Chapter 9
Actuator Design

Henry Haus, Thorsten A. Kern, Marc Matysek and Stephanie Sindlinger

Abstract Actuators are the most important elements of every haptic device, as their selection, respectively, their design influences the quality of the haptic impression significantly. This chapter deals with frequently used actuators structured based on their physical working principle. It focuses on the electrodynamic, electromagnetic, electrostatic, and piezoelectric actuation principle. Each actuator type is discussed as to its most important physical basics, with examples of their dimensioning, and one or more applications given. Other rarely used actuation principles are mentioned in several examples. The previous chapters were focused on the basics of control-engineering and kinematic design. They covered topics of structuring and fundamental character. This and the following chapters deal with the design of technical components as parts of haptic devices. Experience teaches us that actuators for haptic applications can rarely be found "off-the-shelf". Their requirements always include some outstanding features in rotational frequency, power density, working point, or geometry. These specialties make it necessary and helpful for their applicants to be aware of the capabilities and possibilities of modifications of existing actuators. Hence, this chapter addresses both groups of readers: users who want to choose a certain actuator and the mechanical engineer who intends to design a specific actuator for a certain device from scratch.

H. Haus (✉)
Institute of Electromechanical Design, Technische Universität Darmstadt,
Merckstr. 25, 64283 Darmstadt, Germany
e-mail: h.haus@hapticdevices.eu

T.A. Kern
Continental Automotive GmbH, VDO-Straße 1, 64832 Babenhausen, Germany
e-mail: t.kern@hapticdevices.eu

M. Matysek
Continental Automotive GmbH, Babenhausen, Germany
e-mail: m.matysek@hapticdevices.eu

S. Sindlinger
Roche Diagnostics GmbH, Mannheim, Germany
e-mail: s.sindlinger@hapticdevices.eu

C. Hatzfeld and T.A. Kern (eds.), *Engineering Haptic Devices*,
Springer Series on Touch and Haptic Systems, DOI 10.1007/978-1-4471-6518-7_9

9.1 General Facts About Actuator Design

Thorsten A. Kern

Before a final selection of actuators is made, the appropriate kinematics and the control-engineering structure, according to the previous chapters, should have been fixed. However, in order to handle these questions in a reasonable way, some basic understanding of actuators is mandatory. In particular, the available energy densities, forces, and displacements should be estimated correctly for the intended haptic application. This section provides some suggestions and guidelines to help and preselect appropriate actuators based on the typical requirements.

9.1.1 Overview of Actuator Principles

There are a certain number of approaches to transform an arbitrary energy source into mechanical energy. Each of these ways is one actuation principle. The best-known and most frequently used principles are as follows:

Electrodynamic principle A force, so-called LORENTZ force, acting upon a conductor conducting a current.

Electromagnetic principle A force, acting upon a magnetic circuit to minimize the enclosed energy.

Piezoelectric principle A force, acting upon the atomic structure of a crystal and deforming it.

Capacitive principle A force, resulting from charges trying to minimize the energy in a capacitor.

Magnetorheological principle Viscosity change within a fluid resulting from particles trying to minimize the energy contained within a magnetic circuit.

Electrochemical principle Displacement of or pressure within a closed system, whereby a substance emits or bounds a gas and consequently changes its volume due to the application of electrical energy.

Thermal principle Change of length of a material due to controlled temperature changes, making use of the material's coefficient of thermal expansion.

Shape-memory alloy Sudden change of an object's shape made of special material due to relatively small temperature changes ($\approx$500 °C). The object transforms into a root shape embossed during manufacture by the application of high temperatures ($\approx$1,000 °C).

Each of these principles is used in different embodiments. They mainly differ in the exact effective direction of, e.g., a force vector[1] or a building principle.[2] As a

[1] The electromagnet principle for instance is divided into magnetic actuators and actuators based on the reluctance principle; the piezoelectric principle is subdivided into three versions depending on the relative orientation of electrical field and movement direction.

[2] E.g., resonance drives versus direct drives.

consequence, a widespread terminology exists for naming actuators. The major terms are given as follows:

Electric motor The most general term of all. It may describe any electromechanic transformer. However, in most cases, it refers to an actuator rotating continuously whose currents are commutated (mechanically or electronically), or which is equipped with a multiphase alternating current unit. Typically, it is a synchronous motor, a drive with a rotor moving synchronously to the rotating electromagnetic field. In a more general understanding, the term includes hysteresis motors and squirrel-cage rotors. The latter however has not yet reached any relevance for haptic systems, not even in very exceptional cases.

EC-motor Specific embodiment of the synchronous motor and common to haptic applications. Motor based on the electromagnetic or electrodynamic principle with an electronic control unit for the rotating field (electronic-commutated, electronically commutated).

DC-motor Another specific form of a synchronous motor and used among haptic applications because of its cheapness and simplicity. This is an actuator based on the electromagnetic or electrodynamic principle with a mechanical control unit for rotating field using switching contacts (mechanically commutated).

Resonance actuator Generic term for a whole class of actuators with different actuation principles. The term describes an actuator containing one component which is driven in its mechanical resonance mode (or nearby its resonance mode). Typically, parts of this component make an elliptic oscillation driving a second component in small steps via frictional coupling. As a result of the high frequency, the movement of the second component seems uninterrupted. The term is most frequently applied to piezoelectric actuators.

Ultrasonic actuator Resonance actuator performing steps at a frequency within ultrasonic ranges (>15 kHz). These actuators are built almost always based on the piezoelectric principle.

Voice-coil actuator Translational drive based on the electrodynamic principle. Mainly consisting of a conductor wrapped around a cylinder. The cylinder itself is placed in a magnetic circuit, resulting in a Lorentz force when a current is applied to the conductor. There are two major embodiments, one with a "moving coil", another variant with a "moving magnet".

Shaker Another form of a voice-coil actuator with an elastic suspension of the coil. When current is applied to the coil, an equilibrium condition between the suspension's spring and the Lorentz force is achieved at a specific displacement. Actuators based on this structure are frequently used for fast and dynamic movements of masses for vibration testing (this is where its name comes from).

Plunger-type magnet Actuator based on the electromagnetic principle. A rod made of ferromagnetic material is pulled into a magnetic circuit equipped with a coil. These actuators have nonlinear force–displacement characteristics.

Stepper motor Generic term for all actuation principles moving forward step-by-step. In contrast to the resonance drives, no component of a stepper motor is driven in resonance mode. Their step frequency is below any resonance of the system and may vary. These actuators may even be used in a "microstep mode", interpolating movement between so-called "full-steps", which are original to their mechanical design. The term is most frequently used for rotatory drives, for those working based on the reluctance principle or another electromagnetic actuation principle especially.

Pneumatic and Hydraulic These actuation principles do not have a direct electric input value. They transform pressure and volume flow into displacement and force. The media for pressure transmission is air in case of pneumatics and a fluid, typically oil, in case of hydraulics. Usually, the pressure itself is generated via actuators, e.g., electrical actuators attached to a compressor, and controlled via electrical valves.

Bending actuator Actuator with an active layer, frequently made of piezoelectric material—attached to a passive mechanical substrate. By actuating the active layer, mechanical tensions between this layer and the substrate build up, resulting in a bending movement of the whole actuator.

Piezoelectric stack A larger number of piezoelectric layers mechanically connected in series. Small displacements of each layer sum up to a large usable displacement of the whole actuator.

Piezoelectric motor/drive Generic term for all drives based on the piezoelectric principle. It frequently refers to drives moving a rotor or translator with frictional coupling. However, this movement does not need to happen in resonance mode.

Capacitive actuator Actuator based on the capacitive principle and frequently used in microtechnology. Usually, equipped with a comb-like structure of electrode pairs, generating forces in millinewton range with micrometers of displacement.

Shape-memory wire Wire on the basis of shape-memory alloys capable to shorten in the range of percents ($\approx$8 % of its total length) when changing its temperature (e.g., by controlling a current flowing through the wire. The current heats up the wire based on its thermal loss at the wire's electrical resistance).

Surface-wave actuators Generic term for a group of actuators generating high-frequency waves in mechanical structures or exciting the resonance modes of structures. This actuator is frequently based on piezoelectric principles and has been used for the generation of haptic textures for some years.

Each of the above actuation principles can be found in tactile and/or kinaesthetic systems. To simplify the decision process for a new design, all actuators can be grouped into classes. Most of the physical working principles can be grouped either into "self-locking" or "free-wheeling" systems. These groups are identical to:

- Positional sources (x), respectively, angular sources (α)
- Force sources (F), respectively, torque sources (M)

Table 9.1 Typical application areas for actuator principles in haptic systems

Control type		Admittance		Impedance	
Type	Actuator	Closed-l	Open-l	Open-l	Closed-l
Rotatory	Electric motor[a]	X	X	(X)[b]	–
Rotatory and translatory	EC-motor	–	–	X	X
Rotatory and translatory	DC-motor	–	–	X	X
Rotatory and translatory	Resonance actuator	X	X	(X)	–
Rotatory and translatory	Ultrasonic actuator	X	X	(X)	–
Translatory	Voice coil	–	–	X	X
Translatory	Shaker	X	X	–	–
Translatory	Plunger-type magnet	X	–	–	–
Rotatory (and translatory)	Stepper motor	X	X	–	–
Translatory (and rotatory)	Pneumatic	(X)	X	–	–
Translatory (and rotatory)	Hydraulic	–	X	–	–
Translatory	Bending actuator	–	X	–	–
Translatory	Piezo-stack	(X)	X	–	–
Translatory and rotatory	Piezo-actuator	X	X	X	–
Translatory	Capacitive	–	(X)	–	–
Translatory	Shape-memory	–	(X)	–	–
Translatory	Surface wave	–	(X)	–	–

X is frequently used by many groups and even commercialized
(X) Some designs, especially in research
– Very rare to almost none, and if it is used, it is only in the context of research
Type: Gives an idea about which actuator design (translatory or rotatory) is used more often. If the actuator is unusual but does exist, the marker is set into brackets
Annotations
[a]In the meaning of a mechanically commutated drive with a power between 10–100 W
[b]By high-frequency vibrations of the commutation

According to the basic structures of haptic systems (Chap. 6), it is likely that both classes are used within different haptic systems. The correlation between basic structures of haptic systems and actuators is depicted in Table 9.1. This table shows a tendency toward typical applications; however, by adding mechanical elements (springs, dampers), it is possible to use any actuator for any basic structure of haptic systems.

9.1.2 Actuator Selection Aid Based on Its Dynamics

Different actuator designs according to the same physical principle still cover wide performance ranges regarding their achievable displacements or forces. Based on the author's experience, these properties are put in relation to the dynamical ranges relevant for haptic applications. In Fig. 9.1, the most important actuation principles

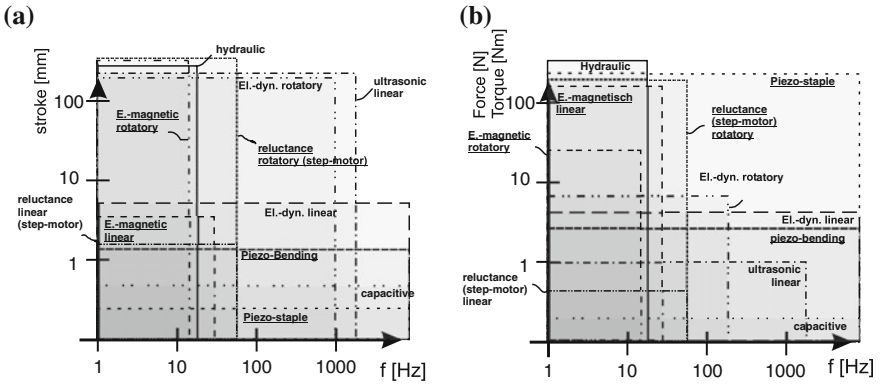

Fig. 9.1 Order of the actuator principles according to the achievable displacement (**a**) and forces respectively torques (**b**) in dependency from their dynamics. Further information can be found in [52]

are visualized in squares scaled according to their achievable displacements (a)[3] and typical output forces and torques (b). The area covered by a specific version of an actuator is typically smaller than the area shown here. The diagram should be read in such a way that, e.g., for haptic applications, electromagnetic linear actuators exist, providing a displacement up to 5 mm at ≈50 Hz. These designs are not necessarily the same actuators that are able to provide ≈200 N, as with electromagnetic systems, the effectively available force increases with smaller maximum displacement (Sect. 9.4). The diagrams in Fig. 9.1 visualize the bandwidths of realization possibilities according to a certain actuation principle and document the preferred dynamic range of their application. Using the diagrams, we have to keep in mind that the borders are fluent and have to be regarded in the context of the application and the actuator's individual design.

9.1.3 Gears

In general machine engineering, the use of gears is a matter of choice for adapting actuators to their load and vice versa. Gears are available in many variants. A simple lever can be a gear; complex kinematics according to Chap. 8 are a strongly nonlinear gear. For haptic applications, specialized gear designs are discussed for specific actuation principles in the corresponding chapters. However, there is one general aspect of the application of gears with relevance to the design of haptic systems, which has to be discussed independently: the scaling of impedances is only in the context of research.

[3] For continuously rotating principles, all displacements are regarded as unlimited.

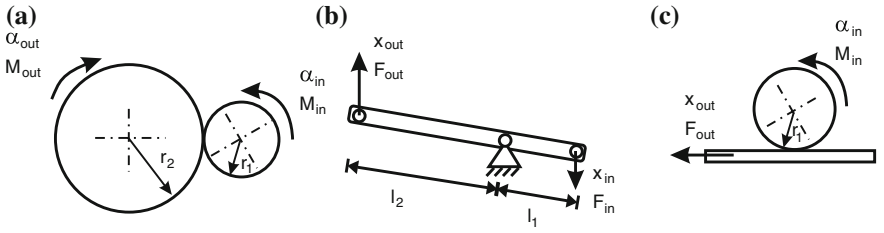

Fig. 9.2 Simple gear design with wheels (**a**), a lever (**b**) and a cable, rope, or belt (**c**)

There is no principal objection to the use of gears for the design of haptic systems. Each gear (Fig. 9.2) be it rotatory/rotatory (gearwheel or frictional wheel), translatory/translatory (lever with small displacements), rotatory/translatory (rope/cable/capstan) has a transmission "tr." This transmission ratio scales forces and torques neglecting loss due to friction according to

$$\frac{F_{\text{out}}}{F_{\text{in}}} = \text{tr} = \frac{l_2}{l_1}\,, \tag{9.1}$$

$$\frac{M_{\text{out}}}{M_{\text{in}}} = \text{tr} = \frac{r_2}{r_1}\,, \tag{9.2}$$

$$\frac{F_{\text{out}}}{M_{\text{in}}} = \text{tr} = \frac{1}{2\pi\, r_1}\,, \tag{9.3}$$

and displacements resp. angles according to

$$\frac{x_{\text{in}}}{x_{\text{out}}} = \text{tr} = \frac{l_2}{l_1}\,, \tag{9.4}$$

$$\frac{\alpha_{\text{in}}}{\alpha_{\text{out}}} = \text{tr} = \frac{r_2}{r_1}\,, \tag{9.5}$$

$$\frac{\alpha_{\text{in}}}{x_{\text{out}}} = \text{tr} = \frac{1}{2\pi\, r_1}\,. \tag{9.6}$$

The velocities and angular velocities scale analogously to the differential of the above equations. Assuming the impedance of the actuator $\underline{Z}_{\text{transl}} = \frac{\underline{F}}{\underline{v}}$ resp. $\underline{Z}_{\text{rot}} = \frac{\underline{M}}{\underline{\dot{\alpha}}}$, one consequence of the load condition of a driven impedance $\underline{Z}_{\text{out}}$ from the perspective of the motor is

$$\underline{Z}_{\text{transl}} = \frac{\underline{F}_{\text{in}}}{\underline{v}_{\text{in}}} = \frac{\underline{F}_{\text{out}}}{\underline{v}_{\text{out}}}\,\frac{1}{\text{tr}^2} = \underline{Z}_{\text{transl out}}\,\frac{1}{\text{tr}^2} \tag{9.7}$$

$$\underline{Z}_{\text{rot}} = \frac{\underline{M}_{\text{in}}}{\underline{\alpha}'} = \frac{\underline{M}_{\text{out}}}{\underline{\alpha}'} \frac{1}{\text{tr}^2} = \underline{Z}_{\text{rot out}} \frac{1}{\text{tr}^2} \tag{9.8}$$

The transmission ratio tr is quadratic for the calculation of impedances. From the perspective of an actuator, the driven impedance of a system gets small with a gear with a transmission ratio larger than one. This is favorable for the actuating system (and the original reason for the application of gears). For haptic applications, especially for impedance controlled ones, the opposite case has to be considered. In an idle situation and with a transmission ratio larger than one,[4] the perceived mechanical impedance of a system $\underline{Z}_{\text{out}}$ increases to the power of two with the transmission ratio. Another aspect makes this fact even more critical, as the increase in output force changes only in a linear way with the transmission ratio, whereas a motor's unwanted moment of inertia is felt to increase quadratically. This effect is obvious to anyone who has tried to rotate a gear motor with a high transmission ratio (e.g., tr >100) at its output. The inertia and the internal frictions upscaled by the gear are identical to a self-locking of the actuator.

As a consequence, the use of gears with force-controlled haptic systems makes sense only for transmission ratios of 1–20 (with emphasis on the lower transmission ratios between 3 and 6). For higher transmission ratios, designs according to Fig. 9.2c and Eq. (9.6) based on ropes or belts have proved valid. They are used in many commercial systems, as with the aid of the definition $\text{tr} = \frac{1}{2\pi\, r_1}$ and the included factor 2π, a comparably high transmission ratio can be achieved easily. In combination with rotatory actuators (typically EC-drives) with low internal impedances, this design shows impressive dynamic properties. Figure 9.3 shows an example for the application of such a gear to drive a delta mechanism [102].

Recently, a new type of gear came into view of several researchers [140]. The twisted-string actuator (TSA) is based on a relatively small motor with large rotation speed that twists a string or a set of strings. Because of the twisting, the strings contract and provide pulling forces in the range of several ten newtons that can be transferred via bowden cables. Applications include exoskeletons as presented in [103] and other devices that are weight sensitive.

Some advice may be given here out of practical experience: Wheel-based gears are applicable for haptic systems but tend to generate unsteady and waving output torques due to toothing. Careful mechanical design can reduce this unsteadiness. The mechanical backlash should be minimized (which is typically accompanied by an increase in friction), for example, by material combinations with at least one soft material. At least one gear should have spur/straight gearing, whereas the other can keep involute gearing.

[4] Which is the normal case, as typically the fast movement of an actuator is transmitted into a slower movement of the mechanism.

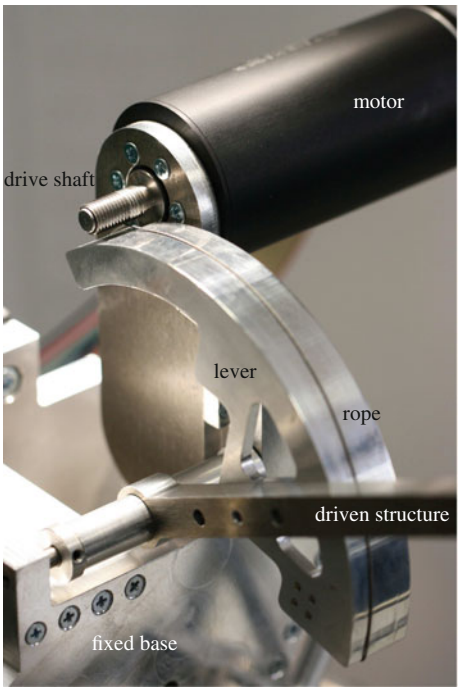

Fig. 9.3 Rope-based gear as widely used in haptic interfaces. The driven structure is connected to a lever on which the driving rope is running. The driving rope is wound around the driving shaft of the motor. The number of revolutions around the shaft is determined by the amount of torque to be transmitted via the gear; threads are used to minimize friction and wearout between individual turns of the driving rope

9.2 Electrodynamic Actuators

Thorsten A. Kern

Electrodynamic actuators are the most frequently used type of drives for haptic applications. This popularity is a result of the direct proportion between their output value (force or torque) from their input values (the electrical current). In case of kinaesthetic applications, they are typically used as open-loop controlled force sources. But even with tactile applications, these very dynamic actuators are frequently applied for oscillating excitements of skin areas. They are equally often used rotatory and translatory. Depending on the design either the electrical coil or the magnet is the moving component of the actuator. This section gives a short introduction to the mathematical basics of electrodynamic systems. Later, some design variants are discussed in detail. The final subsection deals with the drive electronics necessary to control electrodynamic systems.

9.2.1 The Electrodynamic Effect and Its Influencing Variables

Electrodynamic actuators are based on the LORENTZ force

$$\mathbf{F}_{\text{Lorentz}} = \mathbf{i} \cdot l \times \mathbf{B}, \tag{9.9}$$

acting upon moving charges in magnetic fields. The LORENTZ force is dependent on the current **i**, the magnetic induction **B** such as the length of the conductor l, which is typically formed as a coil. This section deals with optimization of each parameter for the maximization of the generated output force F_{Lorentz}. Any electrodynamic actuator is made of three components:

- generator of the magnetic field (coil or most frequently a permanent magnet);
- magnetic flux conductor (iron circuit, magnetic core);
- electrical conductor (frequently formed as coil or a more complex winding).

After a quick look, a recommendation for the maximization of the output force could be to simply increase the current **i** in the conductor. However, with the given limited available space for the conductor's length l (coil's cross section) and a flux density **B** with an upper border (0.8–1.4 T), the effectiveness of this change has to be put into question. This can be shown with a simple calculation example.

9.2.1.1 Efficiency Factor of Electrodynamic Actuators

For example, a straightforward design of an electrodynamic actuator similar to the actor in Fig. 9.4 is analyzed. It contains a wound coil with a permanent magnet in a

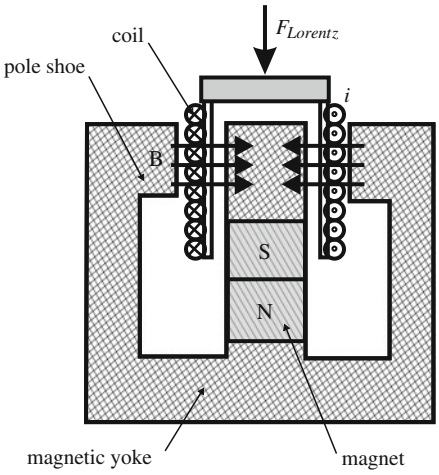

Fig. 9.4 Moving-coil actuator and corresponding functional elements

ferromagnetic core. The electrical power loss P_{el} of this electrodynamic system is generated mainly in a small moving coil with a pure ohmic resistance $R_{\mathrm{coil}} = 3.5\,\Omega$ and a nominal current $i = 0.78\,\mathrm{A}$:

$$P_{\mathrm{el}} = R_{\mathrm{coil}}\, i^2 = 3.5\,\Omega \cdot 0.78\,\mathrm{A}^2 = 2.13\,\mathrm{W}. \tag{9.10}$$

With this electrical power loss, at flux density $\mathrm{B} = 1.2\,\mathrm{T}$, with an orthogonal conductor orientation, and a conductor length within the air-gap $l = 1.58\,\mathrm{m}$, the actuator itself generates the force

$$F_{\mathrm{Lorentz}} = i\, l\, B = 0.78\,\mathrm{A} \cdot 1.58\,\mathrm{m} \cdot 1.2\,\mathrm{T} = 1.48\,\mathrm{N}\,. \tag{9.11}$$

Assuming the system is driven in idle mode—working against the coil's own mass of $m = 8.8\,\mathrm{g}$ only—being accelerated from idleness, and performing a displacement of $x = 10\,\mathrm{mm}$, above electrical power P_{el} is needed for a period of

$$t = \sqrt{2\,\frac{x}{a}} = \sqrt{2\,\frac{xm}{F}} = 0.011\,\mathrm{s} \tag{9.12}$$

seconds. The electrical energy loss sums up to

$$W_{\mathrm{el}} = P_{\mathrm{el}} \cdot t = 23,4\,\mathrm{mJ}. \tag{9.13}$$

This gives an efficiency factor of $\frac{W_{\mathrm{mech}}}{W_{\mathrm{el}}+W_{\mathrm{mech}}} = 38\,\%$ for idle mode and continuous acceleration. Assuming now that the same actuator shall generate a force of 1 N against a fingertip for a period of, e.g., two seconds, an electrical power of $W_{\mathrm{el}} = 2.13\,\mathrm{W} \cdot 2\mathrm{s} = 4.26\,\mathrm{J}$ is needed. This would be identical to an efficiency factor well below 1 %. And indeed, the efficiency factor of electrodynamic actuators in haptic applications lies in the area of low percentages due to the common requirement to generate static forces without much movement. This simple calculation points to one major challenge with electrodynamic actuators: The electrical power loss due to heat transmission extends the mechanically generated power by far. Consequently, during the design of electrodynamic actuators, attention has to be paid to the optimization of power within the given actuator volume and to the thermal management of energy losses.

9.2.1.2 Minimization of Power Loss

Typical designs of electrodynamic actuators either have a winded conductor, which by itself is self-supportive, or which is wound on a coil carrier (Fig. 9.5). The available space for the electrical coil within the homogeneous magnetic flux is limited (A_{Coil}). The number of coil turns $N_{\mathrm{Conductor}}$ is also limited, too, within this area due to the cross-sectional surface; a single turn needs $A_{\mathrm{Conductor}}$. This cross-sectional surface

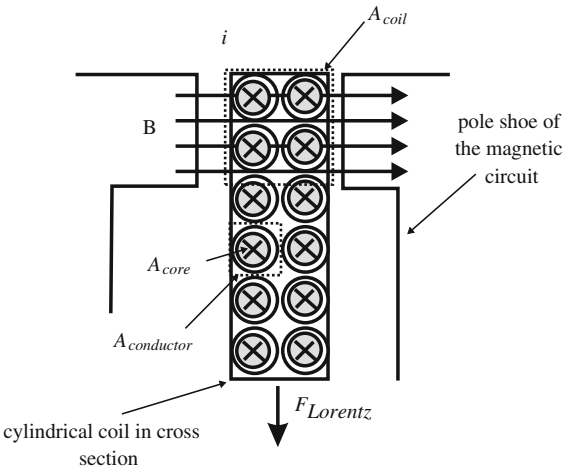

Fig. 9.5 Cross section through a cylindrical electrodynamic actuator based on the moving-coil principle

is typically more than the actual cross section of the conductor, as the winding will have gaps in between single turns [Eq. (9.15)]. Additionally, the actual conducting core with the cross-sectional surface A_{Core} will be smaller than the cross section of the conductor itself due to its isolation. Both parameters describing the geometrical losses in cross sections are available in tables of technical handbooks [95] and are assumed as factors $k \geq 1$ according to Eq. (9.14). The length l of the conductor can be easily calculated by multiplication with the number of turns and the mean circumference *Circ* of the coil [Eq. (9.16)].

The choice of the conductor's diameter influences the resistance of the coil via the conducting area A_{Core} . The specific length-based resistance R_{spezf} of a conductor is given according to Eq. (9.17). Big conducting diameters with large cross sections A_{Core} allow coils to conduct high currents at low voltages but—due to the limited volume available—few windings. Small diameters limit the necessary currents at high voltages and carry more windings. By a careful choice of wire diameter, the winding can be adjusted as a load to the corresponding source to drain the maximum available power.

The power loss P_{Loss} [Eq. (9.18)] acceptable within a given winding is limited. This limit is defined by the generated heat able to dissipate. The technical solutions are dependent on the time of continuous operation, the thermal capacity resulting from the volume of the actuator and the materials it consists of, and a potential cooling system. A calculation of heat transmission is specific to the technical solution and cannot be solved in general within this book. However, the dependency of LORENTZ-force on power loss can be formulated as

$$A_{\text{Conductor}} = k \cdot A_{\text{Core}} \tag{9.14}$$

$$N_{\text{Conductor}} = \frac{A_{\text{Coil}}}{A_{\text{Conductor}}} \tag{9.15}$$

$$l_{\text{Conductor}} = N_{\text{Conductor}} \cdot \text{Circ} \tag{9.16}$$

$$R_{\text{spezf.}} = \frac{l_{\text{Conductor}}\,\rho}{A_{\text{Conductor}}} \tag{9.17}$$

$$P_{\text{Loss}} = i^2 \cdot R_{\text{Coil}} \tag{9.18}$$

From Eq. (9.18) follows

$$i = \sqrt{\frac{P_{\text{Loss}}}{R_{\text{Coil}}}} \tag{9.19}$$

With Eq. (9.17) there is

$$i = \sqrt{\frac{P_{\text{Loss}}\,A_{\text{Core}}}{\rho\,l_{\text{Conductor}}}} \tag{9.20}$$

put into Eq. (9.9) (keeping the direction of current flow $\mathbf{e}_i$) there is

$$F_{\text{Lorenz}} = \sqrt{\frac{P_{\text{Loss}}\,A_{\text{Core}}\,l_{\text{Conductor}}}{\rho}}\mathbf{e}_i \times \mathbf{B} \tag{9.21}$$

by considering Eqs. (9.15)–(9.16) the result is

$$F_{\text{Lorenz}} = \sqrt{\frac{P_{\text{Loss}}\,A_{\text{Coil}}\,N\,\text{Circ}}{\rho\,k}}\mathbf{e}_i \times \mathbf{B} \tag{9.22}$$

Equations (9.15)–(9.18) put into Eq. (9.9) give a precise picture of the influence values on the LORENTZ force [Eq. (9.22)]. The level of Lorentz force is given by the power loss P_{Loss} acceptable within the coil. If there is room for modifications to the geometrical design of the actuator, the cross-sectional area of the coil and the circumference of the winding should be maximized. Additionally, a choice of alternative materials (e.g., alloy instead of copper) may minimize the electrical resistance. Furthermore, the filling factor k should be reduced. One approach could be the use of wires with a rectangular cross-section to avoid empty spaces between the single turns.

The question for the maximum current itself is only relevant in combination with the voltage available and in the context of adjusting the electrical load to a specific electrical source. In this case for i_{Source} and u_{Source}, the corresponding coil resistance has to be chosen based on Eq. (9.23).

$$P_{\text{Source}} = u_{\text{Source}} \cdot i_{\text{Source}} = i_{\text{Source}}^2 \cdot R_{\text{Coil}}$$
$$R_{\text{Coil}} = \frac{P_{\text{Source}}}{i_{\text{Source}}^2} \tag{9.23}$$

Surprisingly, from the perspective of a realistic design, an increase in current is not necessarily the preferred option to increase the LORENTZ force according to Eq. (9.22). The possibility to optimize P_{Loss} by adding cooling or to analyze the temporal pattern of on- and off-times is much more relevant. Additionally, the flux density **B** has—compared to all other influence factors—quadratically higher influence on the maximum force.

9.2.1.3 Maximization of the Magnetic Flux Density

For the optimization of electrodynamic actuators, a maximization of the flux density **B** is necessary within the area where the conducting coils are located. This place is called air-gap and resembles an interruption of the otherwise closed ferromagnetic core conducting the magnetic flux. The heights of the magnetic flux density are influenced by

- the choice of ferromagnetic material for the magnetic core,
- the field winding/exciter winding of the static magnetic field, and
- the geometrical design of the magnetic core.

In the context of this book, some basic design criteria for magnetic circuits are given. For an advanced discussion and optimization, process source [66] is recommended.

Basics for the Calculation of Magnetic Circuits

Calculating magnetic circuits show several parallels to the calculation of electrical networks. As shown in Table 9.2 several analogies between electrical and magnetic variables can be defined.

The direct analogy to the magnetic flux ϕ is the electrical charge Q. For the application of equations, however, it is helpful to regard electrical currents I as a counterpart to the magnetic flux. Please note that this is an aid for thinking and not a mathematical reality, although it is very common. The actual direct analogy for the current I would be a time-dependent magnetic flux $\frac{\mathrm{d}\phi}{\mathrm{d}t}$, which is usually not defined with an own variable name. The exception with this model is the magnetomotive force Θ, which resembles the sum of all magnetic voltages V identical to a rotation within an electrical network. Nevertheless, it is treated differently, as many applications require generating a magnetomotive force Θ by a certain number of winding turns N and a current I, often referred to as ampere turns. The coupling between field and flux variables is given by the permittivity ϵ in case of electrical values and by the permeability μ in case of magnetic values. It is obvious that the field constants

Table 9.2 Analogies between electric and magnetic values

Description	Electric	Magnetic
Flux Differential flux	Charge Q ($C = \mathrm{As}$) $I = \frac{\mathrm{d}Q}{\mathrm{d}t}$ (A)	Magnetic flux ϕ (Vs)
Flux value	Dielectric flux density D ($\mathrm{C/m^2}$) $Q = \int_A \mathbf{D}\mathrm{d}\mathbf{A}$ Current density J ($\mathrm{A/m^2}$) $I = \int_A \mathbf{J}\mathrm{d}\mathbf{A}$	Flux density B ($\mathrm{T} = \mathrm{Vs/m^2}$) $\phi = \int_A \mathbf{B}\mathrm{d}\mathbf{A}$
Electromagnetic coupling formerly:	Voltage U (V) Electromotive force	Flux/ampere turns Θ (A) Magnetomotive force
Induction laws	$U = -N\frac{\mathrm{d}\phi}{\mathrm{d}t}$	$\Theta = N\frac{\mathrm{d}Q}{\mathrm{d}t}$ $\Theta = N\,I$ ($N =$ turns)
Field values	El. field strength E (V/m)	Magn. field strength H (A/m)
Differential values	Voltage U (V) $U = \int_a^b \mathbf{E}\mathrm{d}\mathbf{s}$	Magnetic voltage V (A) $V = \int_a^b \mathbf{H}\mathrm{d}\mathbf{l}$
Mesh equations	$U_{\mathrm{ges}} = \sum_i U_i$	$\Theta = \sum_i V_i$
Resistances	El. resistance R (Ω) $R = \frac{U}{I}$	Magn. resistance R_m (A/Vs) reluctance $R_m = \frac{V}{\phi}$
Coupling factors	Permittivity $\epsilon = \epsilon_0\,\epsilon_r$ ($\epsilon_0 = 8{,}854 \times 10^{-12}$ C/Vm)	Permeability $\mu = \mu_0\,\mu_r$ ($\mu_0 = 1{,}256 \times 10^{-6}$ Vs/Am)
Coupling between field and flux values	$\mathbf{D} = \epsilon\,\mathbf{E}$	$\mathbf{B} = \mu\,\mathbf{H}$
Power (W)	$P_{\mathrm{el}} = U \cdot I$	
Energy (J)	$W_{\mathrm{el}} = P_{\mathrm{el}}\,t$	$W_{\mathrm{mag}} = \phi\,V$ $W_{\mathrm{mag}} = \sum_n H_n\,l_n \cdot B_n\,A_n$

ϵ_0 differ from μ_0 by the factor 10^6. This is the main reason for the electromagnetic effect being the preferred physical realization of actuators in macroscopic systems.[5]

However, there is another specialty with the field constants. The electrical permittivity can be regarded as constant (Sect. 9.5) even for complex actuator designs and can be approximated as linear around an operating point. The permeability μ_r of typical flux-conducting materials, however, shows a strong nonlinear relationship; the materials are reaching saturation. The level of magnetic flux has to be limited to prevent saturation effects in the design of magnetic core.

[5] In micromechanical systems, the energy density relative to the volume becomes more important. The manufacture of miniaturized plates for capacitive actuators is easier to realize with batch processes than the manufacture of miniaturized magnetic circuits.

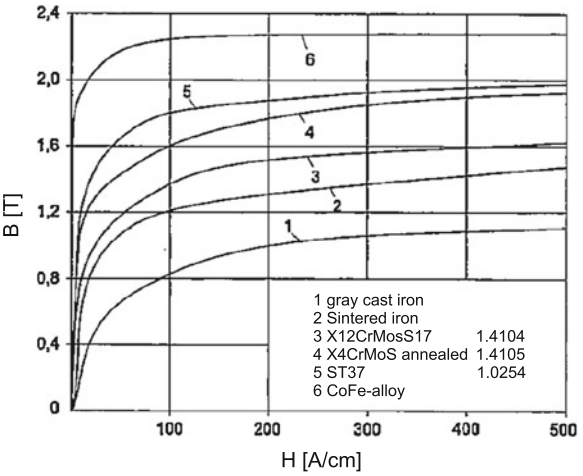

Fig. 9.6 Saturation curve of typical magnetic materials [66]

Magnetic Circuits

For maximization of the magnetic flux density, it is necessary to either analyze the magnetic circuit mathematically, analytically, and/or do a numerical simulation of it. For the simulation of magnetic fields, common CAD and FEM products are available.[6] For classification of the mathematical problem, three solution levels exist: stationary, quasistationary, and dynamic magnetic fields. With stationary magnetic fields, there is no time-dependent change in the magnetic circuit. A steady state of flux density is assumed. With quasistationary field, the induction considered results from changes within the current generating the magnetic field or a linearized change within the geometry of the magnetic circuit (e.g., a movement of an anchor). Dynamic magnetic fields consider additional effects covering the dynamic properties of moving mechanical components up to the change of the geometry of the magnetic circuit and the air-gaps during operation. Dealing with electrodynamic actuators, the analysis of static magnetic circuits is sufficient for first dimensioning. The relevant dynamic drawbacks for electrodynamic actuators are presented in Sect. 9.2.1.4.

There are two principal possibilities to generate magnetic flux densities within the volume of the conducting coil:

1. Generation via winded conductors with another coil (exciter winding);
2. Generation via a permanent magnet.

Both approaches show specific pros and cons: With a winded conductor, the flux density $B = \mu\,(N\,I - H_{\mathrm{Fe}}\,l_{\mathrm{Fe}})$ can be raised without any theoretical limit. In practical

[6] From the very beginning, several free or open software projects are available for electrical and magnetic field simulation, e.g., for rotatory or planar systems, a program by David Meeker named "FEMM".

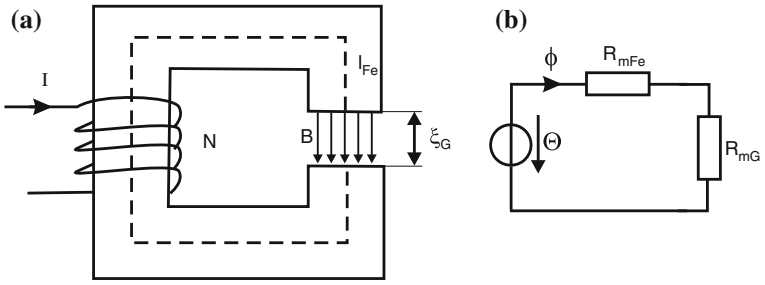

Fig. 9.7 Magnetic field generation B via a current-conducting coil with N turns (**a**) and derived equivalent circuit representation (**b**)

applications, the flux-conducting material will reach saturation (Fig. 9.6) actually limiting the achievable maximum flux density. Additionally, the ohmic resistance of the winding will generate electrical power losses, which will have to be dissipated in addition to the losses resulting from the electrodynamic principle itself (Sect. 9.2.1.1). Abandoning any flux-conducting material and using exciter windings with extremely low electrical resistance, extraordinarily high field densities can be reached.[7] Till date, such a technological effort for haptic devices is yet to be made.

Building a magnetic circuit with a permanent magnet, the practical border for the flux density is given by the remanence flux density B_r of the magnetic material. Such a magnet can be compared to a source providing a certain magnetic power. The flux density—being the relevant quality for electrodynamic actuators—is not independent of the magnetic load attached to the permanent magnet. Additionally, the relevant properties of the magnetic material are temperature dependent, and wrong use of specific magnet materials may harm its magnetic properties.[8]

Nevertheless, modern permanent magnetic materials made of "rare earths" are the preferred source to generate static magnetic fields for electrodynamic actuators. The following section gives some basics on the calculation for simple magnetic circuits. In extension to what is shown here, a more precise analytical calculation is possible [66]. However, it is recommended to use simulation tools early within the design process. Leakage fields are a great challenge in the design of magnetic circuits. Especially, beginners should develop a feeling for the look of these fields with the aid of simulation tools.

[7] MRI systems for medical imaging generate field densities of 2 T and more within air-gaps of up to 1 m diameter by use of supraconducting coils and almost no magnetic circuit at all.

[8] E.g., when removing AlNiCo magnets out of their magnetic circuit after magnetization, they may drop below their coercive field strength actually losing performance.

Direct Current Magnetic Field

Figure 9.7a shows a magnetic circuit of iron with a cross section A and an air-gap of length ξ_G (G = Gap). The magnetic circuit has a winding with N turns conducting a current I. The medium length of the magnetic circuit is l_{Fe}. For calculation, the circuit can be transformed into a magnetic equivalent network (Fig. 9.7b). According to the analogies defined in Table 9.2, the magnetic induction generates a magnetomotive force Θ as a differential value. In combination with two magnetic resistances of the iron circuit R_{mFe} and the air-gap R_{mG}, a magnetic flux ϕ can be identified.

For the calculation of flux density B in the air-gap, it is assumed that this magnetic flux ϕ is identical to the flux within the iron part of the circuit. Leakage fields are disregarded in this example.[9]

$$B = \frac{\phi}{A}$$

The magnetic resistance of materials and surfaces is dependent on the geometry and can be found in special tables [66]. For magnetic resistance of a cylinder of length l and diameter d, a resistance according to Eq. (9.24) is given.

$$R_m = \frac{4\,l}{\mu\,\pi\,d^2} \tag{9.24}$$

For the magnetic circuit, the magnetic resistances $R_{m\mathrm{Fe}}$ and $R_{m\mathrm{G}}$ can be regarded as known or at least calculable. The magnetic flux is given by

$$\phi = \frac{\Theta}{R_{m\mathrm{Fe}} + R_{m\mathrm{G}}}, \tag{9.25}$$

and the flux density by

$$B = \frac{\Theta}{(R_{m\mathrm{Fe}} + R_{m\mathrm{G}})\,A}. \tag{9.26}$$

Using this procedure, a clever approximation of the magnetic resistances of any complex network of magnetic circuits can be made. In this specific case of a simple horseshoe-formed magnet, an alternative approach can be chosen. Assuming that the magnetic flux density in the air-gap is identical to the flux density in the iron (no leakage fields, see above) the flux density B is given by:

$$B = \mu_0 \mu_r\, H \tag{9.27}$$

Assuming that μ_r is given either as a factor or with a characteristic curve (like in Fig. 9.6) only the magnetomotive force Θ within the iron has to be calculated. With

[9] Considering leakage fields would be identical to a parallel connection of additional magnetic resistors to the resistance of the air-gap.

Table 9.3 Magnetic properties of permanent magnet materials [66]

Material	B_r (T)	$H_{c\,B}$ (kA/m)	$(\mathrm{BH})_{\max}$ (kJ/m^3)
AlNiCo (isotropic)	0.5–0.9	10–100	3–20
AlNiCo (anisotropic)	0.8–1.3	50–150	30–70
Hard ferrite (isotropic)	0.2–0.25	120–140	7–9
Hard ferrite (anisotropic)	0.36–0.41	170–270	25–32
SmCo (anisotropic)	0.8–1.12	650–820	160–260
NdFeB (anisotropic)	1.0–1.47	790–1100	200–415

$$\Theta = H_{\mathrm{Fe}}\, l_{\mathrm{Fe}} + H_{\mathrm{G}}\, \xi_G = \frac{B}{\mu_0 \mu_r}\, l_{\mathrm{Fe}} + \frac{B}{\mu_0}\, \xi_G \tag{9.28}$$

the flux density

$$B = \Theta\, \frac{1}{\frac{l_{\mathrm{Fe}}}{\mu_0 \mu_r} + \frac{\xi_G}{\mu_0}}, \tag{9.29}$$

results and can be written down immediately.

Permanent Magnets Generating the Magnetic Field

As stated earlier, the typical approach to generate the magnetic field within an electrodynamic actuator is the choice of a permanent magnet. Permanent magnets cannot simply be regarded as flux or field sources. Therefore, some basic understanding of magnet technology is necessary.

As a simple approach, a magnet is a source of energy that is proportional to the volume of the magnet. Magnets are made of different magnetic materials (Table 9.3) differing in the maximum achievable flux density [remanence flux density B_r), maximum field strengths (coercive field strength $H_{c\,B}$ and $H_{c\,J}$)], and their energy density $BH_{\max}$, such as the temperature coefficient. Additionally, identical materials are differentiated based on being isotropic or anisotropic. With isotropic magnets, the substance is made of homogeneous material, which can be magnetized in one preferred direction. With anisotropic material, a magnetic powder is mixed with a binding material (e.g., epoxy) and formed via a casting or injection-molding process. The latter approach enables almost unlimited freedom for the magnet's geometry and a large influence on the pole distribution on the magnet. However, anisotropic magnets are characterized by slightly worse characteristic values in energy density such as maximum field strengths and flux densities.

Figure 9.8 shows the second quadrant of the $B-H$-characteristic curve (only this quadrant is relevant for an application of a magnet within an actuator) of different magnetic materials. The remanence flux density B_r equals the flux density with short-

circuit pole shoes (a magnet surrounded by ideal iron as magnetic circuit). When there is an air-gap within the magnetic circuit (or even by the magnetic resistance of the real magnetic circuit material itself), a magnetic field strength H appears as a load. As a reaction, an operation point is reached, which is shown here as an example on a curve of NdFeB for a flux density of about 200 kA/m. The actually available flux density at the poles is decreased accordingly. As electrodynamic actuators for haptic applications face high requirements according to their energy density, there are almost no alternatives to the usage of magnet materials based on rare earths (NdFeB, SmCo). This is very accommodating for the design of the magnetic circuit, as nonlinear effects near the coercive field strength such as with AlNiCo or Barium ferrite are of no relevance[10]. Rare earth magnets allow an approximation of their B/H-curve with a linear equation, providing a nice relationship for their magnetic resistance (Fig. 9.9c):

$$R_{\mathrm{Mag}} = \frac{V}{\phi} = \frac{H_c \, l_{\mathrm{Mag}}}{B_r \, A} \tag{9.30}$$

With this knowledge, the magnetic circuit of Fig. 9.9a and the corresponding equivalent circuit (Fig. 9.9b) can be calculated identical to an electrically excited magnetic circuit.

The flux density within the iron is once again given by

$$B = \frac{\phi}{A} \tag{9.31}$$

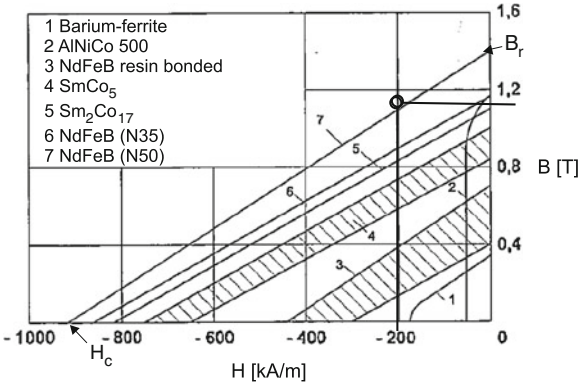

Fig. 9.8 Demagnetization curves of different permanent magnet materials [66]

[10] The small coercive field strength of these materials, e.g., results in the effect, which a magnet magnetized within a magnetic circuit does not reach its flux density anymore once removed and even after reassembly into the circuit again. This happens due to the temporary increase in the air-gap, which is identical to an increase in the magnetic load to the magnet beyond the coercive field strength. Additionally, the temperature dependency of the coercive field strength and of the remanence flux density is critical. Temperatures just below freezing point may result in a demagnetization of the magnet.

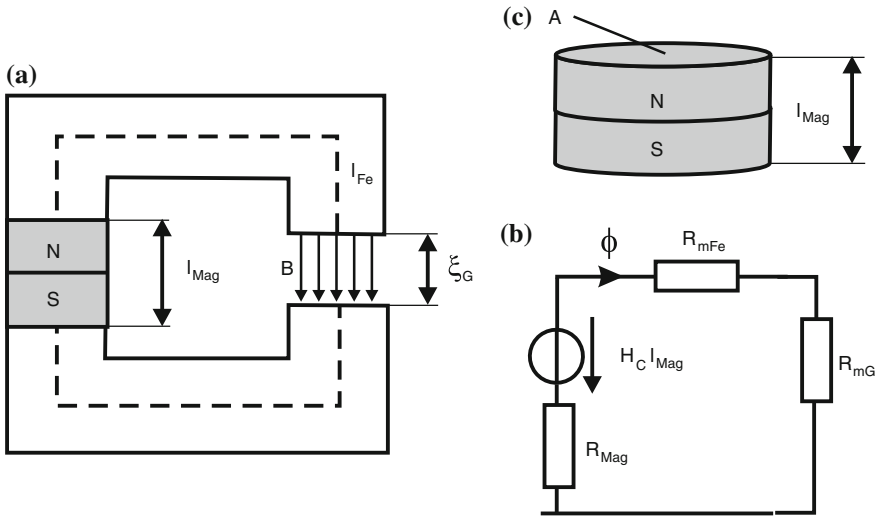

Fig. 9.9 Magnetic field generation B via permanent magnets (**a**), derived equivalent circuit (**b**), and dimensions of the magnet (**c**)

For the given magnetic circuit, the resistances $R_{m\mathrm{Fe}}$ and $R_{m\mathrm{G}}$ are assumed as known or calculable. From Eq. (9.30), the magnetic resistance of the permanent magnet is known. The source within the equivalent circuit is defined by the coercive field strength and the length of the magnets $H_c\, l_{\mathrm{Mag}}$. These considerations result in

$$\phi = \frac{H_c\, l_{\mathrm{Mag}}}{R_{m\mathrm{Fe}} + R_{m\mathrm{G}} + R_{\mathrm{Mag}}}, \tag{9.32}$$

and the flux density

$$B = \frac{H_c\, l_{\mathrm{Mag}}}{(R_{m\mathrm{Fe}} + R_{m\mathrm{G}} + R_{\mathrm{Mag}})\, A}. \tag{9.33}$$

Slightly rearranged and R_{Mag} included gives

$$B = \frac{B_r\, H_c\, \frac{l_{\mathrm{Mag}}}{A}}{(R_{m\mathrm{Fe}} + R_{m\mathrm{G}})\, B_R + H_c\, \frac{l_{\mathrm{Mag}}}{A}}. \tag{9.34}$$

Equation (9.34) states by the factor $B_r\, H_c\, \frac{l_{\mathrm{Mag}}}{A}$ that it is frequently helpful for achieving a maximum flux density B in the air-gap to increase the length of a magnet with at the same time minimized cross-sectional area of the magnetic circuit, which is of course limited by the working distance within the air-gap and the saturation field strengths of the magnetic circuit.

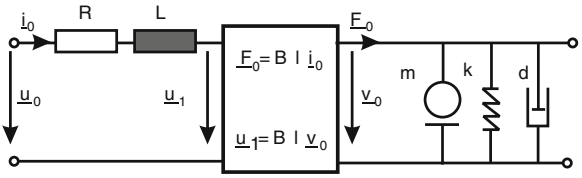

Fig. 9.10 Electrical and mechanical equivalent circuit of an electrodynamic actuator as a transformer

9.2.1.4 Additional Effects in Electrodynamic Actuator

To do a complete characterization of an electrodynamic actuator, there are at least three more effects, whose influences are sketched in the following sections.

Induction

For a complete description of an electrodynamic actuator besides the geometrical design of its magnetic circuit and the mechanical design of its winding and considerations concerning electrical power losses, its other dynamic electrical properties have to be considered. For this analysis, the electrodynamic actuator is regarded as a bipolar transformator (Fig. 9.10).

A current $\underline{i}_0$ generates via the proportional constant $B\,l$ a force $\underline{F}_0$, which moves the mechanical loads attached to the actuator. The movement itself results in a velocity $\underline{v}_0$, which is transformed via the induction law and the proportional constant to an induced voltage $\underline{u}_1$. By measurement of $\underline{u}_1$ and a current source, the rotational velocity or the movement velocity v can be measured, with a voltage source the measurement of $\underline{i}_0$ provides a force- or torque-proportional signal. This is the approach taken by the variant of admittance-controlled devices as a control value (see Sect. 6.4).

The induction itself is a measurable effect, but should not be overestimated. Typically, electrodynamic actuators are used within haptic systems as direct drives at small rotational or translational velocities. Typical coupling factors with rotatory drives are—depending on the size of the actuators—in an area between 100 and 10 $\frac{\text{revolutions}}{s\,V}$. At a rotational speed, which is already fast for direct drives of 10 Hz, induced voltage amplitude $|\underline{u}_1|$ of 0.1 to 1 V can be achieved. This is around 1 to 5 % of the control voltage's amplitude.

Electrical Time Constant

Another aspect resulting from the model according to Fig. 9.10 is the electrical transfer characteristics. Typical inductances L of electrodynamic actuators lie in the area of 0.1–2 mH. The ohmic resistance of the windings largely depends on

the actual design, but as a rule of thumb values between 10 and 100 Ω can be assumed. The step response of the electrical transfer system $\frac{i_0}{u_0}$ shows a time constant $\tau = \frac{L}{R} = 10$ to 30 µs and lies within a frequency range $\gg$10 kHz, which is clearly above the relevant dynamic area of haptics.

Field Response

A factor that cannot so easily be neglected when using electrodynamic actuators for high forces is the feedback of the magnetic field generated by the electromagnetic winding on the static magnetic field. Taking the actuator from the example at the beginning (Fig. 9.4), positive currents generate a field of opposite direction to the field generated by the magnet. This influence can be considered by substitution of both field sources. Depending on the direction of current, this field either enforces or weakens the static field. With awkward dimensioning, this can result in a directional variance of the actuator properties. The problem is not the potential damage to the magnet, modern magnetic materials are sufficiently stable, but a variation in the magnetic flux density available within the air-gap. An intended application of this effect within an actuator can be found in an example in Fig. 9.11.

An detailed discussion of electrodynamic actuators based on concentrated elements can be found in [77].

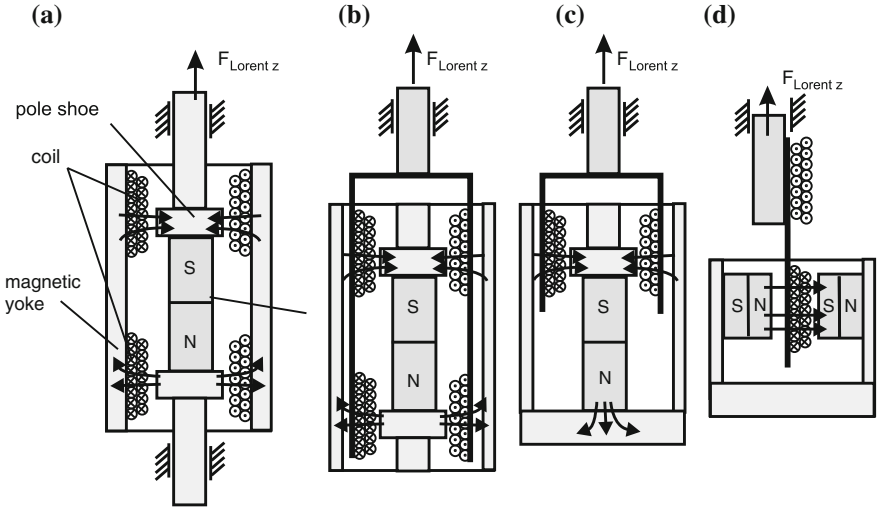

Fig. 9.11 Variants of electrodynamic actuators for translational movement with moving magnets (**a**), moving coils (**b**), as plunger type (**c**), and as flat coil (**d**)

9.2.2 Actual Actuator Design

As stated earlier, electrodynamic actuators are composed of three basic components: coil/winding, magnetic circuit, and magnetic exciter. The following section describes a procedure for the design of electrodynamic actuators based on these basic components. As the common principle for excitation, a permanent magnet is assumed.

9.2.2.1 Actuator Topology

The most fundamental question for the design of an electrodynamic actuator is its topology. Usually, it is known whether the system shall perform rotary or translatory movements. Later, the components' magnetic circuit, the location of magnets, pole shoes, and the coil itself can be varied systematically. A few common structures are shown in Fig. 9.12 for translational actuators and in Fig. 9.11 for rotatory actuators. For the design of electrodynamic actuators in any case, the question to be asked should be whether the coil or the magnetic circuit moves. By this variation, apparently complex geometrical arrangements can be simplified drastically. Anyway, it has to be considered that a moving magnet has more mass and can typically be moved less dynamically than a coil. On the other hand, there is no contact or commutating problem to be solved with non-moving windings.

Moving Coils

Electrodynamic actuators according to the principle of moving coils with a fixed magnetic circuit are named "moving coil" in case of linear movement and "ironless rotor" in case of rotatory actuator. They always combine few moving masses and as a result high dynamics. The translatory version shows displacements of a

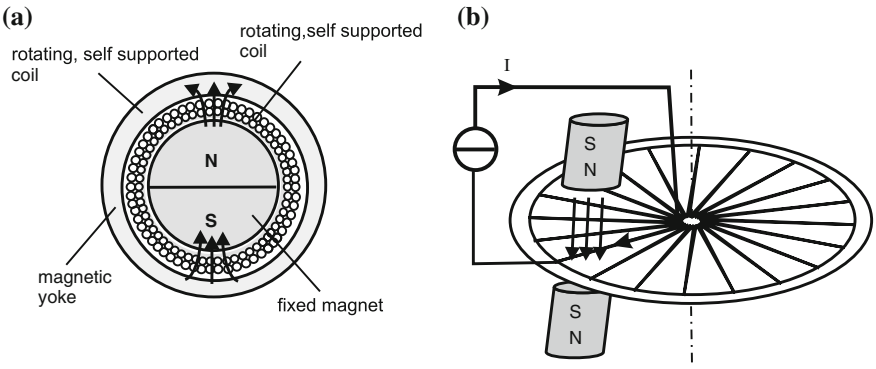

Fig. 9.12 Variants of electrodynamic actuators for rotatory movements with self-supportive winding (**a**), and with disk winding (**b**)

few millimeters and is used especially within audio applications as loudspeaker. Actuators according to the principle of "moving coils" have two disadvantages:

- As the coil is moving, the electrical contact is subject to mechanical stress. With high displacements especially, the contact has to be mechanically robust.
- If there is the idea to design moving coils as pure force sources with large displacements, always only a small area of the conducting coil is within the air-gap and therefore contributes to force generation. With large displacements, moving coils show an even lower efficiency factor. This can be compensated by switching the active coil areas, which again results in the necessity to have more contacts.

A similar situation happens with rotatory systems. Based on the electrodynamic principle, there are two types of windings applicable to rotatory servo-systems: the *Faulhaber* and the *Maxon* winding of the manufacturers with identical names. These actuators are also known as "iron-less" motors. Both winding principles allow the manufacture of self-supportive coils. A diagonal placement of conductors and a baking process after winding generates a structure sufficiently stable for centrifugal forces during operation. The baked coils are connected to the rotating axis via a disk. The complete rotor (Fig. 9.13) is built of these three components. By the very small inertia of the rotor, such actuators show impressive dynamic properties. The geometrical design allows placing the tubular winding around a fixed, diametrally magnetized magnet. This enables another volume reduction compared to conventional actuators as its housing has to close the magnetic circuit only instead of providing additional space for magnets.

Within self-supportive winding, there are areas of parallel-lying conductors combined to poles.[11] With moving coils, there is always the need for a specialized contactor, either via contact rings, or electronic commutation or via mechanical switching.

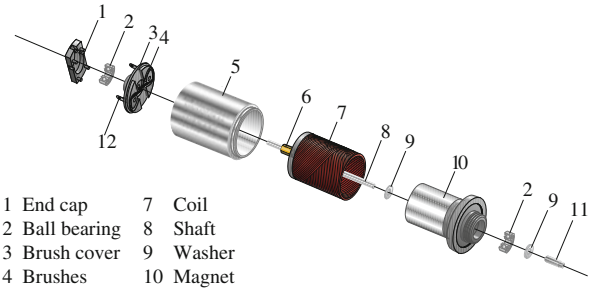

Fig. 9.13 Design of an electrodynamic actuator with self-supportive winding based on the FAULHABER principle. Picture courtesy of *Dr. Fritz Faulhaber GmbH*, Schöneich, Germany

[11] The *Faulhaber* and the *Maxon* excel by a very clever winding technique. On a rotating cylinder, respectively, a flatly pressed rectangular winding pole can be combined by contacting closely located areas of an otherwise continuous wire.

Depending on the number of poles, all coils are contacted at several points. In case of mechanical switching, these contacts are placed on the axis of the rotor and connected via brushes with the fixed part of the actuator named "stator". This design enables a continuous movement of the rotor, whereas a change in the current flow is made purely mechanical by sliding the brushes on the contact areas of the poles on the axis. This mechanical commutation is a switching procedure with an inductance placed in parallel.

As such, an actuator can be connected directly to a direct current source, known as "DC-drives". As stated in Sect. 9.1, the term "DC-drive" is not only limited to actuators according to the electrodynamic principle but is also frequently applied to actuators following the electromagnetic principle (Sect. 9.4).

Moving Magnet

In case of translatory (Fig. 9.11a) systems, actuators based on the principle of a moving magnet are designed to provide large displacements with compact windings. The moving part of the actuator is composed almost completely of magnetic material. The polarity direction of this material may vary in its exact orientation. Actuators according to this principle are able to provide large power but are expensive due to the quantity of magnet material necessary. Additionally, the moving magnet is heavy; the dynamics of the actuator is therefore smaller than in the case of a moving coil. In case of a rotatory system, a design with moving magnet is comparable to a design with moving coil. Figure 9.14 shows such a drive. The windings fixed to the stator are placed around a diametral magnetized magnet. It rotates on an axis, which frequently additionally moves the magnetic circuit, too. Providing the right current feed to the coil the orientation of the rotor has to be measured. For this purpose, sensors based on the Hall effect or optical code-wheels are used.

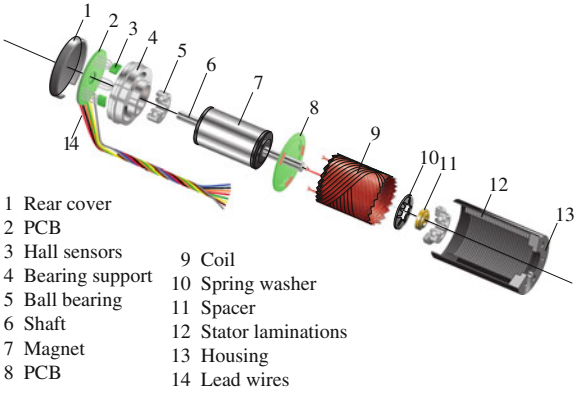

Fig. 9.14 Components of an EC-drive. Pictures courtesy of *Dr. Fritz Faulhaber GmbH*, Schöneich, Germany.

Electrodynamic actuators with moving magnet are known as EC-drives (electronic-commutated). This term is not exclusive to electrodynamic actuators, as there are also electronic-commutated electromagnetic drives. EC-drives—whether electrodynamic or electromagnetic—combined with the corresponding driver electronics are frequently known as servo-drives. Typically, a servo-drive is an actuator able to follow a predefined movement path. Servo-drives are rarely used for haptic devices. However, the use of EC-drives for haptic application is frequent, but they are equipped with specialized driver electronics.

9.2.2.2 Commutation in the Context of Haptic Systems

The necessary commutation of current for rotating actuators has huge influence on the quality of force output with respect to torque output.

Mechanically Commutating Actuators

With mechanically commutating actuators, the current flow is interrupted suddenly. Two effects of switching contacts appear: The voltage at the contact point increases, sparks may become visible—an effect called electrical brush sparking. Additionally, the remaining current flow induces a current within the switched-off part of the winding that itself results in a measurable torque. Depending on the size of the motor, this torque can be felt when interacting with a haptic system and has to be considered in the design.

The current and torque changes can be reduced by he inclusion of resistors and capacitors into the coil. However, this results in high masses of the rotor and worse dynamic properties. Besides, a full compensation is impossible. Nevertheless, mechanically commutating actuators are in use for inexpensive haptic systems. The GEOMAGIC TOUCH from *geomagic* and the FALCON from *Novint* use such actuators.

Electronic-Commutated Electrodynamic Actuators

Electronically commutated electrodynamic actuators differ from mechanically commutated actuators by the measurement technology used as a basis for switching currents. There are four typical designs for this technology:

- In sensor-less designs (Fig. 9.15a), an induced voltage is measured within a coil. At zero-crossing point, one pole is excited with a voltage after an interpolated 30◦ phase delay dependent on the actual revolution speed of the rotor. In combination with measurement of the inductance followed by a switched voltage, a continuous rotation with batch-wise excitation is realized. This procedure cannot be applied to low rotation speeds, as the induced voltage becomes too low, and accordingly, the switching point can hardly be interpolated. Additionally, the concept of using

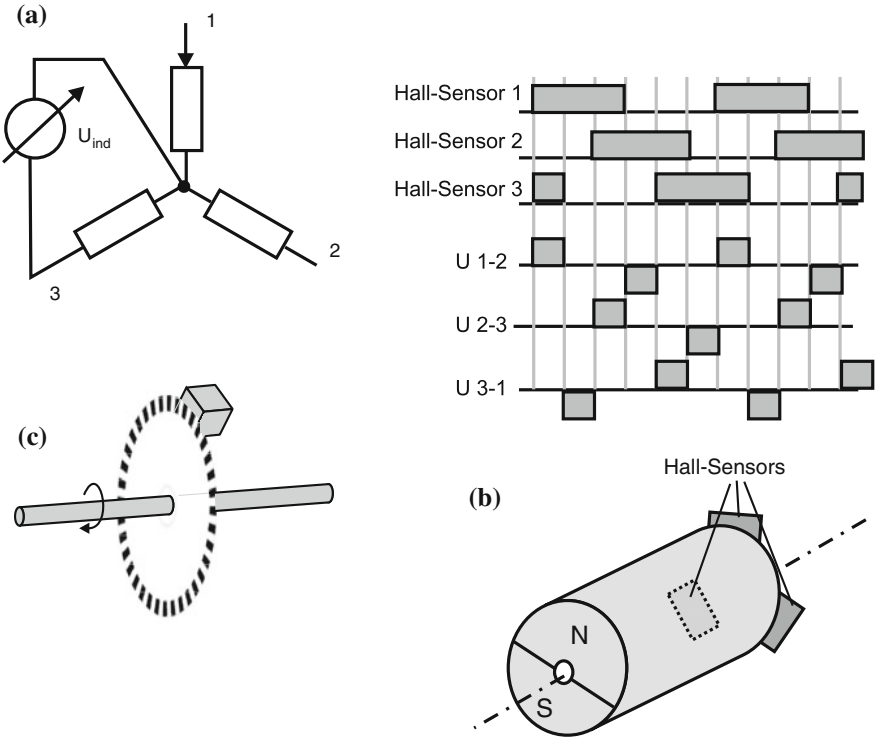

Fig. 9.15 Technologies for different commutation methods: sensorless (**a**), block-commutation (**b**) and optical code-wheel (**c**)

one to two coils for torque generation results in high torque variations at the output of up to 20 %, making this approach not useful for haptic systems.

- Block-commutating procedures (Fig. 9.15 b) are based on the use of simple hall switches or field plates for position detection of the rotor. Three sensors located at 120° angular phase shift allow the detection of six different rotor positions. Reducing positioning information to six orientations per revolution makes this approach equally inappropriate for haptic applications, as the torque varies in a range of >15 % for one revolution.
- Sinus-commutating procedures with analog hall sensors are based on the measurement of the rotor position by at least two sensors. They are placed with an angle of either 120° or 90° at the front of the rotor. They provide voltages in angular phase shift according to their geometrical position. By analyzing the polarity and the absolute height of the voltages, absolute positioning information can be obtained and used for commutating the windings. If the phase lag between both sensor signals is identical to the phase lag between the poles of the winding, a direct control of current drivers can be performed without the need for digitization or a specific calculation step.

- Sinus commutating with digital code-wheels (Fig. 9.15c) are based on the measurement of rotor position by use of, usually optical, code disks. By reflective or transmissive measurement, the rotor position is sampled with high resolution. This relative positioning information can be used for position measurement after initial calibration. Depending on the code-wheels resolution, a smooth sinusoid commutation can be achieved with this method.

The sinus-commutating methods are the preferred solutions used for haptic applications due to the little torque variations and their applicability for slow revolution speeds typical of direct drives.

9.2.3 Actuator Electronics

Electrodynamic actuators require specific electrical circuits. In the following section, the general requirements on these electronics are formulated.

9.2.3.1 Driver Electronics

Driver electronics are electrical circuits transforming a signal of low power (several volts, some milliampere) into a voltage or current level appropriate to drive an actuator. For electrodynamic actuators in haptic applications, driver electronics have to provide a current in a dynamic range from static up to several kilohertz. This section describes general concepts and approaches for such circuits.

Topology of Electric Sources

Driver electronics for actuators—independently from the actuation principle they are used for—are classified according to the flow of electrical energy (Fig. 9.16). There are four classes of driver electronics:

- One-quadrant controllers are capable of generating positive output currents and voltages. An actuator driven by them is able to move in one direction. These controllers use only the first quadrant according to Fig. 9.16a.
- Switched one-quadrant controllers are capable of a direction change by input of a logical signal. They work within the first and third quadrants based on Fig. 9.16a. The switching point is a nonlinear step in their characteristic curve.
- Real two-quadrant controllers are capable of providing a characteristic curve, which is steady around the zero point. They function in the first and third quadrants based on Fig. 9.16a, but are not capable to conduct currents and voltages with opposite directions.
- Four-quadrant controllers function within all four quadrants of Fig. 9.16a. They are able to control currents and voltages in any combination of directions. Four-

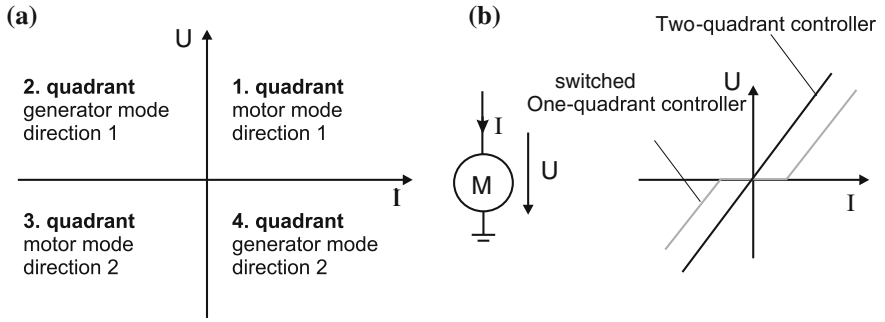

Fig. 9.16 **a** Visualization of the four quadrants of an electric driver, formed by the directions of current and voltage. **b** characteristic curves of a two-quadrant controller and a switched one-quadrant controller

quadrant controllers allow energy recovery by induced current to an energy storage, which is especially relevant for mobile applications.

For haptic application, the switched one-quadrant controller is frequently met, as many haptic systems do not have the necessity to control the device near the voltage- or current-zero point. However, for systems with high dynamics and low impedance, the two-quadrant and the four-quadrant controller are relevant, as the unsteadiness near the zero point is perceivable with high-quality applications.

Pulse-Width Modulation and H-Bridges

With the exception of some telemanipulators, the sources controlling the actuators are always digital processors. As actuators need an analog voltage or current to generate forces and torques, some transformer between digital signals and analog control value is necessary. There are two typical realizations of these transformers:

1. Use of a digital–analog converter (D/A-converter)
2. Use of a ↪ Pulse-Width Modulation (PWM)

The use of D/A-converters as external components or integrated within a microcontroller is not covered further in this book, as it is, if necessary to use, extremely simple. It just requires some additional efforts in circuit layout. The latter results in it being not used much for control of actuators.

With electrodynamic actuators, the method of choice is driver electronics based on PWM (Fig. 9.17a). With the PWM, a digital output of a controller is switched with a high frequency (>10 kHz[12]). The period of the PWM is given by the frequency. The program controls the duty cycle between on- and off-times. Typically, one byte

[12] Typical frequencies lie between 20 and 50 kHz. However, especially within automotive technology for driving LEDs, PWMs for current drivers with frequencies below 1 kHz are in application. Frequencies within this range are not applicable to haptic devices, as the switching in the control

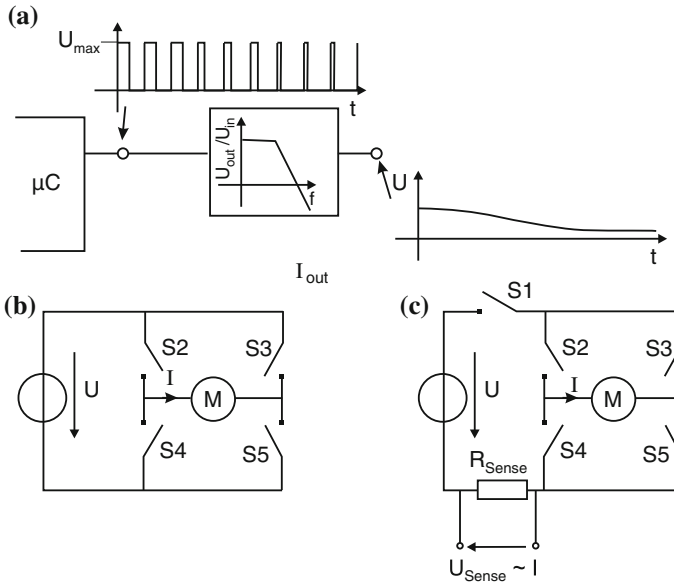

Fig. 9.17 Principle of pulse-width modulation (PWM) at a digital μC-output (**a**), H-bride circuit principle (**b**), and extended H-bridge with PWM (S1) and current measurement at (R_{Sense}) (**c**)

is available to provide a resolution of 256 steps within this period. After filtering the PWM, either via an electrical low-pass or via the mechanical transfer characteristics of an actuator, a smoothed output signal becomes available.

Pulse-width modulation is frequently used in combination with H-bridges (Fig.9.17b). The term H-bridge results from the H-like shape of the motor surrounded by four switches. The H-bridge provides two operation modes for two directions of movement and two operation modes for braking. If according to Fig. 9.17b, the two switches S2 and S5 are on, current I will flow through the motor in positive direction. If instead switches S3 and S4 are switched on, current I will flow through the motor in negative direction. One additional digital signal acting on the H-bridge will change the direction of movement of the motor. This is the typical procedure with switched 1-quadrant controllers. Additional switching states are given by switching the groups S2 and S3, respectively, S4 and S5. Both states result in short circuit of the actuator and stops its movement. Other states like simultaneously switching S2 and S4, respectively, S3 and S5 results in short circuit of the supply voltage, typically destroying the integrated circuit of the driver.

To combine the H-bridge with a PWM, either switch groups S2 and S5 can be switched according to the timing of the PWM, or additional switches S1 (Fig. 9.17c)

---

value may be transmitted by the actuator and will therefore be perceivable especially in static conditions. Typical device designs show mechanical low-pass characteristics even at frequencies in the area of 200 Hz. However, due to the sensitivity of tactile perception in an area of 100–200 Hz, increased attention has to be paid to any switched signal within the transmission chain.

can be placed in series to the H-bridge modulating the supply voltage U. In practical realization, the latter is the preferred design, as the timing of the switches S2 to S5 is critical to prevent likely short circuits in the supply voltage. The effort to perform this timing between the switching is usually higher than the cost of another switch in series. The practical realization of H-bridges is done via field-effect transistors. The discrete design of H-bridges is possible, but not easy. In particular, the timing between switching events, the prevention of short circuits, and the protection of the electronics against induced currents is not trivial. There are numerous integrated circuits available on the market that include appropriate protective circuitry and provide only a minimum of necessary control lines. The ICs L6205 (2A), L293 (2.8A), and VNH 35P30 (30A) are some examples common in test-bed developments. For EC-drives, there are specific ICs performing the timing for the field-effect transistors and reducing the number of necessary PWMs from the microcontroller. The IR213xx series switches three channels with one external half-bridge per channel built from N-MOS transistors with a secure timing for the switching events.

The PWM described above with an H-bridge equals a controlled voltage source. For electrodynamic systems, such a control is frequently sufficient to generate an acceptable haptic perception. Nevertheless, for highly dynamic haptic systems, a counter-induction (Sect. 9.2.1.4) due to movement has to be expected, resulting in a variation in the current within the coils generating an uncontrolled change in the LORENTZ force. Additionally, the power loss within the coils (Sect. 9.2.1.1) may increase the actuator's internal temperature resulting in a change in conductivity in the conductor's material. The increasing resistance with increasing temperatures of the conductor results in less current flow at a constant voltage source. An electrodynamic actuator made of copper as conductive material generates a reduced force when operated. With higher requirements on the quality of haptic output, a controlled current should be considered. In case of a PWM, a resistor with low resistance (R_{Sense} in Fig. 9.17c) has to be integrated, generating a current-proportional voltage U_{Sense}, which itself can be measured with an A/D input of the controller. The control circuit is closed within the microcontroller. However, the A/D-transformation and the closing of the control circuit can be challenging for state-of-the-art electronics with highly dynamic systems with border frequencies of some kilohertz. Therefore, analog circuits should be considered for closed-loop current controls too.

Analog Current Sources

Analog current sources are—to make it simple—controlled resistors within the current path of the actuator. Their resistance is dynamically adjusted to provide the wished current flow. Identical to classical resistors, analog current sources transform the energy that is not used within the actuator into heat. Consequently, in comparison with the switched H-bridges, they are generating a lot of power loss. By use of a discrete current control (Fig. 9.18a), analog current sources for almost any output currents can be built by the choice of one to two field-effect transistor (FET). For heat dissipation, they are required to be attached to adequate cooling elements. There

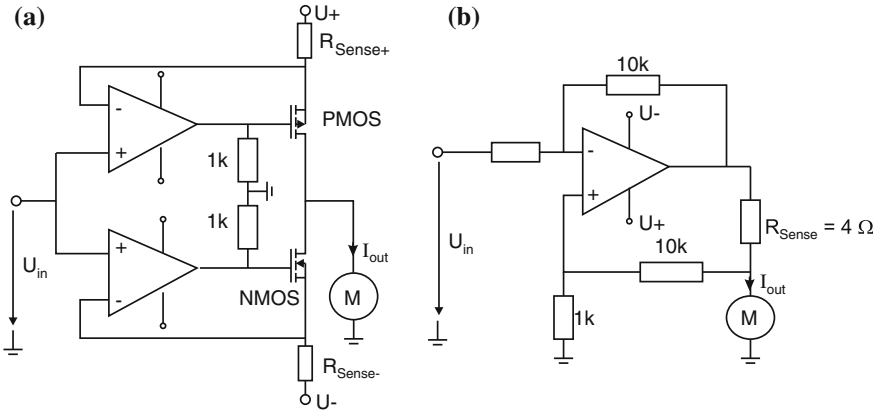

Fig. 9.18 Discrete closed-loop current control [122] (**a**), and closed-loop current control with a power-operational amplifier (**b**)

are only little requirements on the operational amplifiers themselves. They control the FET within its linear range proportional to the current-proportional voltage generated at R_{Sense}. Depending on the quadrant used within operational mode (1 or 3), either the N-MOS transistors or the P-MOS transistor is conductive. An alternative to such discrete designs is the use of power amplifiers (e.g., LM675, Fig. 9.18b). It contains fewer components and is therefore less dangerous to make errors. Realized as non-inverting or inverting operational amplifier with a resistor for measurement R_{Sense}, they can be regarded as a voltage-controlled current source.

9.2.3.2 Monitoring Temperature

Resulting from the low efficiency factor and the high dissipative energy from electrodynamic actuators, it is useful to monitor the temperature nearby the coils. Instead of including a measuring resistor PT100 nearby the coil, another approach monitors the electrical resistance of the windings themselves. Depending on the material of the windings (e.g., cooper, Cu), the conductivity changes proportional to the coil's temperature. With copper, this factor is 0.39 % per Kelvin temperature change. As any driver electronics, either works with a known and controlled voltage or current, measurement of the other component immediately provides all information to calculate resistance and consequently the actual coil temperature.

Fig. 9.19 Electrodynamic tactor by *Audiological Engineering Inc.* with a frequency range from 100 to 800 Hz

9.2.4 Examples for Electrodynamic Actuators in Haptic Devices

Electrodynamic actuators are most frequently used as force and torque sources within kinaesthetic systems. In particular, EC-drives can be found in products of *Quanser*, *ForceDimension*, *Immersion*, and *SensAble/geomagic*. Mechanically commutated electrodynamic actuators are used within less expensive devices, like the GEOMAGIC TOUCH or the NOVINT FALCON. For tactile applications, electrodynamic actuators appear only with linear moving coils or magnets as oscillation sources. The possibility to control frequency and amplitude independently from each other makes them interesting for tactors. Tactors (Fig. 9.19) are small, disk-like actuators that can be integrated in clothes or mobile devices to transmit information via tactile stimulation in small areas of the skin.

9.2.4.1 Cross-Coil System as Rotary Actuator

Besides self-supportive coils, electrodynamic actuators according to the design of cross-coils are one possibility to generate defined torques. Continental VDO developed a haptic rotary actuator device being a central control element for automotive applications (Fig. 9.20). It contains a diametral magnetized NdFeB-magnet. The magnet is surrounded by a magnetic circuit. The field lines reach from the magnet to the magnetic circuit. The coils surround the magnet in an angular phase of 90°, and the electrodynamic active winding section lies in the air-gap between magnetic circuit and magnet. The rotary position control is made via two hall sensors placed in a 90° position. The actuator is able to generate a ripple-free torque of ≈25 m Nm at a geometrical diameter of 50 mm, which is additionally increased by an attached gear to ≈100 m Nm torque output.

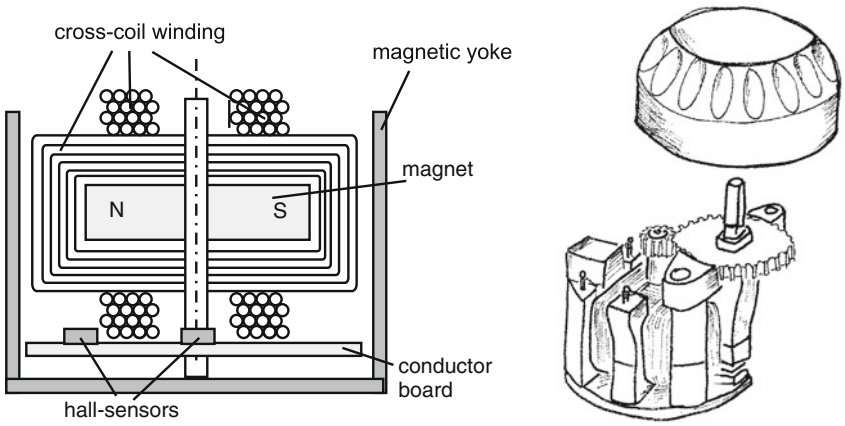

Fig. 9.20 Electrodynamic cross-coil system with moving magnet as haptic rotary actuator

9.2.4.2 Reconfigurable Keypad: HapKeys

The electrodynamic linear actuators building the basis of this device are equipped with friction-type bearings and moving magnets with pole shoes within cylindrically wound fixed coils as shown in Fig. 9.21. The coils have an inner diameter of 5.5 mm and an outer diameter of 8 mm. The magnetic circuit is decoupled from other nearby

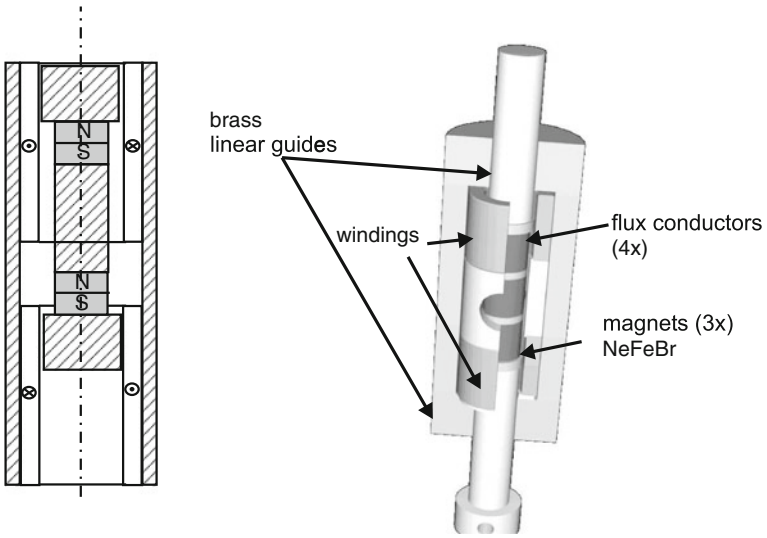

Fig. 9.21 Electrodynamic linear actuator with moving magnet [25]

elements within the actuator array. It is made of a tube with a wall thickness of 0.7 mm of a cobalt–iron alloy with very high saturation flux density. Each actuator is able to generate 1 N in continuous operation mode.

9.2.5 Conclusion About the Design of Electrodynamic Actuators

Electrodynamic actuators are the preferred actuators used for kinaesthetic impedance-controlled haptic devices due to their proportional correlation between the control value "current" and the output values "force" or "torque." The market of DC- and EC-drives offers a wide variety of solutions, making it possible to find a good compromise between haptic quality and price for many applications. Most suppliers of such components offer advice on how to dimension and select a specific model based on the mechanical, electrical, and thermal properties as for example shown in [26].

If there are special requirements to be fulfilled, the design, development, and start of operation of special electrodynamic actuator variants are quite easy. The challenges in thermal and magnetic design are manageable, as long as some basic considerations are not forgotten. The examples of special haptic systems seen in the above section prove this impressively. Just driver electronics applicable to haptic systems and its requirements are still an exceptional component within the catalogs of manufacturers of automation technology. They must either be paid expensively or be built by oneself. Therefore, commercial manufacturers of haptic devices, e.g., *Quanser*, offer their haptic-applicable driver electronics independent of the own systems for sale.

For design of low-impedance haptic systems, currently no alternative to electrodynamic systems is at hand. Other actuation principles that are discussed within this book need a closed-loop control to overcome their inner friction and nonlinear force/torque transmission. This always requires some kind of measurement technology such as additional sensors or the measurement of inner actuator states. The efforts connected with this are still an advantage for electrodynamic actuators, which is gained by a low efficiency factor and as a consequence, the relatively low energy density per actuator volume.

9.3 Piezoelectric Actuators

Stephanie Sindlinger, Marc Matysek

Next to the frequently found electrodynamic actuators, the past few years' piezoelectric actuators were used for a number of device designs. Their dynamic properties in resonance mode especially allow an application for haptics, which is different from the common positioning application they are used for. As variable impedance, a wide spectrum of stiffnesses can be realized. The following chapter gives the

calculation basics for the design of piezoelectric actuators. It describes the design variants and their application in haptic systems. Besides specific designs for tactile and kinaesthetic devices, approaches for the control of the actuators and tools for their dimensioning are presented.

9.3.1 The Piezoelectric Effect

The piezoelectric effect was first discovered by JACQUES and PIERRE CURIE. The term is derived from the Greek word "piedein–piezo" = "to press" [61].

Figure 9.22 shows a scheme of a quartz crystal (chemical: SiO2). With force acting on the crystal mechanical displacements of the charge centers can be observed within the structure, resulting in microscopic dipoles within its elementary cells. All microscopic dipoles sum up to a macroscopic measurable voltage. This effect is called "reciprocal piezoelectric effect." It can be reversed to the "direct piezoelectric effect." If a voltage is applied on a piezoelectric material, a mechanical deformation happens along the crystal's orientation, which is proportional to the field strength in the material [3].

Piezoelectric materials are anisotropic—direction dependent—in their properties. Consequently, the effect depends on the direction of the electrical field applied, and on the angle between the direction of the intended movement and the plane of polarization. For the description of these anisotropic properties, the directions are labeled with indices. The index is defined by a Cartesian space with the axes numbered 1, 2, and 3. The plane of polarization of the piezoelectric material is typically orientated on direction 3. The shear at the axes is labeled with indices 4, 5, and 6.

Among all possible combinations, there are three major effects (Fig. 9.23), commonly used for piezoelectric applications: longitudinal, transversal, and shear effect.

The *longitudinal effect* acts in the same direction as the applied field and the corresponding field strength E_3. As a consequence, the resulting mechanical tensions T_3 and strains S_3 also lie within plane 3. With the *transversal effect*, mechanical

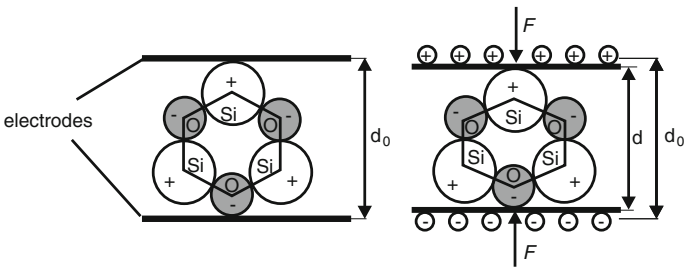

Fig. 9.22 Crystal structure of quartz in initial state and under pressure

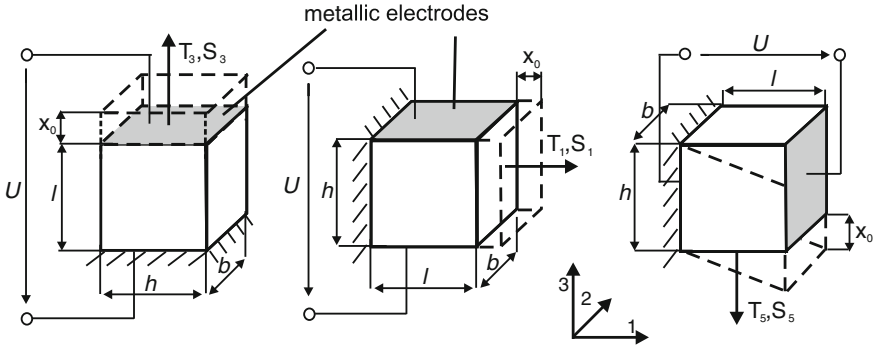

Fig. 9.23 Effects during applied voltage: longitudinal effect (*left*), transversal effect (*center*), shear effect (*right*)

actions show normal to the electrical field. As a result from a voltage U_3 with the electrical field strength E_3, the mechanical tensions T_1 and strains S_1 appear. The *shear effect* happens with electrical voltage U applied along plane 1 orthogonal to the polarization plane. The resulting mechanical tensions appear tangential to the polarization, in the direction of shear, and are labeled with the directional index 5.

9.3.1.1 Basic Piezoelectric Equations

The piezoelectric effect can be described most easily by state equations:

$$P = e \cdot T \tag{9.35}$$

and

$$S = d \cdot E \tag{9.36}$$

with

P = Direction of polarization (in C/m^2)
S = Deformation (non-dimensional)
E = Electrical field strength (in V/m)
T = Mechanical tension (in N/m^2)

The piezoelectric coefficients are

- the piezoelectric coefficient of tension (also: coefficient of force) e (reaction of the mechanical tension on the electrical field)

$$e_{ij,k} = \frac{\partial T_{ij}}{\partial E_k} \partial \tag{9.37}$$

- and the piezoelectric coefficient of strain (also: coefficient of charge) d (reaction of the strain on the electrical field)

$$d_{ij,k} = \frac{\partial \epsilon_{ij}}{\partial E_k} \partial \tag{9.38}$$

The correlation of both piezoelectric coefficients is defined by the elastic constants C_{ijlm}

$$e_{ij,k} = \sum_{lm} \left(C_{ijlm} \cdot d_{lm,k} \right) \tag{9.39}$$

Usually, the tensors shown in the equation above are noted as matrix. In this format, matrices result in six components identical to the defined axes. The matrix shown below describes the concatenation of the dielectrical displacement D, the mechanical strain S, the mechanical tension T, and the electrical field strength E.

	T_1	T_2	T_3	T_4	T_5	T_6	E_1	E_1	E_3
D_1	0	0	0	0	d_{15}	0	ϵ_{11}	0	0
D_2	0	0	0	d_{15}	0	0	0	ϵ_{11}	0
D_3	d_{31}	d_{31}	d_{33}	0	0	0	0	0	ϵ_{11}
S_1	s_{11}	s_{12}	s_{13}	0	0	0	0	0	d_{31}
S_2	s_{12}	s_{11}	s_{13}	0	0	0	0	0	d_{31}
S_3	s_{13}	s_{13}	s_{33}	0	0	0	0	0	d_{33}
S_4	0	0	0	s_{44}	0	0	0	d_{15}	0
S_5	0	0	0	0	s_{44}	0	d_{15}	0	0
S_6	0	0	0	0	0	$2(s_{11} - s_{12})$	0	0	0

This matrix can be simplified for the specific cases of a longitudinal and a transversal actuator. For a longitudinal actuator with electrical contact in direction 3, the following equations are the result:

$$D_3 = \epsilon_{33}^T E_3 + d_{31} T_1 \tag{9.40}$$

$$S_3 = d_{31} E_3 + s_{11}^E T_1. \tag{9.41}$$

Accordingly for a transversal actuator, the correlation

$$D_3 = \epsilon_{33}^T E_3 + d_{33} T_3 \tag{9.42}$$

$$S_3 = d_{33} E_3 + s_{33}^E T_3 \tag{9.43}$$

with becomes valid.

D_3 = dielectric displacement in C/m^2 D = 0: open-ended
E_3 = field strength in V/m E = 0: short cut
S_1, $S_3 = \Delta L/L$ = strains, dimensionless $S = 0$: mech. short cut
T_1, T_3 = mechanical tensions N/m^2 $T = 0$: idle mode
ϵ_{33}^T = relative dielectricity constant at mechanical tension = 0
d_{31}, d_{33} = piezoelectric charge constant in C/N
s_{11}^E, s_{33}^E = elasticity constant at field strength = 0

Therefore, the calculation of piezoelectric coefficients simplifies into some handy equations: The charge constant d can be calculated for the electrical short circuit—which is $E = 0$—to

$$d_{E=0} = \frac{D}{T} \tag{9.44}$$

and for the mechanical idle situation—which is $T = 0$—to

$$d_{T=0} = \frac{S}{E}. \tag{9.45}$$

The piezoelectric tension constant is defined as

$$g = \frac{d}{\epsilon^T}. \tag{9.46}$$

The coupling factor k is given by Eq. (9.47). It is a quantity for the energy transformation and consequently for the strength of the piezoelectric effect. It is used for comparison among different piezoelectric materials. However, note that it is not identical to the efficiency factor, as it does not include any energy losses.

$$k = \frac{\text{converted energy}}{\text{absorbed energy}}. \tag{9.47}$$

A complete description of the piezoelectric effect, a continuative mathematical discussion, and values for piezoelectric constants can be found in the literature, such as [16, 55, 77].

9.3.1.2 Piezoelectric Materials

Till 1944, the piezoelectric effect was observed within monocrystals only. These were quartz, turmalin, lithiumniobat, potassium- and ammonium-hydrogen phosphate (KDP, ADP), and potassium sodium tartrate [3]. With all these materials, the direction of the spontaneous polarization was given by the direction of the crystal lattice [61]. The most frequently used material was quartz.

The development of polarization methods made it possible to retrospectively polarize ceramics by the application of a constant exterior electrical field in 1946. By this approach, "piezoelectric ceramics" (also "piezoceramics") were invented. By this development of polycrystalline materials with piezoelectric properties, the whole group of piezoelectric materials obtained increased attention and technical significance. Today, the most frequently used materials are barium titanate ($BaTiO_3$) or lead zirconate titanate (PZT). C 82 is a piezoelectric ceramic suitable for actuator design due to its high *k-factor*. However, like all piezoelectric ceramic materials, it shows reduced long-term stability compared to quartz. Additionally, it has a pyroelectric effect, which is a charge increase due to temperature changes in the material [77]. Since the 1960s, the semicrystalline synthetic material polyvinylidene fluoride (PVDF) is known. Compared to the materials mentioned before, PVDF excels by its high elasticity and reduced thickness (6–9 µm).

Table 9.4 shows different piezoelectric materials with their specific values.

Looking at these values, PZT is the most suitable for actuator design due to its high coupling factor with large piezoelectric charge modulus and still a high Curie temperature. The Curie temperature represents the temperature at which the piezoelectric properties from the corresponding material are lost permanently. The value of the Curie temperature depends on the material (Table 9.4).

Table 9.4 Selection of piezoelectric materials with characteristic values [77]

Constant	Unit	Quartz	PZT-4	PZT-5a	C 82	PVDF
d_{33}	$\frac{10^{-12}}{\mathrm{m/V}}$	2.3	289	374	540	−27
d_{31}		−2.3	−123	−171	−260	20
e_{33}	$\frac{A \cdot s}{\mathrm{m}^2}$	0.181	15.1	15.8	28.1	108
e_{31}		−0.181	−5.2	−5.4	−15.4	–
s_{33}^E	$\frac{10^{-12}}{\mathrm{m}^2/\mathrm{N}}$	12.78	15.4	18.8	19.2	–
s_{11}^E		12.78	12.3	16.4	16.9	–
c_{33}^E	$\frac{10^{10}}{\mathrm{N/m}^2}$	7.83	6.5	5.3	5.2	–
c_{11}^E		7.83	8.1	6.1	5.9	–
$\frac{\epsilon_{33}^T}{\epsilon_0}$; $\frac{\epsilon_{33}^S}{\epsilon_0}$	–	4.68; 4.68	1,300; 635	1,730; 960	3,400; –	12; 12
$\frac{\epsilon_{11}^T}{\epsilon_0}$; $\frac{\epsilon_{11}^S}{\epsilon_0}$	–	4.52; 4.41	1,475; 730	1,700; 830	3,100; –	–
k_{33}	–	0.1	0.7	0.71	0.72	0.20
k_{31}	–	–	0.33	0.34	0.36	0.15
$\vartheta_{\mathrm{Curie}}$	$\frac{1}{^\circ\mathrm{C}}$	575	328	365	190	80
ρ	$\frac{\mathrm{kg}}{\mathrm{m}^{-3}}$	2,660	7,500	7,500	7,400	1,790

9.3.2 Designs and Properties of Piezoelectric Actuators

Actuators using the piezoelectric effect are members of the group of solid actuators (also: solid-state actuators). The transformation from electrical into mechanical energy happens without any moving parts, resulting in fast reaction time and high dynamics compared to other actuation principles. Additionally, piezoelectric actuators have high durability. The thickness changes are smaller compared to other actuation principles, although the generated forces are higher.

9.3.2.1 Basic Piezoelectric Actuator Designs

Depending on the application, different designs may be used. One may require a large displacement; another one may require self-locking or high stiffness. The most frequently used actuator types are bending actuators and actuator staples. A schematic sketch of each design is given in Fig. 9.24a, c.

Stacked actuator are based on the longitudinal piezoelectric effect. For this purpose, several ceramic layers of opposite polarity are stapled above each other. In between each layer contact, electrodes are located for electrical control. A staple is

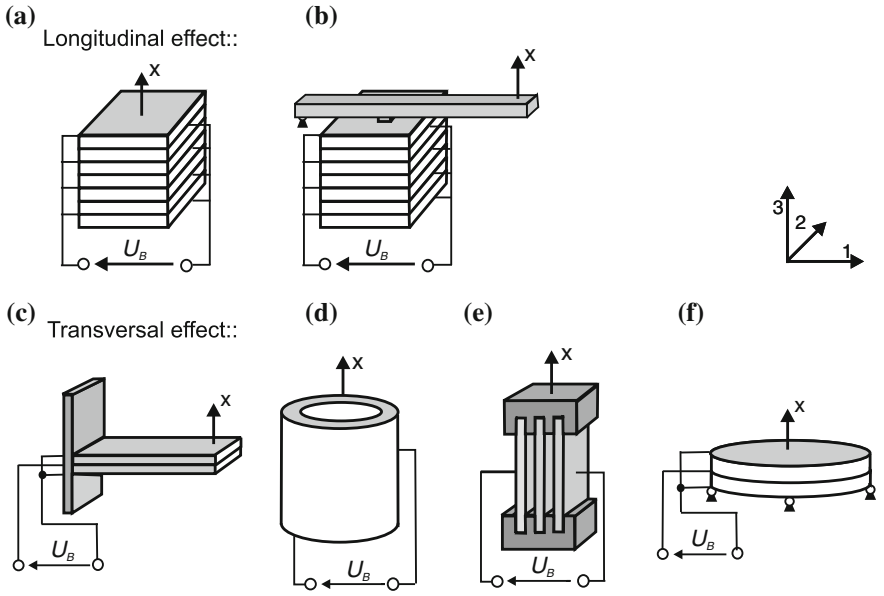

Fig. 9.24 Piezoelectric transducers separated by longitudinal and transversal effect: longitudinal effect: **a** stack, **b** stack with lever transformation, change of length: $x = d_{33} \cdot U_B$ transversal effect: **c** bending actuator, **d** cone, **e** band, **f** bending disk, change of length: $x = -d_{31} \cdot U_B$. Further information can be found in [61]

able to generate high static forces up to several 10 kN. The achievable displacement of 200 µm is low compared to other piezoelectric designs. By use of levers Fig. 9.24, (b) the displacement can be significantly increased (see Fig. 9.24b). Voltages of several 100 V are necessary to drive a piezoelectric actuation staple.

Bending actuators are based on the transversal piezoelectric effect. Designed according to the so-called bimorph principle—with two active layers—they are used in applications requiring large displacements. The transversal effect is characterized by comparably low controlling voltages [3, 61]. These electrical properties and large displacements can be achieved by thin ceramic layers in the direction of the electrical fields, and an appropriate geometrical design. Other geometrical designs using the transversal effect are tubular actuators, film actuators, or bending disks, Fig. 9.24d–f. Due to their geometry, they equal staple actuators in their mechanical and electrical characteristics. The achievable displacements of 50 µm are comparably low, whereas the achievable forces excel bending actuators at several orders of magnitude.

The use of the *shear effect* is uncommon in actuator design. This is somewhat surprising as it shows charge modulus and coupling factor, which is twice as much as the transversal effect. Additionally, it is possible to increase the elongation x_0 in idle mode (displacement without any load) by optimization of the length to thickness (l/h) ratio. However, the clamping force F_k of the actuator is not influenced by these parameters.

Table 9.5 summarizes the properties of different geometrical designs. Typical displacements, actuator forces, and control voltages are shown.

9.3.2.2 Selection of Special Designs for Piezoelectric Actuators

Besides the standard designs shown above, several variations of other geometrical designs exist. In this section, examples of an ultrasonic drive with resonator, oscillatory/traveling waves actuators, and piezoelectric stepper motors are discussed.

Table 9.5 Properties of typical piezoelectric actuator designs based on [61]

Standard designs	Stack	Stack with lever	Bending actuator	Tape actuator	Tubus	Bending disks
Actuator displacements (µm)	20–200	≤1.000	≤1.000	≤50	≤50	≤500
Actuating forces (N)	≤30.000	≤3.500	≤5	≤1000	≤1000	≤40
Control voltages (V)	60–200 200–500 500–1000	60–200 200–500 500–1000	10–400	60–500	120–1000	10–500

Ultrasonic actuators are differentiated according to resonators with bar-like geometry and rotatory ring geometry.

Ultrasonic Actuators with Circular Resonators

As mentioned before, besides actuators providing standing waves, another group of actuators based on traveling waves exists. The traveling wave actuators known best are circular in their design. The first actuator according to this principle was built in 1973 by SASHIDA [125]. Traveling waves actuators count to the group of ultrasonic actuators as their control frequencies typically lie between 20 and 100 kHz.

This section is reduced to the presentation of ring-shaped traveling wave actuators with a bending wave. Other design variants for linear traveling wave actuators can be found in the corresponding literature [29, 46, 47].

Figure 9.25 shows an actuator's stator made of piezoelectric elements. They have an alternating polarization all around the ring. The stator itself carries notches actually enabling the formation of the rotating traveling wave.

Each point on the surface of the stator performs a local elliptic movement (trajectory). This movement is sketched schematically in Fig. 9.25. These individual elliptic movements overlie to a continuous wave on the stator. With frictional coupling, this movement is transferred on the rotor, resulting in a rotation. The contact between stator exists with the same number of contact points anytime during operation.

The movement equation of the traveling wave actuator is given by

$$u(x,t) = A\cos(kx - \omega t) \tag{9.48}$$

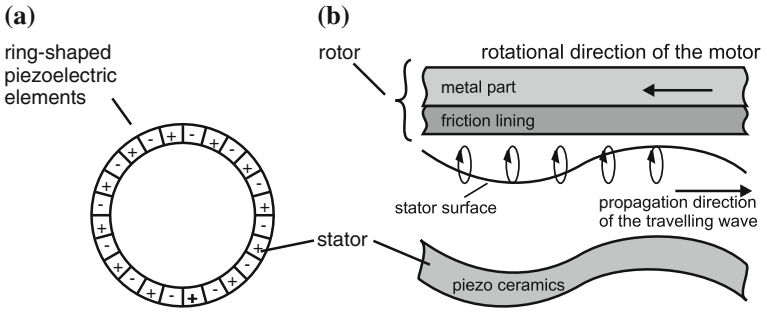

Fig. 9.25 Piezoelectric traveling wave motor: **a** stator disk with piezoelectric elements. **b** schematic view of the functionality of a ring-shaped piezoelectric traveling wave motor [61]

By reshaping it, the following form results in

$$u(x,t) = A(\cos(kx))(\cos(wt)) + A(cos(kx - \pi/2))(cos(kx + \pi/2)) \quad (9.49)$$

The second term of Eq. (9.49) includes important information for the control of traveling wave actuators. A traveling wave can be generated by two standing waves being spatially and timely different. Within typical realization, the spatial difference of $x_0 = \lambda/4$ is chosen, and a time phase lag of $\Phi_0 = \pi/2$. The use of two standing waves is the only practical possibility for generating a traveling wave. The direction of rotor movement can be switched by changing the phase lag from $+\pi/2$ to $-\pi/2$ [43, 49, 50, 125].

Figure 9.26 shows the practical realization of a traveling wave motor. The advantages of a traveling wave motor are the high torques possible to achieve at low rotational speeds. It has low overall size and is of little weight. This enables a thin design as shown in Fig. 9.26 . In passive mode, the traveling mode motor has high locking torque of several Nm.

Other advantages are given by the good control capabilities, high dynamics, and robustness against electromagnetic noise such as the silent movement [65]. Typical applications of traveling wave actuators are autofocus functions in cameras.

Piezoelectric Stepper Motors

Another interesting design can be found with the actuator PI Nexline. It combines the longitudinal effect with the piezoelectric shear effect, resulting in a piezoelectric stepper motor.

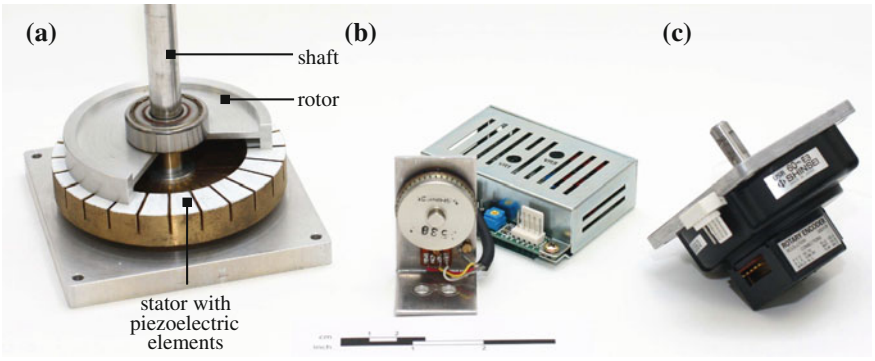

Fig. 9.26 Realization of a traveling wave motor. **a** cross-sectional model with functional parts, **b** motor model USR30 with a maximum speed of 300 rpm and a nominal torque of 0.05 Nm with driver D6030, **c** model USR60 with attached rotary encoder, maximum speed of 150 rpm and a nominal torque of 0.05 Nm. Scale shown is cm (*top*) and inch (*bottom*), valid for all parts of the figure. All examples by *Shinsei Corporation*, Tokyo, JP

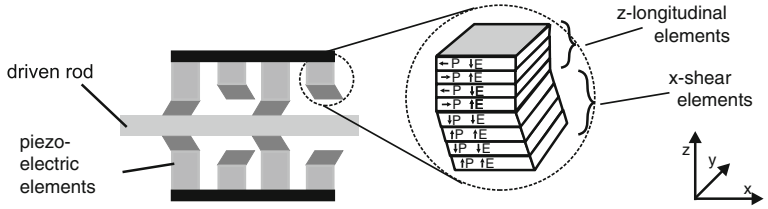

Fig. 9.27 Piezoelectric stepper motor using the shear effect and the longitudinal effect [101]

The principal design is sketched in Fig. 9.27. The movement of the motor is similar to the inchworm principle. Drive and release phases of the piezoelectric elements produce a linear movement of the driven rod. The piezoelectric longitudinal elements generate the clamping force in z-direction, the shear elements rotated by 90° a translational movement in y-direction is also possible.

The advantage of this design is given by the high positioning resolution. Over the whole displacement of 20 mm, a resolution of 0.5 nm can be achieved. The stepping frequency is given by—dependent on the control—up to 100 Hz and enables, depending on its maximum step-width, velocities of up to 1 mm/s. The step-width can be chosen continuously between 5 nm and 8 µm. The intended position can be achieved either closed loop or open loop controlled. For closed-loop control, a linear encoder has to be added to the motor. In open-loop control, the resolution can be increased to 0.03 nm in a high-resolution dithering mode.

The actuator can generate push and pull forces of 400 N maximum. The self-locking reaches up to 600 N. The typical driving voltage is 250 V. The specifications given above are based on the actuator N-215.00 Nexline® of the company *Physik Instrumente* (*PI*) *GmbH & Co. KG*, Karlsruhe, Germany [101]. Besides the impressive forces and positioning resolutions that can be achieved, these actuators have high durability compared to other designs of piezoelectric actuators, as no friction happens between moving parts and stator.

Olsson et al. presented a haptic glove to display stiffness properties based on such an actuator as shown in Fig. 9.28 [96].

9.3.3 Design of Piezoelectric Actuators for Haptic Systems

Within the preceding section, the basic designs of piezoelectric actuators have been discussed and special variants were shown. This section transfers this knowledge about the design of piezoelectric actuators focusing on haptic applications now.

First of all, the principal approach for designing is sketched. Hints are given about designs appropriate for such applications. Later, three tools for practical engineering are shown: description via electromechanic networks, analytical formulations, and finite-element simulations.

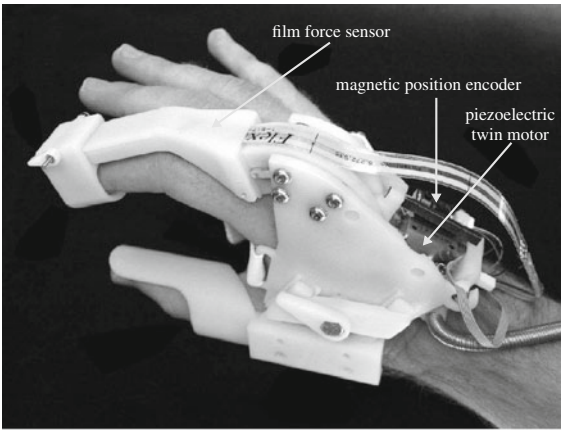

Fig. 9.28 Hand exoskeleton for the display of stiffness parameters. Forces exerted by the user are recorded with thin force sensors and the actuator position is tracked magnetically. Figure taken from [96]

9.3.4 Procedure for the Design of Piezoelectric Actuators

Figure 9.29 gives the general procedure for the design of piezoelectric actuators.

The choice of a general design based on those shown in the previous section is largely dependent on the intended application. For further orientation, Fig. 9.30 shows a decision tree for classifying the own application.

The following section describes the appropriate designs for specific application classes according to this scheme. The list has to be regarded as a point for orientation, but it does not claim to be complete. The creativity of an engineer will be able to find and realize other and innovative solutions besides those mentioned here.

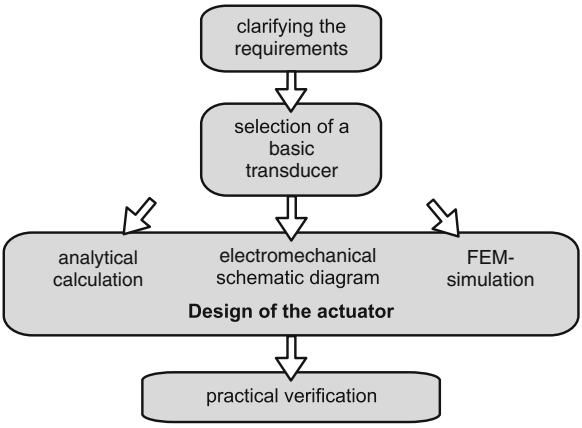

Fig. 9.29 Procedure of designing piezoelectric actuators

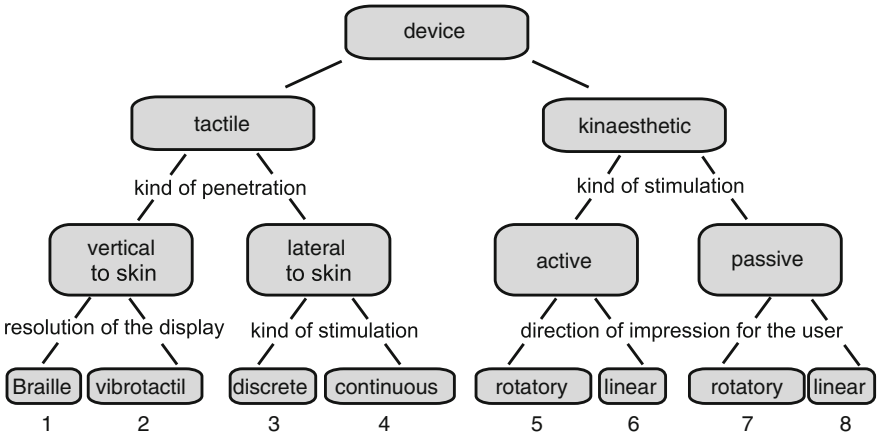

Fig. 9.30 Decision tree for the selection of a type of piezoelectric actuator

Nevertheless, especially for the design of tactile devices, some basic advice can be given based on the classification in Fig. 9.30:

1. Braille displays have to act against the finger's force. At typical resolutions, this requires forces in the area of mN at displacement of around 100 µm. The requirements on the dynamics are in the lower range of several Hertz. The smallest resolution of a pixel has to be in the area of $1 \times 1\,\text{mm}^2$ and is defined by the lowest resolution at the finger's tip. Looking at the force–amplitude diagram of Fig. 9.31 bending actuators fit well to these requirements.
2. In comparison with Braille displays, there are vibrotactile displays, which need higher frequencies and smaller displacements and forces to present a static shape to the user. With the diagram in Fig. 9.31, especially bending disk or staple actuators would be appropriate to fulfill these requirements, although these are overpowered concerning the achievable forces.

3, 4 Such displays are subject to current research and are not yet applied in broad range. Their design is typically based on bending actuators, as shear on the

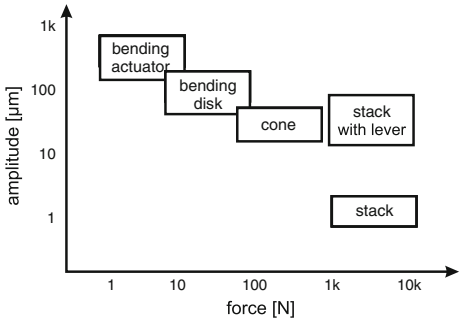

Fig. 9.31 Force–amplitude diagram for classification of the piezoelectric actuating types

skin requires less force than forces acting normal to the skin by generating a comparable perception.

5–8 In contrast to tactile displays, the actuator selection for kinaesthetic systems is more dependent on the actual application. Forces, displacement, and degrees of freedom influenced by the kinematics alter in wide ranges. Additionally, the actuator's volume may be a criterion for selection. Figure 9.31 gives an overview of piezoelectric actuation principles and has to be interpreted based on the specific kinaesthetic problem at hand. Generally speaking, ultrasonic piezoelectric actuators are usually a matter of choice for kinaesthetic devices, although they have to be combined with a closed-loop admittance control.

Figure 9.31 gives an overview of piezoelectric actuation principles and has to be interpreted according to the specific kinaesthetic problem at hand. Generally speaking, ultrasonic piezoelectric actuators are usually a matter of choice for kinaesthetic devices, although they have to be combined with a closed-loop admittance control.

Additional reference for actuator selection found in Sect. 9.3.2 are suitable for haptic applications, but still need some care in their use due to high voltages applied and their sensitivity on mechanical damage. This effort is often rewarded by piezoelectric actuation principles, which can be combined to completely new actuators. The only thing required is the creativity of the engineer.

After choosing the general actuator, the design process follows. For this purpose, three different methods are available, which are presented in the following and discussed with their pros and cons. In addition, some hints on further references are given.

9.3.4.1 Methods and Tools for the Design Process

There are three different engineering tools for the design of piezoelectric actuators:

- Description via the aid of electromechanical concentrated networks
- Analytical descriptions
- Finite-element simulations

Description via the Aid of Electromechanical Concentrated Networks

The piezoelectric basic equations from Sect. 9.3.1.1 are the basis for the formulation of the electromechanic equivalent circuit of a piezoelectric converter.

The piezoelectric actuator can be visualized as an electromechanical circuit. Figure 9.32 shows the converter with a gyratory coupling (a), alternatively a transformatory coupling (b) is also possible. For gyratory coupling, Eqs. (9.50)–(9.53) summarize the correlations for calculation of values for the concentrated elements. They are derived from the constants e, c, ϵ such as the actuator's dimensions l and A [77].

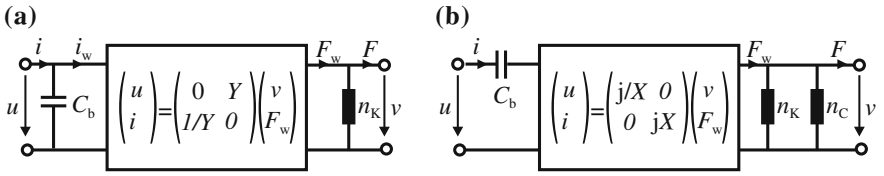

Fig. 9.32 Piezoelectric actuator as a electromechanical schematic diagram **a** gyratory and **b** transformatory combination [77]

$$C_b = \epsilon \cdot \frac{A}{l} = (\epsilon - d^2 \cdot c)\frac{A}{l} \quad \text{with} \quad v = 0 \tag{9.50}$$

$$n_K = \frac{1}{C} \cdot \frac{l}{A} = s \cdot \frac{A}{l} \qquad \text{with} \quad U = 0 \tag{9.51}$$

$$Y = \frac{1}{e} \cdot \frac{l}{A} = \frac{s}{d} \cdot \frac{l}{A} \tag{9.52}$$

$$k^2 = \frac{e^2}{\epsilon \cdot c} = \frac{d^2}{\epsilon \cdot c} \tag{9.53}$$

With the piezoelectric force constants

$$e = d \cdot c = \frac{d}{s} \tag{9.54}$$

This makes for the transformatory coupling

$$X = \frac{1}{\omega C_b \cdot Y} \quad \text{and} \quad n_C = Y^2 \cdot C_b \tag{9.55}$$

Figure 9.33 shows the sketch of an element Δx taken out of a piezoelectric bimorph bending actuator (dimensions $\Delta l \times \Delta h \times \Delta b$) as a electromechanical equivalent circuit.

It is:

$$C_b = 4\epsilon_{33}^T \left(1 - k_L^2\right) \frac{b \cdot \Delta x}{h}$$

$$\Delta n_{RK} \approx 12\, s_{11}^E \frac{(\Delta x)^3}{b \cdot h^3}$$

$$\frac{1}{Y} = \frac{1}{2} \frac{d_{31}}{s_{11}^E} \frac{b \cdot h}{\Delta x}$$

The piezoelectric lossless converter couples the electrical with the mechanical rotatory coordinates first, which are torque M and angular velocity Ω. To calculate the force F and the velocity v, additional transformatory coupling between rotatory and translatory mechanical network has to be introduced. As a result, the complete description of a subelement Δx of a bimorph is given in a ten-pole equivalent circuit.

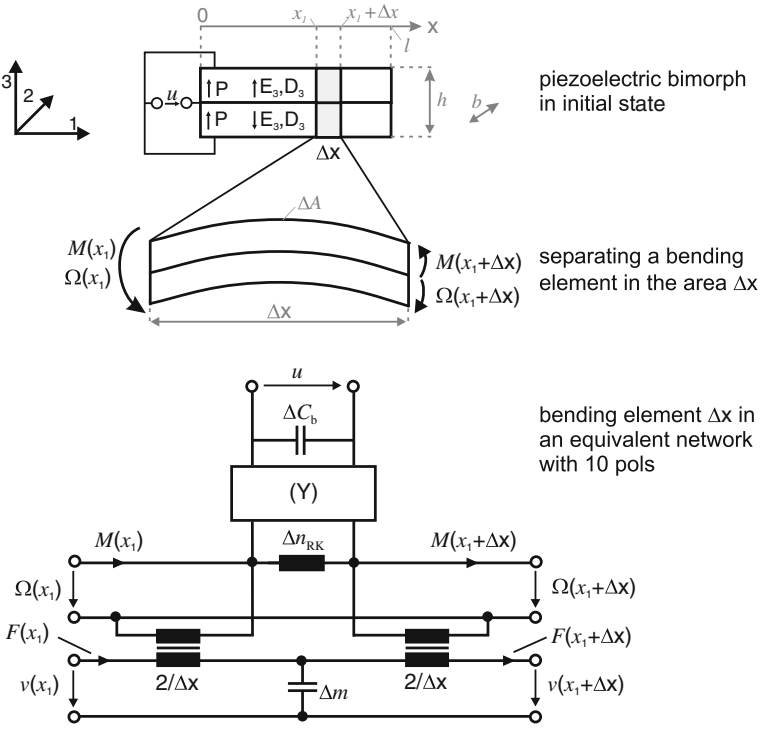

Fig. 9.33 Piezoelectric bimorph bending element in a electromechanical schematic view in quasi-static state [77]

Analytical Calculations

A first approach for the design of piezoelectric actuators is given by the application of analytical equations. The advantage of analytical equations lies in the descriptive visualization of physical interdependencies. The influence of different parameters on a target value can be derived directly from the equations. This enables high flexibility in the variation of dimensions and material properties. Additionally, the processing power for the solution of equations can—compared to simulations—be neglected.

A disadvantage of analytical solution results from the fact that they can only be applied to simple and frequently only symmetrical geometrical designs. Although already limited to such designs, even simple geometries may result in complex mathematical descriptions requiring a large theoretical background for their solution.

The following gives the relevant literature for familiarization with specific analytical challenges faced with during the design of piezoelectric actuators:

- Compelling and complete works on the design of piezoelectric actuators are [124–127].
- The theory of the piezoelectric effect and piezoelectric elements are discussed in [16, 55, 56].

- The mathematical description of traveling wave actuators can be found in [108, 141].
- The contact behavior between stator and rotor with piezoelectric multilayer bending actuators is analyzed in [42, 118, 133, 142].
- In the static and dynamic behavior of multilayer beam bending actuators is described.
- The description of the mechanical oscillations for resonance shapes is discussed in [8, 27, 30, 112, 114, 135] elaborately.

Finite-Element Simulation

The application of both approaches given before is limited to some limited geometrical designs. In reality, complex geometrical structures are much more frequent that cannot be solved with analytical solutions or mechanical networks. Such structures can be analyzed according to the method of finite-element simulation (FEM).

For design of piezoelectric actuators, the use of coupled systems is relevant. One example of a FEM simulation for a piezoelectric traveling wave motor is shown in Fig. 9.34.

9.3.5 Piezoelectric Actuators in Haptic Systems

Piezoelectric actuators are among the most frequently used actuation principles in haptic systems. The designs shown before can be optimized and adapted for a reasonable number of applications. One of the most important reasons for their use is their effectiveness at a very small required space, which is identical to a high power density. To classify the realized haptic systems, a division into tactile and kinaesthetic is done for the following sections.

9.3.5.1 Piezoelectric Actuators for Tactile Systems

For design of tactile systems, the application area is of major importance. The bandwidth ranges from macroscopic table-top devices, which may be used for embossed printings in Braille being placed below a PC keyboard, up to highly integrated sys-

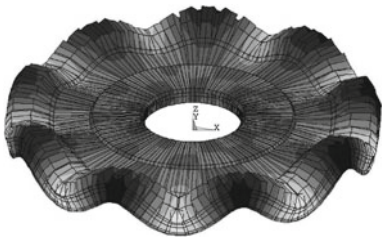

Fig. 9.34 Example FEM simulation of the oscillation shape of the stator of a piezoelectric traveling wave motor (view highly exaggerated)

tems, which may be used for mobile applications. In particular for the latter use, the requirements on volume, reliable, and silent operation, but also on low weight and energy consumption are enormous. The following examples are structured into two subgroups. Each of them addresses one of two directions of the penetration of the skin: lateral and normal.

Tactile Displays with Normal Stimulation

Braille Devices

A Braille character is encoded by a dot pattern formed by embossed points on a flat surface. By touching this pattern made of eight dots (two columns with four rows of dots each), combinations of up to 256 characters can be addressed. Since the 1970s reading tablets for visually handicapped people have been developed who are capable to present these characters with a 2×4 matrix of pins. The most important technical requirements are a maximum stroke of $0.1-1$ mm and a counter-force of 200 mN. Early in this development, electromagnetic drives have been replaced by piezoelectric bimorph bending actuators. These actuators enable a thinner design, are more silent during operation, and are faster. At typical operating voltages of $\pm 100-200$ V and at nominal current of 300 mA, they additionally need less energy than the electromagnetic actuators used before. Figure 9.35 shows the typical design of a Braille character driven by a piezoelectric bimorph actuator. A disadvantage of this system is the high price, as for 40 characters with eight elements each, altogether 320 bending actuators are needed. Additionally, they still require a large volume as the bending elements have to show a length of several centimeters to provide the required displacements. This group of tactile devices is part of the shape-building devices. The statically deflected pins enable the user to detect the displayed symbol.

In the HYPERBRAILLE project, a two-dimensional graphics-enabled display for blind computer users based on piezoelectric bending actuators is realized. The pin matrix of the portable tablet display consists of 60 rows with 120 pins each to present objects such as text blocks, tables, menus, geometric drawings, and other elements of a graphical user interface. The array is an assembly of modules that integrate 10

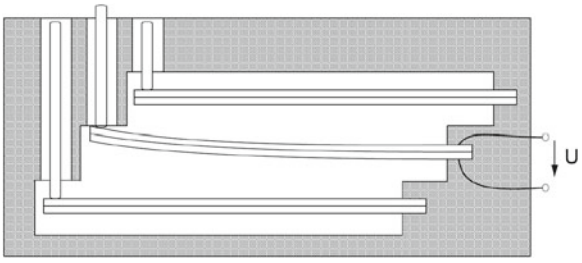

Fig. 9.35 Schematic setup of a Braille row with piezoelectric bending actuators

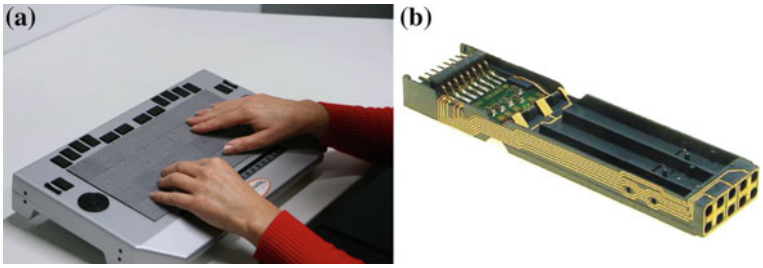

Fig. 9.36 HyperBraille display: whole device (**a**) [54], and single actuator module (**b**) [87]. Pictures courtesy of *metec AG*, Stuttgart, Germany

pins, spaced at intervals of 2.5 mm as shown in Fig. 9.36. The benders raise the pins above the plate by 0.7 mm [130].

Vibrotactile Devices

With vibrotactile devices, the user does not detect the displacement of the skin's surface but the skin itself is put into oscillations. At smaller amplitude, the sensation is similar to the static elongation. The general design of vibrotactile displays equals an extension of the Braille character to an $N \times N$ matrix, which is actuated dynamically. The tactile image generated is not perceived by the penetration depth but by the amplitude of the oscillation [58]. Another impact factor is the oscillation frequency, as the tactile perception depends extremely on the frequency. With the knowledge of these inter-dependencies, optimized tactile displays can be built generating a well-perceivable stimulation of the receptors. Important for displays according to this approach is a large surface, as movements performed by the own finger disturb the perception of the patterns.

The TEXTURE EXPLORER presented in [57] is designed as a vibrating 2×5 pin array. It is used for research on the perception of tactile stimulation, such as the overlay of tactile stimulation with force feedback. The surfaces displayed change according to their geometry and roughness within the technical limits of the device. The contact pins have a size of $0.5 \times 0.5\,\text{mm}^2$ with a point-to-point distance of 3 mm. Each pin is actuated separately by a bimorph bending actuator at a driving voltage of 100 V and a frequency of 250 Hz. The maximum displacement of these pins with respect to surface level is 22 µm and can be resolved down to 1 µm resolution.

An even more elaborate system is based on 100 individually controlled pins [116]. It can be actuated dynamically in a frequency range of 20−400 Hz. Figure 9.37 shows a schematic sketch. Twenty piezoelectric bimorph bending actuators (PZT-5H, *Morgan Matrinic, Inc.*) in five different layers one above the other are located in a circuit around the stimulation area. Each bending actuator carries one stimulation pin, which is placed 1 mm above the surface in idle state. The pins have a diameter of 0.6 mm and are located equally spaced at 1 mm distance. At a maximum voltage of $\pm$ 85 V, a displacement of $\pm$ 50 µm is achieved. A circuit of equally high passive pins is located around the touch area to mark the borders of the active display.

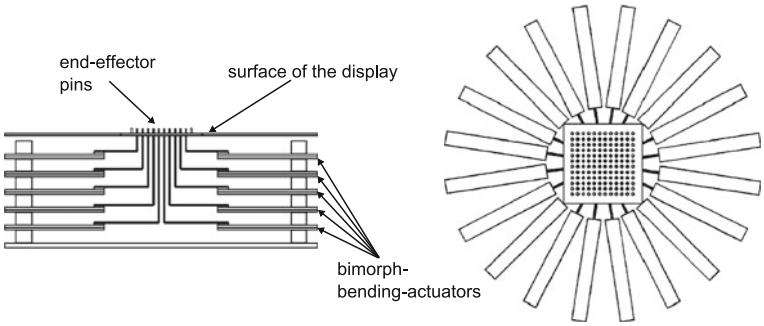

Fig. 9.37 Schematic setup of the 100 pin array [116]

Another even more compelling system can be found in [75] (Fig. 9.38). The very compact 5 × 6 array is able to provide static and dynamic frequencies of up to 500 Hz. Once again, piezoelectric bending actuators are used to achieve a displacement of 700 µm. However, the locking force is quite low with a maximum of 60 mN.

Ubi-Pen

The "Ubi-Pen" is one of the highest integrated tactile systems. Inside of a pen, both components, a spinning disk motor and a tactile display, are assembled. The design of the tactile display is based on the "TULA35" ultrasonic linear drive (*Piezoelectric Technology Co.*, Seoul, South Korea). A schematic sketch of the design is given in Fig. 9.39. The actuator is made of a driving component, a rod, and the moving part. The two piezoelectric ceramic disks are set to oscillation resulting in the rod oscillating upwards and downwards. The resulting movement is elliptical. To move upwards, the following procedure is applied: in the faster downward movement, the inertial force is excelled by the speed of the operation and the element remains in the upper position. Whereas in the upwards movement, the speed is controlled slow enough to carry the moving part up by the frictional coupling between moving

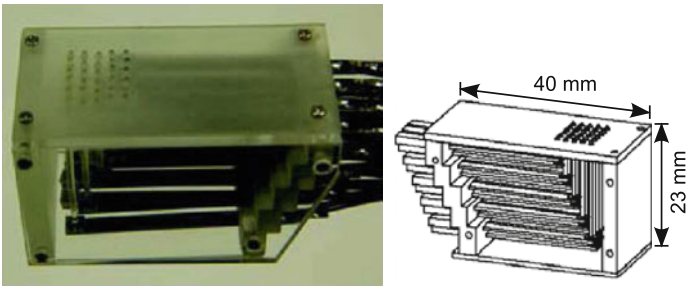

Fig. 9.38 Schematic setup of the 5 × 6 pin array [75]

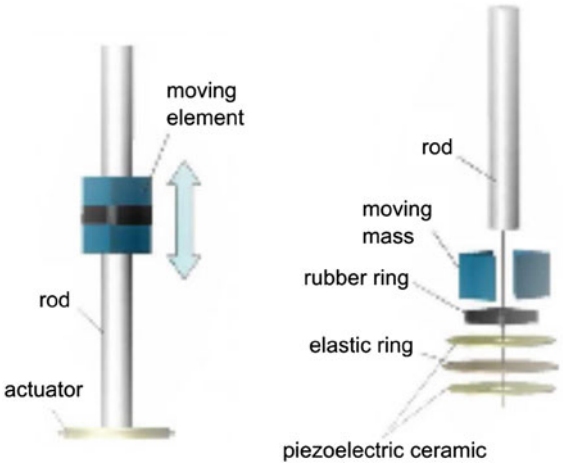

Fig. 9.39 Schematic setup of the ultrasonic motor "TULA35" [74]

element and central rod. The actuator disks have a diameter of 4 mm and height of 0.5 mm. The rod has a length of 15 mm and a diameter of 1 mm. It can be used as contact pin directly. The actuator's blocking force is larger than 200 mN and at a control frequency of 45 kHz velocities of 20 mm/s can be reached.

Figure 9.40 shows the design of a 3 x 3 pin array. In particular, the very small size of the design is remarkable: All outer dimensions have a length of 12 mm. The pins are distributed in a matrix of 3 mm. On the area of 1.44 cm^2, nine separate drives are located. To achieve such a high actuator density, the lengths of the rods have to be different, allowing the moving parts to be placed directly next to each other. If this unit is placed at the upper border of the display, all pins move in, respectively, out of the plane. The weight of the whole unit is 2.5 g. When the maximum displacement of 1 mm is used, a bandwidth of up to 20 Hz can be achieved.

The integration in a pen including another vibratory motor at its tip is shown in Fig. 9.41. This additional drive is used to simulate the contact of the pen with a surface. The whole pen weighs 15 g.

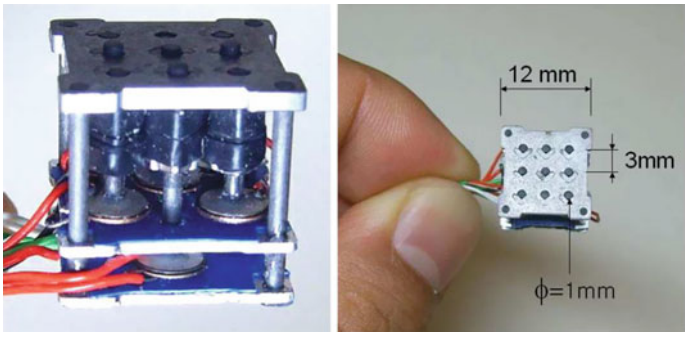

Fig. 9.40 Tactile 3 × 3 pin array [75]

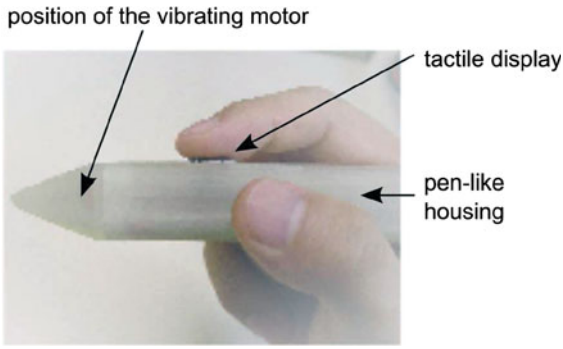

Fig. 9.41 Prototype of the "Ubi-Pen" [74]

The Ubi-Pen provides surface structures such as roughness and barriers or other extreme bumpy surfaces. To realize this, vibrations of the pins are superimposed with the vibratory motor. If the pen is in contact with a touch-sensitive surface (touch panel), the shown graphical image may be displayed in its grayscale values by the pins of the tactile display. The system has been used for a number of tests for recognition of information displayed in different tactile modalities [73]. The results are good with a mean recognition rate of 80 % with untrained users.

Tactile Displays with Lateral Stimulation

Discrete Stimulation

The concept of discrete stimulation is based on an excitation lateral to the skin's surface ("laterotactile display") [45]. Figure 9.42a shows the schematic sketch of a one-dimensional array of actuators. An activation of a piezoelectric element results in its elongation and a deformation of the passive contact comb (crown). If the skin of a touching finger is stretched by this movement, a contact point is perceived. Part (b) of Fig. 9.42 shows a two-dimensional display on the right. With the extension from 1D to 2D array, it is necessary to consider the more complex movement patterns resulting from it. A deeper analysis of the capabilities of such a system and the application for the exploration of larger areas can be found in [79, 134], proving the applicability of a laterotactile display as a virtual 6-point Braille device and to render surface properties. Further tests prove the generated tactile impression very realistic, it can hardly be distinguished from a moving pin below the finger surface.

Continuous Stimulation

The transfer from the discrete points to a piezoelectric traveling wave drive is shown in [12]. The touching finger faces a closed and continuous surface. Due to this design, the tactile display itself becomes less sensitive in its performance to movements of the finger. With the contact surface beyond the skin being excited as a standing wave, the user perceives a surface texture. With relative movement between wave and finger

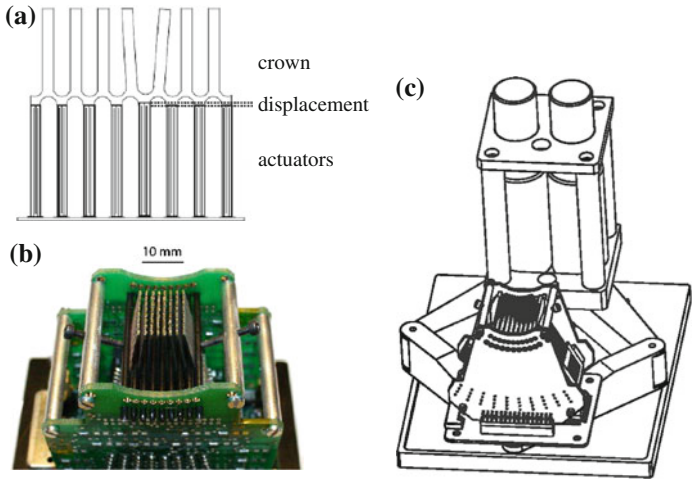

Fig. 9.42 **a** 1D array of the "laterotactile display" [45]. **b** 2D STReSS^2 display [79], **c** integration of an optimized version of the 2D display mounted on a Pantograph haptic device to simulate texture on large surfaces [134]

even a roughness can be perceived. By modifying the shape of the traveling wave, a simulation of a touch force perceivable by the moving finger can be achieved. Figure 9.43 shows the schematic sketch of the contact between finger and traveling wave, such as the corresponding movement direction.

In a test-bed application [12], the stator of a traveling actuator USR60 from *Shinsei* has been used. This actuator provides a typical exploration speed by its tangential wave speed of 15 cm/s and forces up to ≈2 N. This system enables to generate continuous and braking impressions by the change of wave shapes. An additional modulation of the ultrasonic signals with low frequency periodical signal generates the sensation of surface roughness. Actual research is performed on the design of linear ultrasonic traveling wave displays.

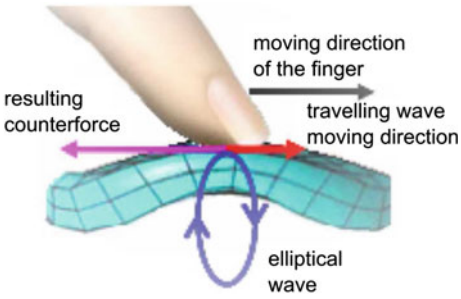

Fig. 9.43 Contact area of finger and traveling wave [12]

9.3.5.2 Piezoelectric Actuators for Kinaesthetic Systems

Piezoelectric actuators used in kinaesthetic systems are usually part of active systems (in a control-engineering sense). The user interacts with forces and torques generated by the actuator. A classic example is a rotational knob actuated by a traveling wave motor. With passive systems, the actuator is used as a switching element, which is able to consume power from an actuator or user in either time-discrete or continuous operation. Examples are breaks and clutches.

Active Kinaesthetic Systems

Piezoelectric traveling wave actuators show a high torque to mass ratio compared to other electrical actuation principles. They are predestined for use in applications with high torque at small rotational velocity, as they do not need additional bearing or other transmission ratios. Kinaesthetic systems require exactly these properties. A very simple design can be used to build a haptic knob: A rotationally mounted plate with a handle attached for the user is pressed on the stator of a traveling wave piezoelectric motor. A schematic sketch of the critical part is shown in Fig. 9.25. Due to the properties specific to the traveling wave motor, the rotational speed of the rotor can be adjusted easily by increasing the wave's amplitude w at the stator. As this actuation principle is based on a mechanical resonance mode, it is actuated and controlled with frequencies nearby its resonance. Coincidentally, this is the most challenging part of the design, as the piezoelectric components show nonlinear behavior at the mechanical stator–rotor interface. Hence, the procedures for its control and electronics have a large influence on its performance.

Figure 9.44 shows the speed versus torque characteristics for different wave amplitudes *w* of the actuator [39]. The torque is highly dependent on the actual rotational speed and amplitude. By monitoring the speed and controlling the phase and wave amplitude, the system can be closed-loop controlled to a linear torque–displacement

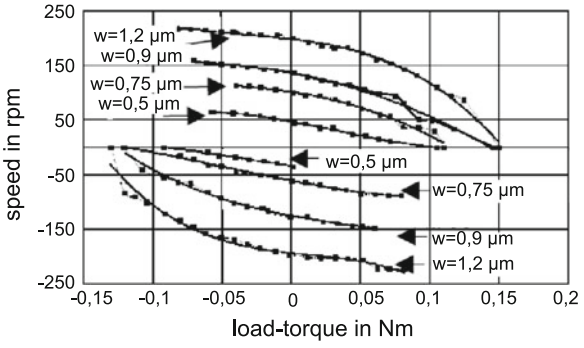

Fig. 9.44 Speed/load torque characteristics for different wave amplitudes. Figure taken from [39]

characteristic. In this mode, a maximum torque of about 120 mNm can be achieved with this example. A deeper discussion of the phase control for a piezoelectric traveling wave motor according to this example is given in [38]. A specialized design of such a device is used in neurological research for application with magneto-resonance tomography [31]. For closed-loop control, the admittance of the device the torque has to be measured. In the specific application, near a large magnetic field, glass fibers are used, measuring the reflection at a bending polymer body. Preventing disturbance from the device on the switching gradients of MRI and vice versa, the device is designed from specific non-conductive materials. It was based on a traveling wave motor in a special MR-compatible version of the "URS60" from *Shinsei*.

Hybrid Systems

Another class of kinaesthetic systems are so-called hybrid systems. If there is need for generating a wide bandwidth of forces and elongations with a single device, there is no actuator fulfilling all requirements alone. Due to this reason, several hybrid systems are designed with two (or more) components complementing each other. A typical example is the combination of a dynamic drive with a brake; the latter is used to provide large blocking torques. As seen in the above section, the closed-loop control of a traveling wave motor's impedance is a challenging task. A simple approach to avoid this problem is the combination of a traveling wave actuator with a clutch. The main difference between a traveling wave actuator and other types of actuators is given by its property to rotate with a load-independent velocity. Providing a certain torque, this system is accompanied with a clutch. Other designs add a differential gear or a break. Such a system is presented in [21]. If the system experiences a mechanical load, the operation of the break is sufficient to increase friction or even block the system completely. Consequently, the system provides the whole dynamic range of the traveling motor in active operation, whereas passive operation is improved significantly by the break. Due to the simple mechanical design and the reduction of energy consumption, such systems are suitable for mobile applications as well.

Passive Kinaesthetic Systems

Objects can be levitated by standing acoustic waves. To achieve this, an ultrasonic source has to provide a standing wave first. Within the pressure nodes of the wave, a potential builds up, attracting a body placed nearby the node. The size of the object is important for the effect to take place, as with a large size, the influence on the next node may be too high. A system based on this principle is described in [72]. It shows the design of an exoskeleton in the form of a glove with external mechanical guides and joints. The joints are made of piezoelectric clutches with a schematic design shown in Fig. 9.45. In their original state, both disks are pressed together by an external spring generating a holding torque. With the vibrator being actuated, the levitation mode is achieved between rotor and stator creating a gap h. This reduces the friction drastically allowing to make both disks almost free of each other.

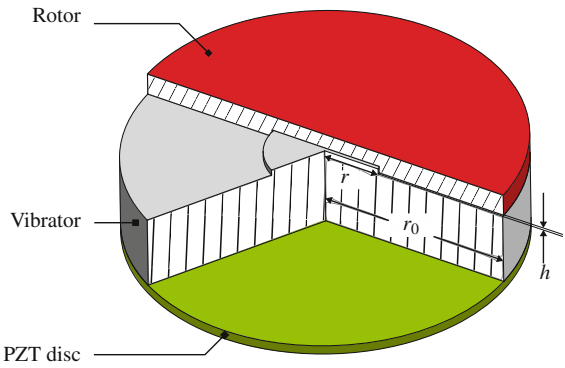

Fig. 9.45 Schematic setup of the "levitation clutch" presented in [72]

9.3.5.3 Summary

Tactile systems are distinguished according to their direction of movement. With a normal movement into the direction of the skin, additional differences are made between passive systems simulating a more or less static surface by their pins, and active systems—so-called vibrotactile systems—providing information by a dynamic excitement of the skin's surface. The user integrates this information into a static perception. The advantages of this approach are given by the reduced requirements on the necessary force and displacements, as the dynamical perception of oscillations is higher than the perception of static slow-changing movements. When the display is not fixed to the finger, however, its fast movements will be a problem. With a static display in a fixed frame the user is able to repeatedly touch the display, increasing the dynamics of the haptic impression by own movements. With a dynamic display, this interaction does not work as well anymore as periods of oscillations from the vibrating elements are lost.

Another alternative is tactile systems with lateral movement of the skin. With appropriate control, the human can be "fooled" to feel punctual deformations analogous to an impression of a normal penetration. Systems with a closed surface are comfortable variants of such displays, but their dynamic control is demanding for finger positions moving across larger surfaces. Typically, today's solutions show smaller contact areas than with other variants, as the actuator elements cannot be placed as close together as necessary.

Kinaesthetic (force feedback) systems can be distinguished in active and passive systems in a control-engineering sense. Active systems are able to generate counterforces and supportive forces. The spectrum of movements is only limited by the degrees-of-freedom achieved by the mechanical design. A stable control for active system tends to become very elaborate due to the required measurement technology and complex control algorithm of sufficient speed. As with all active systems, a danger that remains is: an error in the functionality of the system may harm the user. This danger increases for piezoelectric actuators, as the available forces and torques are high. Passive systems with breaks and clutches enable the user to feel the

resistance against their own movement as reactive forces. These designs are simpler to build and less dangerous by definition of passivity. The general disadvantages of passive systems can be found in their high reaction times, change in their mechanical properties in long-time applications, and their comparably large volume. Hybrid systems combining both variants—usually including another actuation principle—may enlarge the application area of piezoelectric actuators. Although the mechanical design increases in volume and size, the requirements on control may become less and large holding forces and torques can be achieved with low power consumption. From the standpoint of haptic quality, they are one of the best actuator solutions for rotating knobs with variable torque/angle characteristics available today.

9.4 Electromagnetic Actuators

Thorsten A. Kern

Electromagnetic actuators are the most frequently used actuator type within the general automation industry. Due to their simple manufacture and assembly, they are a matter of choice. Additionally, they do not necessarily need a permanent magnet, and their robustness against exterior influences is high. They are used within coffee machines, water pumps, and for redirecting paper flow within office printers. But nevertheless, their applicability for haptic devices, especially kinaesthetic devices, is limited. Their main fields of application are tactile systems. This can be reasoned by several special characteristics of the electromagnetic principle. This chapter gives the theoretical basics for electromagnetic actuators. Technical realizations are explained with examples. First, the general topology and later the specific designs are shown. The chapter closes with some examples of haptic applications of electromagnetic actuators.

9.4.1 Magnetic Energy

The source responsible for the movement of a magnetic drive is the magnetic energy. It is stored within the flux-conducting components of the drive. These components are given by the magnetic core (compare Sect. 9.2.1.3) and the air-gap, such as all leakage fields, which are neglected for the following analysis. It can be seen from Table 9.2 that stored magnetic energy is given by the products of fluxes and magnetic voltages in each element of the magnetic circuit:

$$W_{\mathrm{mag}} = \sum_{n} H_n \, l_n \cdot B_n \, A_n \tag{9.56}$$

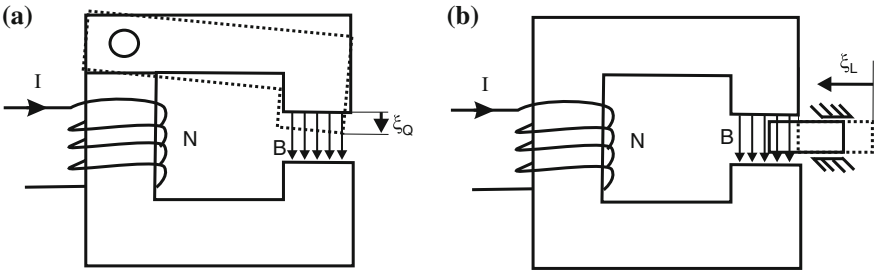

Fig. 9.46 Electromagnetic transversal effect (**a**) and longitudinal effect (**b**)

As every other system does, the magnetic circuit tries to minimize its inner energy.[13] Concentrating on electromagnetic actuators, the minimization of energy almost always refers to reduction in the air-gap's magnetic resistance R_{mG}. For this purpose, two effects may be used, which can be found within electrostatic for electrical fields too (Sect. 9.5):

- Electromagnetic longitudinal effect (Fig. 9.46a) (also: reluctance effect)
- Electromagnetic transversal effect (Fig. 9.46b)

The forces, respectively, torques generated with the individual effects are the derivations of the energy according to the corresponding direction,

$$\mathbf{F}_{\xi} = \frac{\mathrm{d}\, W_{\mathrm{mag}}}{d\xi}, \tag{9.57}$$

being equal to a force in the direction of the change of the air-gap

$$\mathbf{F}_{\xi} = -\frac{1}{2}\phi^2 \frac{\mathrm{d}\, R_{\mathrm{mG}}}{\mathrm{d}\xi}. \tag{9.58}$$

9.4.1.1 Example: Transversal Effect

The magnetic resistance of an arbitrary homogeneous element of length l between two boundary surfaces (Fig. 9.47a) with the surface A is calculated as

$$R_{\mathrm{m}} = \frac{l}{\mu\, A}. \tag{9.59}$$

This gives the stored energy W_{mag} within the magnetic resistance:

[13] Minimizing potential energy is the basis for movements in all actuator principles. Actuators may therefore be characterized as "assemblies aiming at the minimization of their inner energy."

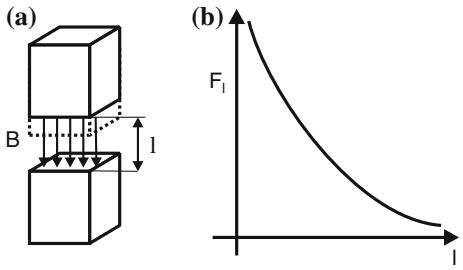

Fig. 9.47 Electromagnetic transversal effect in the air-gap (**a**) and with a qualitative force plot (**b**)

$$W_{\text{mag}} = (B\,A)^2\,\frac{l}{\mu\,A}. \tag{9.60}$$

The flux density B is dependent on the length of the material. Assuming that the magnetic core contains one material, only the magnetomotive force Θ is calculated as

$$\Theta = \frac{B}{\mu l} = NI, \tag{9.61}$$

which gives

$$B = NI\,\frac{\mu}{l}. \tag{9.62}$$

This equation used to replace the flux density in Eq. (9.60), with several variables canceled, finally results in the magnetic energy

$$W_{\text{mag}} = (NI)^2 A\mu\,\frac{1}{l}. \tag{9.63}$$

With the assumption about the magnetic energy concentrating within the air-gap—which is identical to the assumption that the magnetic core does not have any relevant magnetic resistance—the approximation of the force for the transversal effect in the direction of l can be formulated as

$$F_l = -\frac{1}{2}(NI)^2\,A\mu\,\frac{1}{l^2}. \tag{9.64}$$

The force shows an anti-proportional quadratic coherence (Fig. 9.47b) to the distance l. The closer the poles become, the higher the force attracting the poles increases.

9.4.1.2 Example: Longitudinal Effect, Reluctance Effect

The same calculation can be repeated for the longitudinal effect. Assuming that the surface A from Eq. (9.63) is rectangular and its edge lengths are given by a and b,

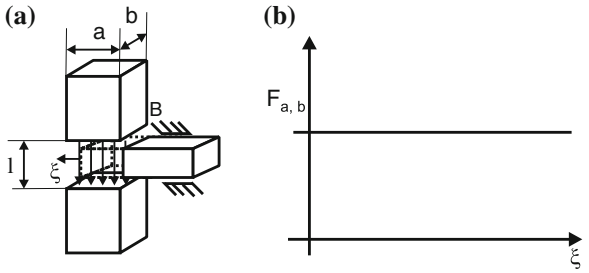

Fig. 9.48 Electromagnetic longitudinal effect in the air-gap (**a**) and as qualitative force plot (**b**)

and further assuming that a flux-conducting material is inserted into direction a, the forces in longitudinal direction can be calculated as

$$F_a = (NI)^2 \, b\mu \, \frac{1}{l}, \tag{9.65}$$

and in direction b as

$$F_b = (NI)^2 \, a\mu \, \frac{1}{l}. \tag{9.66}$$

The reluctance effect is—in contrast to the transversal effect—linear (Fig. 9.48b). The force is dependent on the length of the mobbing material's edge only. Consequently, the stored energy within the magnetic circuit is necessary for the design of an electromagnetic actuator. The above examples have the quality of rough estimations. They are sufficient to evaluate the applicability of an actuation principle—no more, no less. The magnetic networks sufficient for a complete dimensioning should contain effects with magnetic leakage fields and the core's magnetic resistance. Therefore, it is necessary to further deal with the design of magnetic circuits and their calculation.

9.4.2 Design of Magnetic Circuits

The basic interdependencies for the design of magnetic circuits have already been discussed in Sect. 9.2.1.3 in the context of electrodynamic actuators. Taken from the approach of longitudinal and transversal effect, several basic shapes (Fig. 9.49) can be derived applicable to electromagnetic actuators. In contrast to electrodynamic actuators, the geometrical design of the air-gap within electromagnetic actuators is freer. There is no need to guide an electrical conductor within the air-gap anymore. Besides the designs shown in Fig. 9.49, there are numerous other geometrical variants. For example, all shapes can be transferred to a rotational-symmetrical design around one axis. Additional windings and even permanent magnets can be added. There are however two limits to their design:

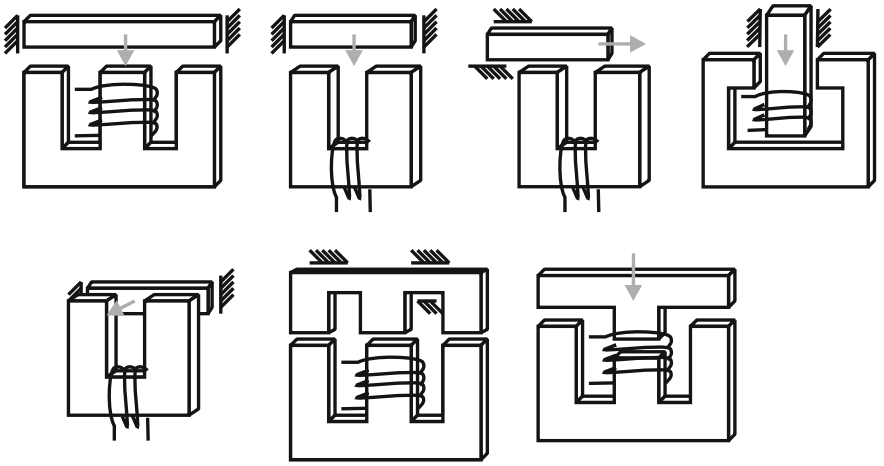

Fig. 9.49 Basic shapes of electromagnetic actuators

- A sufficient cross section of the flux-conducting elements has to be guaranteed to prevent the material from getting into saturation.
- A sufficient distance between flux-conducting elements has to be kept to prevent a magnetic leakage-field via the air.

9.4.2.1 Cross Section Surface Area: Rough Estimation

The calculation of the cross section surface area for dimensioning the magnetic core is simple. A common, easily available and within precision engineering and prototype-design gladly used material is steel ST37. The B/H-characteristic curve with its saturation is given in Fig. 9.8. For this example, we choose a reasonable flux density of 1.2 T. This equals a field intensity of $H \approx 1{,}000$ A/m. Within the air-gap a flux density of 1 T should be achieved. The magnetic flux within the air-gap is given as

$$\phi = A_{\mathrm{G}}\, B_{\mathrm{G}}. \tag{9.67}$$

As the magnetic flux is conducted completely via the magnetic core—neglecting leakage fields and other side bypasses—the relation

$$A_{\mathrm{Iron}}\, B_{\mathrm{Iron}} = A_{\mathrm{G}}\, B_{\mathrm{G}}, \tag{9.68}$$

is given, and consequently with the concrete values from above:

$$\frac{A_{\mathrm{Iron}}}{A_{\mathrm{G}}} = \frac{B_{\mathrm{G}}}{B_{\mathrm{Iron}}} = 0,833\,. \tag{9.69}$$

At its tightest point, the magnetic core may have 83 % of the cross section of the air-gap. More surface of the cross section results in lower field intensities, which should be aimed at if geometrically possible. Please note that $A_G \leq A_{Iron}$ is with almost all technical realization, as the boundary surface of the magnetic core is always one pole of the air-gap.

9.4.2.2 Magnetic Energy in the Magnetic Core and Air-Gap

In the above examples, the assumption that the energy stored within the magnetic core is clearly less than the energy within the air-gap should now be checked for validity. Calculating the magnetic resistance of an arbitrary element

$$R_m = \frac{l}{\mu A}, \tag{9.70}$$

the relation of two elements with identical length and cross section scales via the magnetic resistance with permeability μ:

$$\frac{R_{m1}}{R_{m2}} = \frac{\mu_2}{\mu_1} \tag{9.71}$$

The permeability $\mu_r = \frac{B}{H\mu_0}$ is given by the relation between flux density versus field strength relatively to the magnetic constant. It is nonlinear (Fig. 9.50) for all typical flux-conducting materials within the flux-density areas relevant for actuator design between 0.5 and 2 T. It is identical to the inverse gradient of the curves given in diagram 9.8. The maximum permeability values are given in tables frequently, but refer to field strengths within the material only. They range from 6,000 for pure iron over 10,000 for nickel alloys up to 150,000 for special soft-magnetic materials.

Mechanical processing of flux-conducting materials and the resulting thermal changes within its microstructure will result in considerable degradation of its magnetic properties. This change can be restored by an annealing process.

Generally speaking, however, even outside an optimum value for flux density the stored energy within typical materials is always several orders of magnitudes below the energy within the air-gap. This legitimates to neglect this energy portion

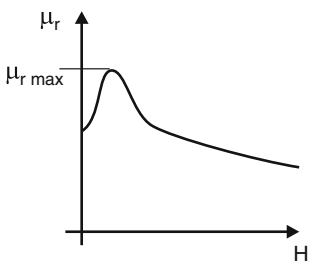

Fig. 9.50 Qualitative change permeability for common flux-conducting materials

for the rough estimations in actuator design, but also shows that there is potential within the optimization of electromagnetic actuators. This potential can be used by the application of FEM-software, which is typically available as module for CAD software.[14]

9.4.2.3 Permanent Magnets in Electromagnetic Actuators

Permanent magnets do not differ significantly in their properties from coils conducting DC current. They generate a polarized field, which—in combination with another field—provide attraction or repulsion. For calculating combined magnetic circuits, a first approach can be taken by substituting the sources within the magnetic equivalent circuit (neglecting saturation effects). The calculation is analogous to the methods mentioned in this chapter on electrodynamic actuators (Sect. 9.2.1.3). A permanent magnet within a circuit either allows

- the realization of a state held without any current applied
- or switching between two states with just one winding powered.

A good example for a currentless held state [66] shows the calculation of a polarized magnetic clamp (Fig. 9.51). With non-active winding, the flux is guided through the upper anchor and held securely. With active coil, the magnetic flux via the upper anchor is compensated. The magnetic bypass above the coil prevents the permanent magnet from being depolarized by a counter field beyond the kink in the B/H-curve.

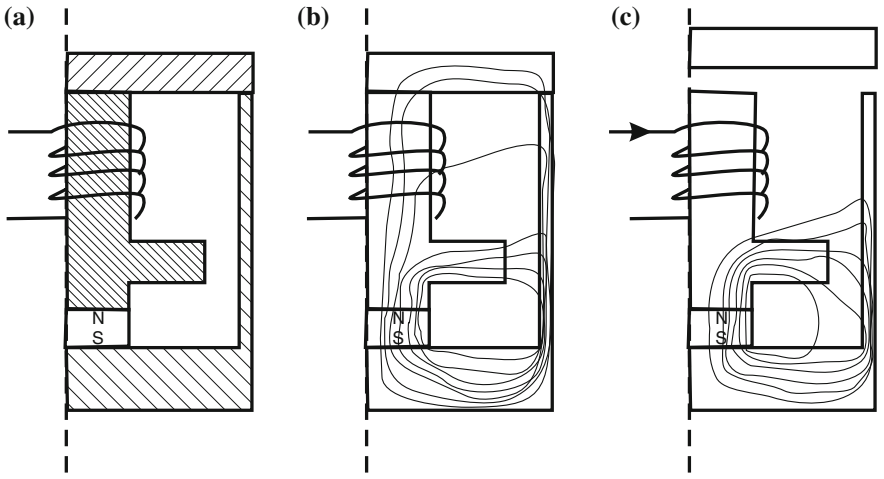

Fig. 9.51 Permanent magnet in the magnetic circuit in shape (**a**), field lines with inactive coil (**b**) and field lines with active coil (**c**), releasing the anchor

[14] Or as free software, e.g., the tool "FEMM" from David Meeker

9.4.3 Examples for Electromagnetic Actuators

Electromagnetic actuators are available in many variants. The following section gives typical designs for each principle and shows the corresponding commercial products. Knowledge of the designs will help to understand the freedom in the design of electromagnetic circuits more broadly.

9.4.3.1 Claw-Pole Stepper Motor

The electromagnetic claw-pole stepper motor (Fig. 9.52) is one of the most frequently used rotatory actuation principles. These actuators are made of two stamped metal sheets (1, 2) with the poles—the so-called claws—bent by 90° to the interior of the motor. The metal sheets are the magnetic core for conducting the flux of one coil each (3). The permanent magnet rotor (4) with a pole subdivision equalizing the claw pattern orientates to the claws in currentless state. In stepper mode, the coils are powered subsequently, resulting in a combined attraction and repulsion of the rotor. The control of the coil currents may happen either by simply switching them or by a microstep mode with different current levels being interpolated between discrete steps. The latter generates stable states for the rotor not only in the positions of the claws but also in between.

Claw-pole stepper motors are available with varying number of poles, different numbers of phases, and varying loads to be driven. As a result of the permanent magnet, they show a large holding torque with respect to their size. The frequency of single steps may reach up to 1 kHz for fast movements. By counting the steps, the position of the rotor can be detected. Step losses—the fact that no mechanical step happens after a control signal—are not very likely with a carefully designed power chain. Claw-pole stepper motors are the working horses in the electrical automation technology.

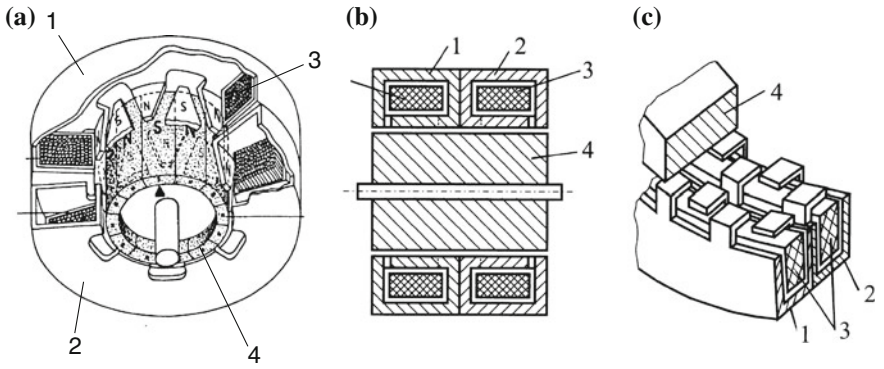

Fig. 9.52 Two-phase stepper motor made of stamped metal sheets and with a permanent magnet rotor in a 3D-sketch (**a**), cross section (**b**), and with details of the claw-poles (**c**). (Figure based on Kallenbach et al.)

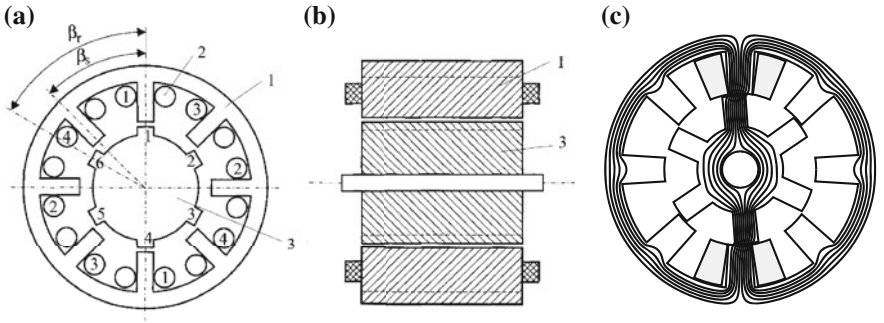

Fig. 9.53 Switched reluctance drive with pole- and coil-layout (**a**), in cross section (**b**), and with flux lines of the magnetic excitation (**c**). Figure based on [65]

9.4.3.2 Reluctance Drives

The rotatory reluctance drives (Fig. 9.53) are based on the electromagnetic longitudinal effect. By clever switching of the windings (2), it is possible to keep the rotor (3) in continuous movement with minimal torque ripples. To make this possible, the rotor has to have fewer poles than the stator. The rotor's pole angle β_r is larger than the pole angle β_s. Reluctance drives can also be used as stepper motors by the integration of permanent magnets. Generally speaking, it excels by high robustness of the components and a high efficiency factor with—for electromagnetic drives—comparably little torque ripples.

9.4.3.3 Electromagnetic Brakes

Electromagnetic brakes (Fig. 9.54) are based on the transversal effect. They make use of the high force increase at electromagnetic attraction to generate friction on a spinning disk (1). For this purpose, usually rotational-symmetrical flux-conducting magnetic cores (2) are combined with embedded coils (3). The frontal area of the magnetic core and braking disk (1) itself is coated with a special layer to reduce abrasion and influence positively the reproducibility of the generated torque. The current/torque characteristic of electromagnetic brakes is strongly nonlinear. On one hand, this is the result of the quadratic proportion between force and current of the electromagnetic transversal effect, and on the other hand, it is also a result of the friction pairing. Nevertheless, they are used in haptic devices for simulation of "hard contacts" and stop positions. A broad application for haptic devices is nevertheless not visible. This is likely a result of their limits in reproducibility of the generated torque, the resulting complex control of the current, and the fact that they can only be used as a break (passive) and not for active actuation.

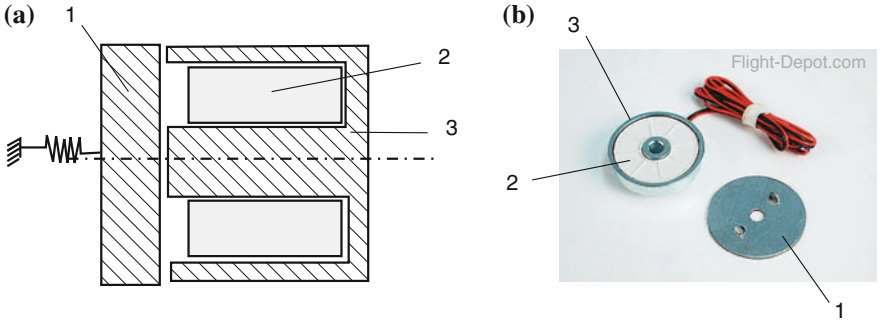

Fig. 9.54 Electromagnetic brake in cross section (**a**) and as technical realization for an airplane model (**b**)

9.4.3.4 Plunger-Type Magnet

Electromagnetic plunger-type magnets (Fig. 9.55) are frequently based on the electromagnetic transversal effect. Their main uses are switching and control applications, requiring actuation in specific states. With a magnetic core frequently made of bended iron steel sheets, (2) a coil-induced (3) flux is guided to a central anchor, which itself is attracted by a yoke (4). The geometry of the yoke influences significantly the characteristic curve of the plunger-type magnet. By varying its geometry, a linearization of the force–position curve is possible within certain limits. Even strongly nonlinear pulling-force characteristics can be achieved by such a modification. Plunger-type magnets are available with additionally magnets and with more coils. In these more complex designs, they provide mono- and bi-stable switching properties. By variation of the wires diameter and the number of turns, they can be adapted easily to any power level.

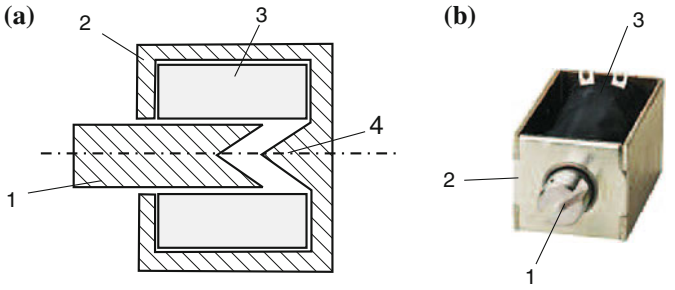

Fig. 9.55 Plunger-type magnet (**a**) with altered force–position curve (*4*), and realization as pulling anchor (**b**) with metal-sheet-made magnetic circuit (*2*)

9.4.4 Magnetic Actuators in Haptic Devices

For haptic applications, electromagnetic actuators are mainly used within tactile devices. Nevertheless, admittance-controlled devices can be found providing impressive output forces of high quality even by use of stepper motors. Besides commercial systems such as HAPTICMASTER of *Moog FCS* (Sect. 6.4) especially an idea of LAWRENCE has attracted increased attention in the past few years.

9.4.4.1 Spring-Tendon Actuator

In [76], LAWRENCE describes an inexpensive actuator for kinaesthetic haptic systems (Fig. 9.56) based on an electromagnetic stepper motor coupled via a tendon to a pen and with a spring mechanically connected in parallel. Analogous to other haptic devices, the pen is the interface to the user. Between pen and tendon and spring, there is a bending body with DMS as a force sensor. To additionally minimize the torque ripples of the stepper drive resulting from the latching of the poles, a high-resolution external encoder is attached to the motor and a torque/angle curve measured. A mathematical spline fit of this curve is used for the actuator's control to compensate the torque oscillations. In addition, the closed loop control of the actuator via the force sensor near the pen also includes a compensation of frictional effects. The result of these efforts is a force source, providing a force transmission with little noise and high stiffness up to 75 kN/m with movements of limited dynamics.

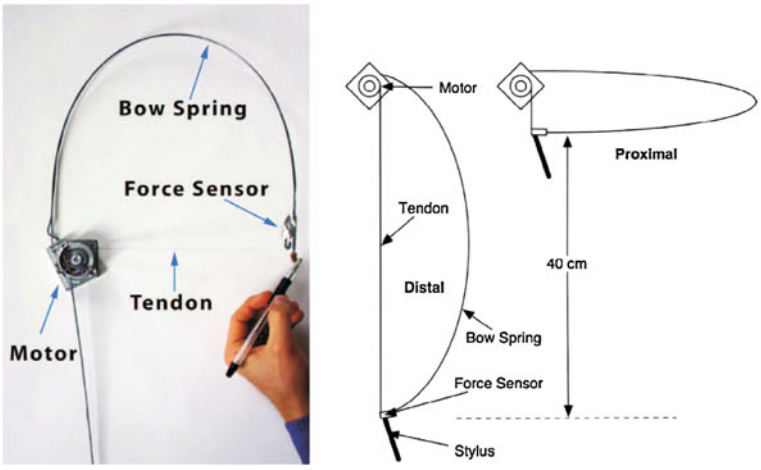

Fig. 9.56 Electromagnetic stepper motor with spring, actuated in closed-loop admittance control mode [76]

9.4.4.2 Electromagnetic Pin Array

The use of electromagnetic actuators for control of single pins in array design is very frequent. The earliest uses for haptic applications go back to printer heads of dot matrix printers that were used in the 1980s and early 1990s of the previous century. Modern designs are more specific to haptics and make use of manufacturing technologies available from microtechnology. In [24], an actuator array (Fig. 9.57) is shown made of coils with 430 windings each and a 0.4 mm-wide iron core. Above it, a magnet is embedded in a polymer layer attracted by the flux induced into the core. With such an actuator and diameter of 2 mm, a maximum force of up to 100 mN is possible. A position measure is realized via inductive feedback. Further realizations of tactile arrays based on electromagnetic actuators and different manufacturing techniques can be found in the work of STREQUE ET AL. [115].

9.4.4.3 Electromagnetic Plunger-Type Magnet for the Tactile Transmission of Speech Information

One fundamental motivation for the design of haptic devices is the partial substitution of lost senses. In particular, methods to communicate information from the sense of sight or hearing by aid of tactile devices have some tradition. BLUME designed and tested an electromagnetic plunger-type magnet based on the reluctance effect 1986 at the University of Technology, Darmstadt. Such actuators were attached to the forearm and stimulated up to eight points by mechanical oscillations encoded from speech signals. The actuator (Fig. 9.58) was made of two symmetrical plunger-type magnets (on the horizontal axis) acting upon a flux-conducting element integrated into the plunger. The whole anchor takes a position symmetrically within the actuator due to the integrated permanent magnet. In this symmetrical position, both magnetic

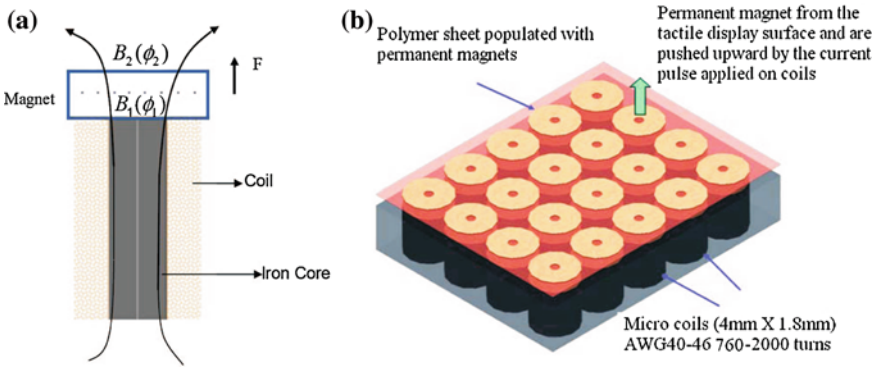

Fig. 9.57 Electromagnetic monostable actuator with permanent magnet: principal sketch (**a**) and actuator design (**b**) [24]

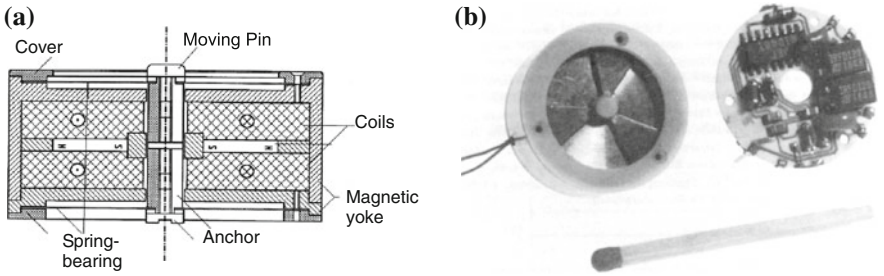

Fig. 9.58 Electromagnetic actuator according to the reluctance principle in a "counteractive plunger-type" design with permanent magnet: cross section (**a**) and design incl. driver electronics (**b**) [13]

circuits conduct a magnetic flux resulting in identical reluctance forces. In active mode, the flux in the upper or lower magnetic circuit is amplified depending on the direction of current flow. The reluctance forces on the amplified side pull the anchor in a current-proportional position working against the magnetic pretension from the permanent magnets, the mechanic pretension from the springs, and the load of the actuator. The plunger is displaced in the direction of the weakened magnetic field. At diameter of 20 mm, this actuator covers a dynamic range of 500 Hz at a efficiency factor of 50 %. The forces lie in the range of about 4 N per ampere.

9.4.5 Conclusion on the Design of Magnetic Actuators

Electromagnetic actuators are—identical to electrodynamic systems —mainly force sources. In rotary drives, especially the reluctance effect is used to generate a continuous movement. With linear drives, mainly plunger-type magnets are used based on the nonlinear transversal effect, although there are exceptions to both showing some surprising properties (Sect. 9.4.4.3). The translational systems are used to actuate as either bistable switches between two discrete states or monostable against a spring (plunger type, break, and valve). There are applications within haptics based on either or both effects. Whereas reluctance-based actuators can be found equally often within kinaesthetic applications as drives and in an admittance-controlled application in tactile systems as vibrating motor, switching actuators are almost exclusively found in tactile devices with single pins or pin arrays. In contrast to the highly dynamic electrodynamic drives, electromagnetic actuators excel in less dynamic applications with higher requirements on torque and self-holding. During switching between two states, however, acceleration and deceleration at the mechanical stop are a highly dynamic but almost uncontrollable action. The dynamic design of switching actions are not the subject of this chapter, but are usually based on modeling a nonlinear force source of the electromagnet and assuming the moving parts as concentrated elements of masses, springs, and dampers. Due to their relatively high masses within the moving parts, the hard to control nonlinearities of fluxes and forces, and the low efficiency factor of the transversal effect in many designs, electromagnetic actuators

occupy niches within haptic applications only. However, in those niches, there is no way around for their use. If an appropriate area is found, they excel by an extremely high efficiency factor for the specific design and huge robustness against exterior influences.

9.5 Electrostatic Actuators

Henry Haus, Marc Matysek

Electrostatic transformers are part of the group of electric transformers, such as piezoelectric actuators. *Electric transformers* show direct coupling between the electrical value and the mechanical value. This is contrary to electrodynamic and electromagnetic actuators, which show an intermediate transformation into magnetic values as part of the actuation process. In principle, the transformation may be used in both directions. Hence, all these actuators can be used as sensors as well.

Electrostatic field actuators are used due to their simple design and low power consumption. As a result of the technical progress of micro-engineering, the advantages of integrated designs are fully utilized. For miniaturized systems especially, electrostatic field actuators gain increased importance compared to other actuator principles. This is more surprising as their energy density is significantly lower in macroscopic designs. However, during miniaturization the low efficiency factor and the resulting power loss and heat produced become limiting factors for magnetic actuators [78].

An important subgroup of electrostatic field actuators is given *by solid-state actuators*, with an elastomeric dielectric. It has high breakdown field strength compared to air, builds the substrate of the electrodes, and can simultaneously provide an isolating housing.

In addition to the classic field actuators mentioned above, *electrorheological* fluids are part *of electrostatic actuators* as well. With these actuators, an electric field of arbitrary external source results in a change in the physical (rheological) properties of the fluid.

9.5.1 Definition of Electric Field

The following sections define the electric field and relevant variables for the design of electrostatic actuators.

9.5.1.1 Force on Charge

The magnitude of a force F acting on two charges Q_1 and Q_2 *with* a distance r is given by Coulomb's law [Eq. (9.72)].

$$F = \frac{1}{4\pi\epsilon_0}\frac{Q_1 Q_2}{r^2}. \tag{9.72}$$

9.5.1.2 Electric Field

The electric field E describes the space where these forces are present. The field strength is defined as the relation of the force **F** acting on the charge in the field and the charge's magnitude Q.

$$\mathbf{E} = \frac{\mathbf{F}}{Q} \tag{9.73}$$

The charges cause the electric field; the forces on the charges within an electric field are the effect. Cause and effect are proportional. With the electric constant $\epsilon_0 = 8{,}854 \times 10^{-12}$ C/Vm within vacuum and air Eq. (9.74) results:

$$\mathbf{D} = \epsilon_0 \mathbf{E} \tag{9.74}$$

The electric displacement field **D** describes the ratio of the bound charges and the area of the charges. The direction is given by the electric field pointing from positive to negative charges. If the electric field is filled with an insulating material (dielectric), the electric displacement field is bound partly due to the polarizing of the dielectric. Accordingly, the field strength drops from E_0 to E (with still the same electric displacement field). Consequently, the ratio of the weakened field depends on the maximum polarization of the dielectric and is called "permittivity" $\epsilon_r = E_0/E$.

9.5.1.3 Capacity

The electrical capacity is defined as the ratio of charge Q on each conductor to the voltage U between them. A capacitor with two parallel plates charged contrary to a surface of the plates A and a fixed distance d shows a capacity C depending on the dielectric:

$$C = \frac{Q}{U} = \epsilon_0 \epsilon_r \frac{A}{d}. \tag{9.75}$$

9.5.1.4 Energy Storage

Work must be done by an external influence to move charges between the conductors in a capacitor. When the external influence is removed, the charge separation persists and energy is stored in the electric field. If charge is later allowed to return to its equilibrium position, the energy is released. The work done in establishing the electric field, and hence, the amount of energy stored, is given by Eq. (9.76) and for the parallel-plate capacitor by the use of Eq. (9.75) according to Eq. (9.77).

$$W_{\mathrm{el}} = \frac{1}{2} \mathrm{CU}^2 = \frac{1}{2} \frac{Q^2}{C} \tag{9.76}$$

$$W_{\text{el}} = \frac{1}{2}\epsilon_0\epsilon_r \frac{A}{d} U^2 \tag{9.77}$$

This stored electric energy can be used to perform mechanical work according to Eq. (9.78).

$$W_{\text{mech}} = Fx. \tag{9.78}$$

9.5.2 Designs of Capacitive Actuators with Air-Gap

A preferred setup of electrostatic actuators is given by parallel-plate capacitors with air-gap. In these designs, one electrode is fixed to the frame, while the other one is attached to an elastic structure enabling the almost free movement in the intended direction (DoF). All other directions are designed stiff enough to prevent a significant displacement of this electrode. To perform physical work (displacement of the plate), the energy of the electric field according to Eq. (9.77) is used. Considering the principle design of these actuators, two basic variants can be distinguished: The displacement may result in a change in the distance d, or the overlapping area A. Both variants are discussed in the following sections.

9.5.2.1 Movement Along Electric Field

Looking at the parallel-plate capacitor from Fig. 9.59, the capacity C_L can be calculated with

$$C_L = \epsilon_0 \cdot \frac{A}{d} \tag{9.79}$$

As shown before, the stored energy W_{el} can be calculated for an applied voltage U:

$$W_{\text{el}} = \frac{1}{2}CU^2 = \frac{1}{2}\epsilon_0 \frac{A}{d} U^2 \tag{9.80}$$

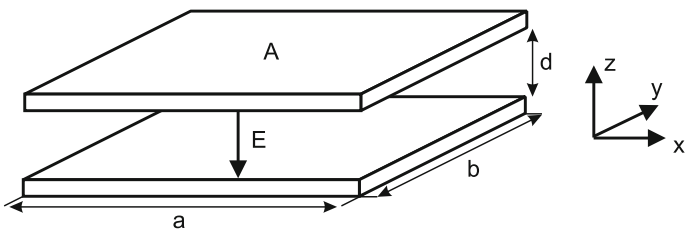

Fig. 9.59 Parallel-plate capacitor with air-gap

The force between both plates in z-direction can be derived by the principle of virtual displacement:

$$F_{z,\mathrm{el}} = \frac{\partial W}{\partial z} = \frac{1}{2} U^2 \frac{\partial C}{\partial z} \tag{9.81}$$

$$\mathbf{F}_{z,el} = -\epsilon_0 \frac{A}{2d^2} U^2 \mathbf{e}_z \tag{9.82}$$

The inhomogeneities of the electric field at the borders of the plates are neglected for this calculation, which is an acceptable approximation for the given geometrical relations of a large plate surface A and a comparably small plate distance d. A spring pulls the moving electrode into its idle position. Consequently, the actuator has to work against this spring. The schematic sketch of this actuator is shown in Fig. 9.60. The plate distance d is limited by the thickness of the insulation layer d_I. Analyzing the balance of forces according to Eq. (9.83), the interdependency of displacement z and electrical voltage U can be calculated as

$$F_z(z) = F_{\mathrm{spring}}(z) + F_{z,\mathrm{el}}(U, z) = 0 \tag{9.83}$$

$$-k \cdot z - \frac{1}{2} \epsilon_0 A \frac{U^2}{(d+z)^2} = 0 \tag{9.84}$$

$$U^2 = -2 \frac{k}{\epsilon_0 A} (d+z)^2 \cdot z \tag{9.85}$$

Analyzing the electrical voltage U in dependency of the displacement z, a maximum can be identified as

$$\frac{\mathrm{d}U^2}{\mathrm{d}z} = -2 \frac{k}{\epsilon_0 A} (\mathrm{d}^2 + 4\mathrm{d}z + 3z^2) = 0 \tag{9.86}$$

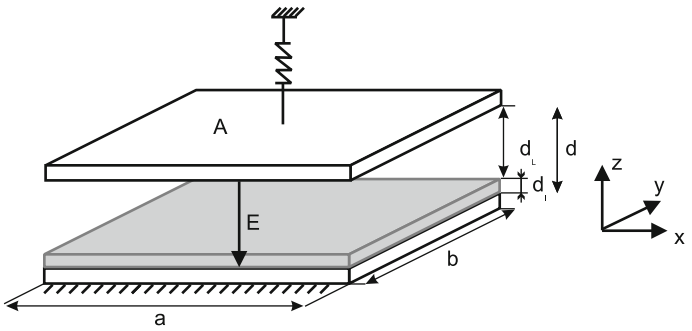

Fig. 9.60 Schematic setup of an actuator with variable air-gap

$$z^2 + \frac{4}{3}\mathrm{d}z + \frac{1}{3}d^2 = 0$$

$$z_1 = -\frac{1}{3}d;\ z_2 = -d \tag{9.87}$$

To use the actuator in a stable state, the force of the retaining spring has to be larger than the attracting forces of the charged plates. This condition is fulfilled for distances z

$$0 > z > -\frac{1}{3}d$$

Smaller distances cause attracting forces larger than the retaining force, and the moving plate is strongly pulled onto the fixed plate ("pull-in" effect). As this would immediately result in an electric shortcut, typical designs include an insulating layer on at least one plate. Equations (9.85) and (9.87) are used to calculate the operating voltage for the pull-in:

$$U_{pull-in} = \sqrt{\frac{8}{27}\frac{k}{\epsilon_0 A}d^3} \tag{9.88}$$

The retention force to keep this state is much less than the actual force at the point of pull-in. It should be noted that force increases quadratically with decreasing distance. A boundary value analysis for $d \to 0$ provides the force $F \to \infty$. Consequently, the insulation layer fulfills the purpose of a force limitation.

9.5.2.2 Moving Wedge Actuator

A special design of air-gap actuators with varying plate distance is given by the moving wedge actuator. To increase displacement, a bended flexible counter-electrode is placed on a base electrode with a non-conductive layer. The distance between the electrodes increases wedge-like from the fixation to its free end. The resulting electrical field is higher inside the area where the flexible electrode is closest to the counter-electrode and decreases with increasing air-gap. When designing the stiffness of the flexible electrode, it has to be guaranteed that it is able to roll along with the tightest wedge on the isolation. Figure 9.61 shows the underlying principle in idle state and during operation [109].

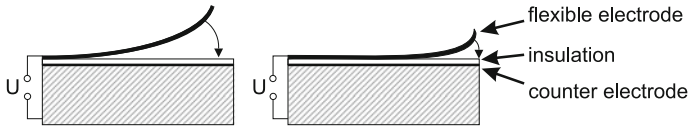

Fig. 9.61 Schematic view of a moving wedge actuator

9.5.2.3 Movement Perpendicular to Electric Field

The major difference compared to the prior design is given by the fact that the plates are moving parallel to each other. The plate distance d is kept constant, whereas the overlapping area varies. Analogous to Eq. (9.80), the forces for the displacement can be calculated in both directions of the plane:

$$F_x = \frac{\partial W}{\partial x} = \frac{1}{2} U^2 \frac{\partial C}{\partial x} \tag{9.89}$$

$$\mathbf{F}_x = \frac{1}{2} \epsilon_0 \frac{b}{d} U^2 \mathbf{e}_x \tag{9.90}$$

$$F_y = \frac{\partial W}{\partial y} = \frac{1}{2} U^2 \frac{\partial C}{\partial y} \tag{9.91}$$

$$\mathbf{F}_y = \frac{1}{2} \epsilon_0 \frac{a}{d} U^2 \mathbf{e}_y \tag{9.92}$$

The forces are independent on the overlapping length only. As a consequence, they are constant for each actuator position. Figure 9.62 shows the moving electrode attached to a retaining spring.

If an electrical voltage is applied on the capacitor, the surface A increases along the border a. Hence, the spring is deflected and generates a counter-force $\mathbf{F}_F$ according to

$$\mathbf{F}_F = -kx\mathbf{E}_x \tag{9.93}$$

The equilibrium of forces acting upon the electrode is given by

$$F_x(x) = F_F(x) + F_{x,el}(U) \tag{9.94}$$

From idle position ($F_x(x) = 0$), the displacement of the electrode in x-direction is given as

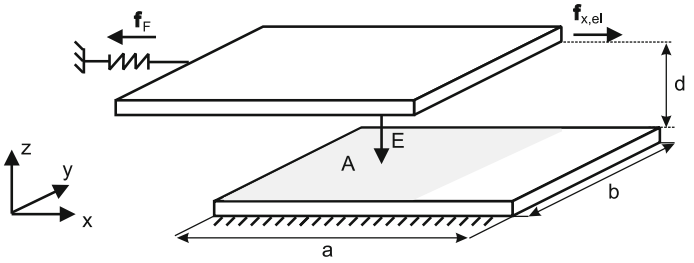

Fig. 9.62 Electrostatic actuator with variable overlapping area

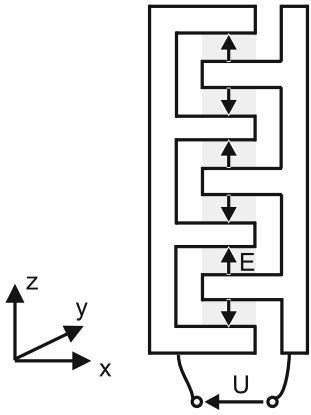

Fig. 9.63 Actuator with comb electrodes and variable overlapping area

$$x = \frac{1}{2}\epsilon_0 U^2 \frac{b}{d}\frac{1}{k} \tag{9.95}$$

Typically, this design is realized in a comb-like structure, with one comb of electrodes engaged in a counter-electrode comb. This equals an electrical parallel circuit of n capacitors, which is identical to a parallel circuit of force sources complementing each other. Figure 9.63 shows such a design. The area of the overlapping electrodes is given by a in x-direction and b in y-direction. With the plate distance d, the capacity based on Eq. (9.96) can be calculated.

$$C_Q = \epsilon_0 \cdot \frac{ab}{d} \cdot n \tag{9.96}$$

By differentiating the energy according to the movement direction, the electromotive force can be calculated as

$$F_x = \frac{\partial W}{\partial x} = \frac{1}{2}U^2 \frac{\partial C}{\partial x} = \frac{1}{2}U^2 \epsilon_0 \frac{b}{d} \cdot n. \tag{9.97}$$

9.5.2.4 Summary and Examples

For all actuators shown, the electrostatic force acts indirectly against the user and is transmitted by a moveable counter-electrode. A simpler design of tactile displays makes use of the user's skin as a counter-electrode, which experiences the whole electrostatic field force. Accordingly, tactile electrostatic applications can be distinguished in direct and indirect principles.

Direct Field Force

The simplest design combines one electrode, respectively, a structured electrode array and an isolating layer. A schematic sketch is given in Fig. 9.64. The user and his finger resemble the counter-electrode. With the attractive force between the conductive skin and the electrodes, a locally distributed increase in friction can be achieved. It hinders a relative movement and can be perceived by the user. Such systems can be easily realized and excellently miniaturized. Their biggest disadvantage is their sensitivity on humidity on the surface, which is brought onto the electrodes during any use in form of sweat. This leads to a blocking of the electrical by the conductive sweat layer above the isolation, preventing the user to feel any relevant force.

Indirect Field Force

With these systems, the field force is used to move an interacting surface. The finger of the user interacts with these surfaces (sliders) and experiences their movements as a perceivable stimulation. A realization with a comb of actuators moving orthogonal to the field direction is given in Fig. 9.65. The structural height is 300 µm, providing 1 mN at operating voltages of up to 100 V. The same design with an actuator made of parallel electrodes can achieve displacements of 60 µm. The comb electrodes shown here displace 100 µm.

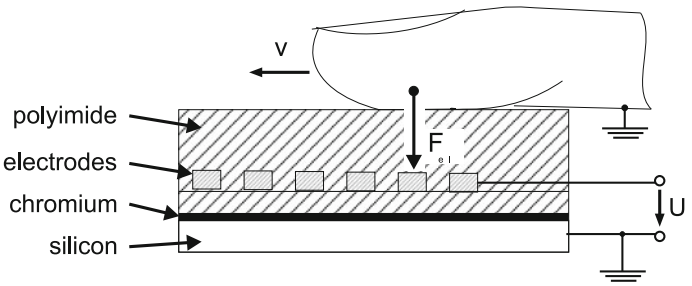

Fig. 9.64 Electrostatic stimulator with human finger as counter-electrode as presented in [119]

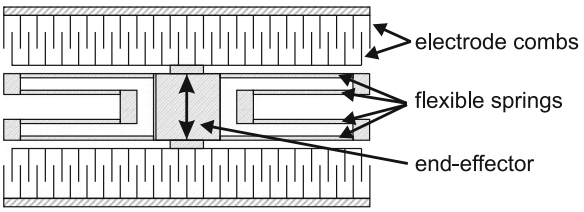

Fig. 9.65 Electrostatic comb-actuator for tangential stimulation [37]

Summary

Electrostatic drives with air-gap achieve force in the range of mN–N. As the actuators are driven by fields, the compromise between plate distance and electrical operation voltage has to be validated for each individual application. The breakdown field strength of air (approx. $3\,V/\mu m$) is the upper, limiting factor. The actuators' displacement is limited to several μm. At the same time, the operating voltages reach several hundred volts. Due to the very low achievable displacement, the application of electrostatic actuators is limited to tactile stimulation only.

For the concrete actuator design, it is recommended to deal with the modeling of such actuators, e.g., based on concentrated network parameters (see Sect. 4.3.2). This allows the analysis of the complete electromechanical system starting from the applicable mechanical load situation to the electrical control with a single methodological approach.

9.5.3 Dielectric Elastomer Actuators

As with many other areas, new synthetic materials replace classic materials such as metals in actuator design. Thanks to the enormous progress in material development their mechanical properties can be adjusted to a large spectrum of possible applications. Other advantages are the cheap material costs. Additionally, almost any geometrical shape can be manufactured with relatively small efforts.

Polymers are called "active polymers" if they are able to change their shape and form under the influence of external parameters. The causes for these changes may be manifold: electric and magnetic fields, light, and even pH-value. Being used within actuators, their resulting mechanical properties like elasticity, applicable force, and deformation at simultaneously high toughness and robustness are comparable to biological muscles [4].

To classify the large variety of "active polymers," they are distinguished according to their physical working principle. A classification into "non-conductive polymers" is activated, e.g., by light, pH-value, or temperature, and "electrical polymers" is activated by an arbitrary electrical source. The latter are called "electroactive polymers" (EAP) and are further distinguished into "ionic" and "electronic" EAPs. Generally speaking, electronic EAP are operated at preferably high field strengths near the breakdown field strength. Depending on the thickness layer of the dielectrics, $1-20\,kV$ are considered typical operation voltages. Consequently, high energy densities at low reaction times (in the area of milliseconds) can be achieved. In contrast, ionic EAP are operated at obviously lower voltages of $1-5\,V$. However, an electrolyte is necessary for transportation of the ions. It is frequently provided by a liquid solution. Such actuators are typically realized as bending bars, achieving large deformations at their tip with long reaction times (several seconds).

All EAP technologies are the subject of actual research and fundamental development. However, two actuator types are already used in robotics: "Ionic polymer

Table 9.6 Comparison of human muscle and DEA according to PEI [98]

Parameter	Human muscle	DEA
Strain (%)	20−40	10 bis > 100
Stress (MPa)	0, 1−0, 35	0, 1−2
Energy density (kJ/m^3)	8−40	10−150
Density (kg/m^3)	1, 037	≈1,000
Velocity of deformation (%/s)	>50	450 (acrylic) 34,000 (silicone)

metal composite" (IPMC) and "dielectric elastomer actuators" (DEA). A summary and description of all EAP-types is offered by KIM [69]. Their functionality is discussed in the following sections as they affiliate to the group of electrostatic actuators. A comparison between characteristic values of dielectric elastomer actuators and the muscles of the human is shown in Table 9.6. By use of an elastomer actuator with large expansion, additional mechanical components such as gears or bearings are needless. Additionally, the use of these materials may be combined with complex designs similar to and inspired by nature. One application is the locomotion of insects and fish within bionic research [5].

9.5.3.1 Dielectric Elastomer Actuators: Electrostatic Solid-State Actuators

The design of dielectric elastomer actuators is identical to the design of a parallel-plate capacitor, but with an elastic dielectric (a polymer, respectively, elastomer) sandwiched by compliant electrodes. Hence, it is a solid-state actuator. The schematic design of a dielectric elastomer actuator is visualized in Fig. 9.66, left. In an uncharged condition, the capacity and the energy stored is identical to an air-gap actuator [Eqs. (9.75) and (9.76)]. A change in this condition happens by application of a voltage U and is visualized in Fig. 9.66, on the right: The charged capacitor contains more charges ($Q + \Delta Q$), the electrode area increases ($A + \Delta A$), while the distance ($z - \Delta z$) simultaneously decreases. The change of energy after an infinitesimal change $\mathrm{d}Q$, $\mathrm{d}A$, and $\mathrm{d}z$ is calculated in Eq. (9.98):

$$\mathrm{d}W = \left(\frac{Q}{C}\right)\mathrm{d}Q + \left(\frac{1}{2}\frac{Q^2}{C}\frac{1}{z}\right)\mathrm{d}z - \left(\frac{1}{2}\frac{Q^2}{C}\frac{1}{A}\right)\mathrm{d}A \tag{9.98}$$

$$\mathrm{d}W = U\mathrm{d}Q + W\left[\left(\frac{1}{z}\right)\mathrm{d}z - \left(\frac{1}{A}\right)\mathrm{d}A\right] \tag{9.99}$$

The internal energy change equals the change of the electrical energy by the voltage source and the mechanical energy used. The latter depends on the geometry (parallel ($\mathrm{d}z$) and normal ($\mathrm{d}A$) to the field's direction). In comparison with the air-gap actuator in Sect. 9.5.2, an overlay of decreasing distance and increasing electrodes'

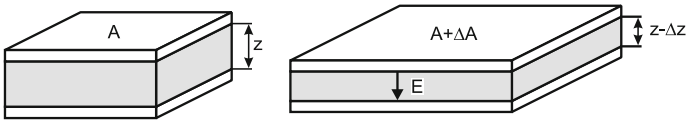

Fig. 9.66 DEA in initial state (*left*) and charged state (*right*)

area occurs. This is caused by a material property that is common to all elastomers and to almost all polymers: the aspect of volume constancy. A body compressed in one direction will extend in the remaining two dimensions if it is incompressible. This gives a direct relation between distance change and the change in electrodes' area. As a consequence, Eq. (9.100) results

$$A\,\mathrm{d}z = -z\mathrm{d}A \tag{9.100}$$

simplifying Eq. (9.99) to

$$\mathrm{d}W = U\mathrm{d}Q + 2W\left(\frac{1}{z}\right)\mathrm{d}z \tag{9.101}$$

The resulting attractive force of the electrodes can be derived from this electrical energy. With respect to the electrode surface A, the electrostatic pressure p_{el} at $\mathrm{d}Q = 0$ is given according to Eq. (9.102)

$$p_{\mathrm{el}} = \frac{1}{A}\frac{\mathrm{d}W}{\mathrm{d}z} = 2W\frac{1}{Az} \tag{9.102}$$

and by application of Eq. (9.76)

$$p_{\mathrm{el}} = 2\left(\frac{1}{2}\epsilon_0\epsilon_r Az\frac{U^2}{z^2}\right)\frac{1}{Az} = \epsilon_0\epsilon_r E^2 \tag{9.103}$$

Comparing this result with Eq. (9.81) as a reference for a pressure of an air-gap actuator with variable plate distance, dielectric elastomer actuators are capable of generating a pressure twice as high with otherwise identical parameters [99]. Additional reasons for the obviously increased performance of the dielectric elastomer actuators are also based on their material. The relative permittivity is given by $\epsilon_r > 1$, depending on the material $\epsilon_r \simeq 3 - 10$. By chemical processing and implementation of fillers, the relative permittivity may be increased. However, it may be noted that other parameters (such as the breakdown field strength and the E-modulus) may become worse, possibly the positive effect of the increased ϵ_r gets lost. The breakdown field strength especially is one of the most limiting factors. With many materials, an increase in breakdown field strength can be observed after planar prestrain. In these cases, breakdown field strengths of $100-400\,\mathrm{V/\mu m}$ are typical [17].

The pull-in effect does not happen at $z = 1/3 \cdot z_0$ (air-gap actuators), but at higher deflections. With some materials mechanical prestrain of the actuator allows to displace the pull-in further, reaching the breakdown field strength before. The reason for this surprising property is the volume constant dielectric layer showing viscoelastic properties. It complies with a return spring with strong nonlinear force–displacement characteristics for large extensions. Its working point is displaced along the stress–strain curve of the material as an effect of the mechanical prestrain.

For application in dielectric elastomer actuators, many materials may be used. The material properties cover an extreme wide spectrum ranging from gel-like polymers up to relatively rigid thermoplastics. Generally speaking, every dielectric material has to have a high breakdown field strength and elasticity besides high relative permittivity. Silicone provides highest deformation velocities and a high temperature resistance. Acrylics have high breakdown field strength and achieve higher energy densities. The following list is a selection of the dielectric materials frequently used today:

- silicone
  - HS 3 (Dow Corning)
  - CF 19-2186 (Nusil)
  - Elastosil P7670 (Wacker)
  - Elastosil RT625 (Wacker)
- acrylics
  - VHB 4910 (3M)

The most frequently used materials for the elastic electrodes are graphite powder, conductive carbon, and carbon grease.

9.5.4 Designs of Dielectric Elastomer Actuators

As mentioned before, dielectric elastomer actuators achieve high deformations (compression in field direction) of 10−30 %. To keep voltages within reasonable ranges, layer thicknesses of 10−100 μm are used depending on the breakdown field strength. The resulting absolute displacement in field direction is too low to be useful. Consequently, there are several concepts to increase it. Two principle movement directions are distinguished for this purpose: the longitudinal effect in parallel to the field (thickness change) and the transversal effect orthogonal to field (surface area change). The importance of this discrimination lies in the volume constancy of the material: uniaxial pressure load equals a two-axial tension load in the remaining spatial directions. Hence, two transversal tensions within the surface result in a surface change. For materials fulfilling the concept of "volume constancy," Eq. (9.104) is valid, providing the following properties for the longitudinal compression S_z and the transversal elongation S_x:

- with a longitudinal compression of 62 %, both extensions are identical;
- for smaller values of the longitudinal compression, the resulting transversal extension is smaller;
- for a longitudinal compression >62 % them, transversal extensions increases faster than the longitudinal compression.

$$S_x = \frac{1}{\sqrt{1 - S_z}} - 1 \tag{9.104}$$

The extension of the surface area S_A depends on the longitudinal compression S_z according to Eq. (9.105):

$$S_A = \frac{dA}{A} = \frac{S_z}{1 - S_z} \tag{9.105}$$

The increase of the area with uniaxial compression is always larger than the change in thickness. Actuators built according to this principle are the most effective ones. Figure 9.67 shows three typical designs. A roll-actuator (left) built as full or tubular cylinder can achieve length changes of more than 10 %. KORNBLUH [71] describes an acrylic roll-actuator achieving a maximum force of 29 N with an own weight of no more than 2.6 g at a extension of 35 mm. The manufacture of electrodes with a large area is very simple. On the other hand, the rolling of the actuators with simultaneous pre-strain (up to 500 %) can be challenging. With a stack-actuator (middle), very thin dielectric layers down to 5 µm with minimized operational voltages can be achieved, depending mainly on the manufacturing technique [81]. As the longitudinal effect is used, extension is limited to approximately 10 %. However, due to their design and fabrication process, actuator arrays at high density can be built [63] and offer typically lifetimes of more than 100 million cycles depending on their electrical interconnection [84]. The most simple and effective designs are based on a restrained foil, whose complete surface change is transformed into an up-arching (diaphragm-actuator, right) [70]. If this actuator experiences a higher external load, such as from a finger, an additional force source, e.g., a pressure, has to be provided to support the actuators own tension.

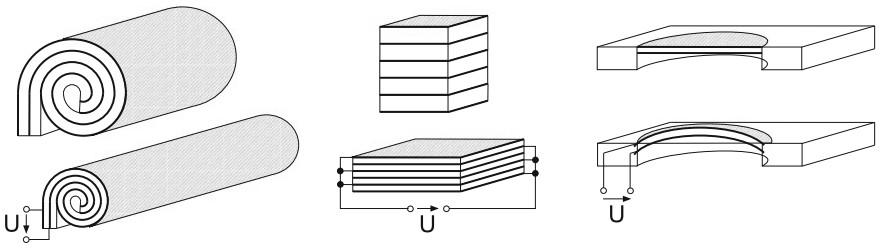

Fig. 9.67 Typical designs of Dielectric Elastomer Actuators: roll-actuator (*left*), stack-actuator (*center*), and diaphragm-actuator (*right*)

9.5.4.1 Summary and Examples

As with air-gap actuators, a dielectric solid-state actuator's major limit is given by the breakdown field strength of the dielectric. However, in contrast to the air-gap actuators, a carefully chosen design can easily avoid any pull-in effect. Consequently, these actuators show larger workspace, and with the high number of different design variants a wide variety of applications can be realized depending on the requirements of displacement, maximum force, and actuator density.

Tactile Displays

The simplest application of a tactile display is a Braille device. Such devices are meant to display Braille letters in patterns of small, embossed dots. In standard Braille, six dots are used, in computer compatible Euro-Braille eight dots. These points are arranged in a 2×3 or 2×4 matrix, respectively (Fig. 9.68). In a display device, 40 to 80 characters are displayed simultaneously. In state-of-the-art designs, each dot is actuated with one piezoelectric bending actuator (Sect. 9.3.5). This technical effort is the reason for the high price of these devices. As a consequence, there are several functional samples existing, which prove the applicability of less expensive drives with simplified mechanical designs, but still sufficient performance. Each of the three variants for dielectric elastomer actuators has already been used for this application.

Figure 9.68 shows the schematic sketch of roll-actuators formed to an actuator column [107]. Each roll-actuator moves one pin, which itself is pushed up above the base plate after applying a voltage. The elastomer film is coiled around a spring of 60 mm length with diameter of 1.37 mm. With an electric field of 100 V/μm applied, the pre-tensioned spring can achieve a displacement of 1 mm at a force of 750 mN. The underlying force source is the spring with spring constant 225 N/m pre-tensioned by a passive film. The maximum necessary displacement of 500 μm is achieved at field strengths of 60 V/μm.

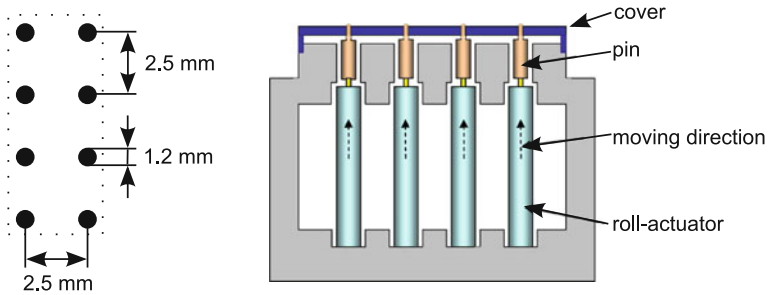

Fig. 9.68 Presenting a Braille sign with roll-actuators, *left* geometry, *right* schematic setup of a Braille row [107]

The application of stack-actuators according to JUNGMANN [63] is schematically sketched in Fig. 9.68, left. The biggest advantage of this variant is given by the extremely high actuator density combined with a simple manufacturing process. Additionally, the closed silicone elements are flexible enough to be mounted on an almost arbitrary formed surface. The surface—by itself made of silicone—shows an adequate roughness and temperature conductivity. It is perceived as "convenient" by many users. With a field strength of 30 V/μm, a stack made of 100 dielectric layers displacements of 500 μm can be achieved. The load of a reading finger on the soft substrate generates a typical contact pressure of 4 kPa, resulting in a displacement of 25 μm. This extension is considerably less than the perception threshold of 10 % of the maximum displacement. For control of the array, it has to be noted that the actuators are displaced in a negative logic. With applied voltage, the individual pin is pulled downwards.

A remote control providing tactile feedback based on the same type of stack-actuators is presented in [85]. The mobile user interface consists of five independent actuating elements. Besides the presentation of tactile feedback, the stack transducers offer to acquire user's input using the transducers intrinsic sensor functionality. The actuators are driven with a voltage of up to 1,100 V generated out of a primary lithium-ion battery cell. A free-form touch pad providing tactile feedback to the human palm is described in [89]. Four actuators are integrated in a PC-mouse to enhance user experience and substitute visual feedback during navigation tasks (see Fig. 9.69). The stacks consist of 40 dielectric layers, each 40 μm in thickness and are supplied by a maximum voltage of 1 kV in a frequency range from 1.5 to 1 kHz. The mouse contains all the required driving electronics and can be customized by a software configuration tool.

The design of a Braille display with diaphragm-actuators according to HEYDT [48] demonstrates the distinct properties of this variant. The increase of elastomer surface results in a notable displacement of a pin from the device's contact area. However, a mechanical prestrain is necessary to provide a force. This can be either generated by a spring or air pressure below the actuator. Figure 9.70 on the right

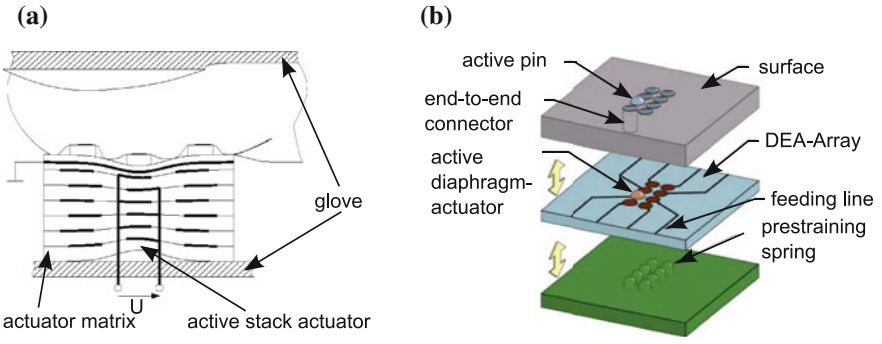

Fig. 9.69 Tactile feedback enhanced PC-mouse: CAD model (**a**), and demonstration device (**b**) [89]

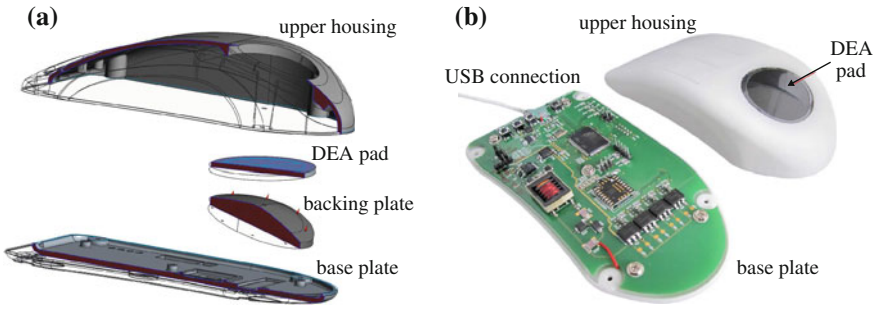

Fig. 9.70 **a** Actuator row with stack-actuators [63]; **b** Use of diaphragm-actuators [48]

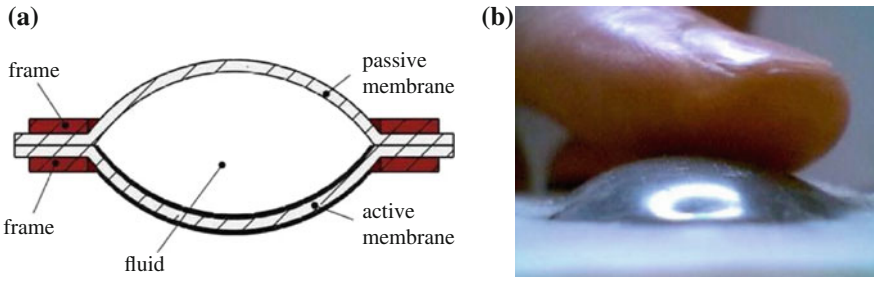

Fig. 9.71 Hydrostatically coupled membrane actuator: **a** schematic drawing, **b** and finger touching active display as presented in [19]

gives a schematic sketch for a single point being pretensioned by a spring with a diameter of 1.6 mm. At an operating voltage of 5.68 kV, the actuator displaces in idle mode 450 µm.

CARPI combines the principle of the diaphragm-actuators with fluid-based hydrostatic transmission [19]. The result is a wearable tactile display intended for providing feedback during electronic navigation in virtual environments. As shown in Fig. 9.71, the actuators are based on an incompressible fluid that hydrostatically couples a dielectric elastomer membrane to a passive membrane interfaced to the user's finger. The transmission of actuation from the active membrane to the finger, without any direct contact, allows suitable electrical safety. However, the actuator is driven with comparatively high voltages up to 4 kV.

9.5.5 Electrorheological Fluids

Fluids influenced in their rheological properties (especially the viscosity) by electrical field varying in direction and strength are called ↪ Electrorheological Fluid (ERF). Consequently, ERF are classified as non-Newton fluids, as they have a variable

viscosity at constant temperature. The electrorheological effect has been observed for the first time in 1947 at a suspension of cornstarch and oil by WILLIS WINSLOW.

Electrorheological fluids include dipoles made of polarized particles, which are dispersed in a conductive suspension. These particles are aligned in an applied electrical field. An interaction between particles and free charge carriers happens. Chain-like microstructures are built between the electrodes [23, 51, 111] in this process. However, it seems as if this is not the only effect responsible for the viscosity change, as even when the microstructures [97] were destroyed, a significant viscosity increase remained. The exact analysis of the mechanism responsible for this effect is a subject of actual research.

The viscosity of the fluid changes depending on the strength of the applied electrical field. With an electric field of 1−10 kV/mm, the viscosity may change up to a factor of 1,000 compared to the field-free state. This enormous change equals a viscosity difference between water and honey. An advantage of this method can be found in the dynamics of the viscosity change. It is reversible and can be switched within one millisecond. Therefore, electrorheological fluids are suitable for dynamic applications.

If large field strengths are assumed, the ERF can be modeled as BINGHAM fluid. It has a threshold for linear flow characteristics: starting at a minimum tension $\tau_{F,d}$ (flow threshold) the fluid actually starts to flow. The fluid starts flowing right below this threshold. The shear forces τ are calculated according to Eq. (9.106):

$$\tau = \mu\dot{\gamma} + \tau_{F,d} \tag{9.106}$$

with μ the dynamic viscosity, $\dot{\gamma}$ the shear rate, and $\tau_{F,d}$ the dynamic flow limit. The latter changes quadratically with the electrical field strength [Eq. (9.107)]. The proportional factor C_d is a constant provided with the material's specifications.

$$\tau_{F,d} = C_d E^2 \tag{9.107}$$

For complex calculations modeling the fluid's transition to and from the state of flow, the model is extended to a nonlinear system according to Eq. (9.108) [for $n = 1$ this equals Eq. (9.106)].

$$\tau = \tau_{F,d} + k\dot{\gamma}^n \tag{9.108}$$

This general form describes the shear force for viscoplastic fluids with flow limit according to VITRANI [129]. For analysis of idle state with shear rate $\dot{\gamma} = 0$, the static flow limit $\tau_{F,s}$ with $\tau_{F,s} > \tau_{F,d}$ is introduced. When exceeding the static flow limit, the idle fluid is deformed. With the specific material constants, C_s and E_{ref} Eq. (9.109) can be formulated as

$$\tau_{F,s} = C_s(E - E_{\text{ref}}) \tag{9.109}$$

The materials used for the particles are frequently metal oxides, silicon anhydride, poly urethane, and polymers with metallic ions. The diameter of particles is 1–

100 µm; their proportion on the fluid's volume is 30–50 %. As carrier medium, typically oils (such as silicone oil) or specially treated hydrocarbon are used. To additionally improve the viscosity change, nanoscale particles are added in the electrorheological fluids ("giant electrorheological effect" [40, 137]). In [28] and [105] further mathematical modeling is presented for the dynamic flow behavior of ER-fluids.

The central property of ERF—to reversibly change the viscosity—is used for force-feedback devices, haptic displays, and artificial muscles and joints. As the change in viscosity is mainly a change in counter-forces but not in shape or direct forces, ERF-actuators are counted to the group of "passive actuators." For the characterization of their performance, the ratio between stimulated and idle state is used. They are built in three principle design variants [14] as described in the following sections.

9.5.5.1 Shear Mode

The ER-fluid is located between two parallel plates, one fixed and the other moving relatively to the fixed one. The only constraint is given by a fixed inter-plate distance d. If a force F is applied on the upper plate, it is displaced by a value x at a certain velocity v. For the configuration shown in Fig. 9.72, the mechanical control ratio λ can be calculated according to Eq. (9.112) from the ratio of dissipative forces (field-dependent flow stresses, Eq. (9.115)) and the field-independent viscosity term (Eq. (9.110)) [100]. η gives the basis viscosity of the ER-fluid (in idle state) and τ_y the low-stress depending on the electrostatic field.

$$F_\eta = \frac{\eta v a b}{d} \tag{9.110}$$

$$F_\tau = \tau_y a b \tag{9.111}$$

$$\lambda = \frac{F_\tau}{F_\eta} = \frac{\tau_y d}{\eta v}. \tag{9.112}$$

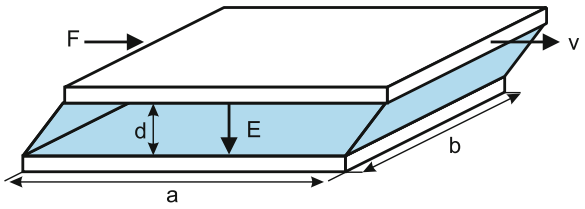

Fig. 9.72 Using ERF to vary the shear force

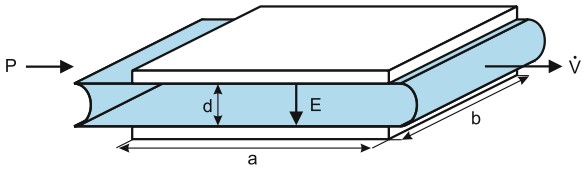

Fig. 9.73 Varying the flow channel's resistivity with ERF-actuators

9.5.5.2 Flow Mode

The schematic sketch of this configuration is shown in Fig. 9.73. Both fixed plates form a channel, with the fluid flowing through it due to an external pressure difference p and a volume flow $\dot{V}$. With an electric field E applied between the plates, the pressure loss increases along the channel and the volume flow is reduced. Analogous to the prior design, a field-independent viscosity-based pressure loss p_η and a field-dependent pressure loss p_τ can be calculated [100]as

$$p_\eta = \frac{12\eta\dot{V}a}{d^3 b} \tag{9.113}$$

$$p_\tau = \frac{c\tau_y a}{d} \tag{9.114}$$

The mechanical control ratio equals

$$\lambda = \frac{p_\tau}{p_\eta} = \frac{c\tau_y d^2 b}{12\eta\dot{V}} \tag{9.115}$$

At an adequate dimensioning of the fluid, the flow resistance can be increased by the electrical field to such a degree that the fluid stops completely when exceeding a specific voltage. This makes the channel a valve without any moving mechanical components.

9.5.5.3 Squeeze Mode

A design to generate pressure is schematically sketched in Fig. 9.74. In contrast to the variants shown before, the distance between both plates is subject to change now. If a force acts on the upper plate, it moves downwards. This results in the fluid being pressed outside. A plate distance d_0 is assumed at the beginning and a relative movement of v of the plate moving downwards. The velocity-dependent viscosity force F_η and the field-dependent tension term F_τ [62] are calculated according to:

$$F_\eta = \frac{3\pi\eta v r^4}{2(d_0 - z)} \tag{9.116}$$

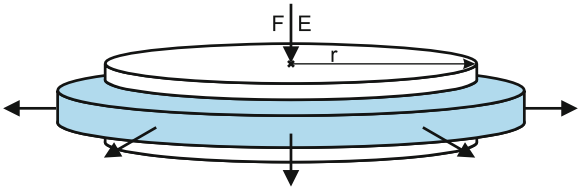

Fig. 9.74 Varying the acoustic impedance with ERF-actuators under external forces

$$F_\tau = \frac{4\pi\,\tau_y r^3}{3(d_0 - z)}, \tag{9.117}$$

which gives the mechanical control ratio:

$$\lambda = \frac{8\tau_y 3(d_0 - z)^2}{9\eta v r} \tag{9.118}$$

With pressure (force on the upper plate), the fluid is pressed out of the gap. In this configuration, the force–displacement characteristics are strongly influenced by the electrical field strength. An analysis of the dynamic behavior of such an actuator is described in [132].

9.5.5.4 Designing ERF-Actuators

The maximum force F_τ and the necessary mechanical power P_{mech} are the input values for the design of ERF-actuators from the perspective of an application engineer. Equations (9.110) and (9.118) can be combined to calculate the necessary volume for providing a certain power with all three actuator configurations.

$$V = k\frac{\eta}{\tau_y^2}\lambda P_{\text{mech}} \tag{9.119}$$

Consequently, the volume is defined by the mechanical control ratio, the fluid-specific values η and τ_y, such as a constant k dependent on the actual configuration. The electrical energy W_{el} necessary to generate the electrostatic field of the actuator (volume dependent) is calculated according to Eq. (9.120).

$$W_{\text{el}} = V\left(\frac{1}{2}\epsilon_0\epsilon_r E^2\right). \tag{9.120}$$

9.5.5.5 Comparison to Magnetorheological Fluids

↪ Magnetorheological Fluids (MRF) are similar to electrorheological fluids. However, the physical properties of the fluids are influenced by magnetic fields. All calculations shown before are also applicable to MRF. Looking at the volume necessary for an actuator according to Eq. (9.119), considering the viscosities of electrorheological and magnetorheological fluids being comparable, a volume ratio proportional to the reciprocal ratio of the fluid-tensions' square according to Eq. (9.121) results in

$$\frac{V_{\mathrm{ERF}}}{V_{\mathrm{MRF}}} = \frac{\tau_{\mathrm{MRF}}^2}{\tau_{\mathrm{ERF}}^2} \tag{9.121}$$

In a rough but good approximation, the flow stress of a magnetorheological fluid is one magnitude larger than an ERF, resulting in a smaller (approximately factor 100) volume of an MRF-actuator compared to the ERF. However, a comparison between both fluids going beyond the pure volume analysis for similar output power is hard: for an ERF high voltages at relatively small currents are required. The main power leakage is lost by leakage currents through the medium (ERF) itself. With MRF-actuators, smaller electrical voltages at high currents become necessary to generate an adequate magnetic field. The energy for an MRF-actuator is calculated according to Eq. (9.122) with the magnetic flux density B and the magnetic field strength H.

$$W_{\mathrm{el,MRF}} = V_{\mathrm{MRF}} \left(\frac{1}{2} BH \right) \tag{9.122}$$

The ratio between the energies for both fluids is calculated according to Eq. (9.123)

$$\frac{W_{\mathrm{el,ERF}}}{W_{\mathrm{el,MRF}}} = \frac{V_{\mathrm{ERF}}}{V_{\mathrm{MRF}}} \frac{\epsilon_0 \epsilon_r E^2}{BH} \tag{9.123}$$

With typical values for all parameters, the necessary electrical energy for actuator control is comparable for both fluids. An overview of the design of actuators for both types of fluids is given in [18].

9.5.5.6 Summary and Examples

Electrorheological fluids are also called partly active actuators, as they do not transform the electrical values into a direct movement, but change their properties due to the electrical energy provided. The change in their properties covers a wide range. Naturally, their application in haptics ranges from small tactile displays to larger haptic systems.

Tactile Systems

The first application of ERF as tactile sensor in an artificial robot hand was made in 1989 by KENALEY [67]. Starting from this work, several ideas developed to use ERF in tactile arrays for improving systems for virtual reality applications. Several tactile displays, among them a 5×5 matrix from TAYLOR [121] and another one from BÖSE [15], were built. Figure 9.75 shows the schematic design of such a tactile element. A piston is pressed in an ERF filled chamber by the user. Varying counter-forces are generated depending on the actuation state of the ERF. Elastic foam is connected to the piston as a spring to move it back to its resting position. With an electric field of 3 V/µm a force of 3.3 N can be achieved at a displacement of 30 mm. Switching the electrical voltages is realized by light emitting diodes and corresponding receivers (GaAs-elements) on the backplane.

Haptic operating controls

Another obvious application for ERF in haptic systems is their use as a "variable brake." This is supported by the fact that typical applications beside haptic systems are variable brakes and bearings (e.g., adaptive dampers). There are several designs with a rotary knob mobbing a spinning disk within an ERF or MRF generating varying counter-torques as shown in [80]. In this case, the measurement of the rotary angle is solved by a potentiometer. In dependency on the rotary angle, the intended counter-force, respectively, torque is generated. The user can perceive a "latching" of the rotary knob with a mature system. The latching depth itself can be varied in a wide range. By the varying friction, hard stops can be simulated, too, such as sticking and of course-free rotation.

An extension of the one-dimensional system is presented in [136]. Two systems based on ERF are coupled to a joystick with two DoF. A counter-force can be generated in each movement direction of the joystick. As ERF are able to generate higher

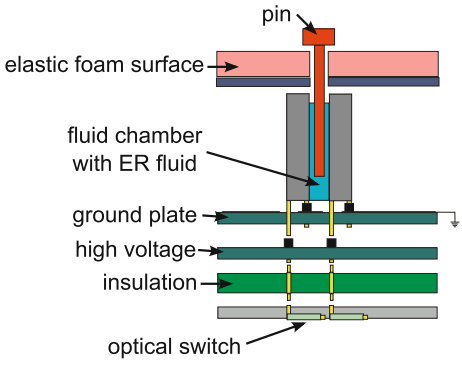

Fig. 9.75 Schematic setup of a tactile actuator based on ER-fluids [15]

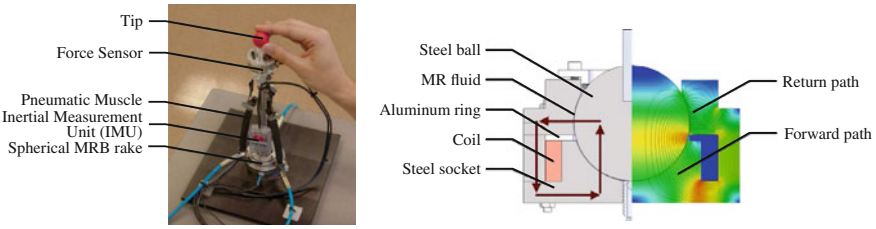

Fig. 9.76 Haptic joystick based on pneumatic actuators and a MRF-brake as presented in [110]

torques with less energy required compared to a normal electrical drive, they are especially suitable to mobile applications like in cars.

SENKAL ET AL. presented a combination of an MRF-brake and pneumatic actuators for a 2D joystick as shown in Fig. 9.76. This hybrid concept uses pneumatic actuators because of the high energy density and the MR brake to increase the fidelity of rigid objects [110]. Further realizations of MRF operating controls can be found in [1].

Force-Feedback Glove

A force-feedback glove was designed as a component for a simulator of surgeries [6]. Surgical interventions shall be trained by the aid of haptic feedback. The system "remote mechanical mirroring using controlled stiffness and actuators" (MEMICO) enables a surgeon to perform treatment with a robot in telemanipulation, whereas the haptic perception is retained. ERF-actuators are used for both ends: on the side of the end-effector, and for the haptic feedback to the user. The adjustable elasticity is based on the same principle as tactile systems. For generating forces, a force source is necessary. A new "electronic controlled force and stiffness" actuator (ECFS) is used for this application. The schematic design is shown in Fig. 9.77. It is an actuator according to the inchworm principle, wherein both brakes are realized by the ER-fluid surrounding it. The driving component for the forward and backward movement is realized by two electromagnets. Both actuators are assembled within a haptic

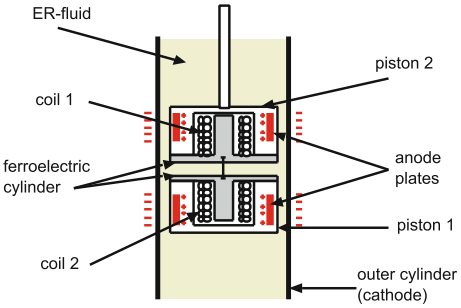

Fig. 9.77 Schematic setup of an ERF-Inchworm motor [6]

exoskeleton. They are mounted on the rim of a glove to conserve the mobility of the hand. With the actuators in between all finger-joints, arbitrary forces and varying elasticities can be simulated independently. The ECFS actuators are operated at voltages of 2 kV and generate a force of up to 50 N.

9.6 Special Designs of Haptic Actuators

Thorsten A. Kern, Christian Hatzfeld

The actuation principles discussed so far are the most common approaches to the actuation of haptic devices. Besides these principles, there are numerous research projects, singular assemblies, and special classes of devices. The knowledge of these designs is an enrichment for any engineer, yet it is impossible to completely cover all the haptic designs in a single book. This section, nevertheless, intends to give a cross section of alternative, quaint, and unconventional systems for generating kinaesthetic and tactile impressions. This cross section is based on the authors' subjective observations and knowledge and does not claim to be exhaustive. The discussed systems have been selected, as examples suited best to cover one special class of systems and actuators, each. They are neither the first systems of their kind, nor necessarily the best ones. They are thought to be crystallization points of further research, if specific requirements have to be chosen for special solutions. The systems shown here are meant to be an inspiration and an encouragement not to discard creative engineering approaches to the generation of haptic impressions too early during the design process.

9.6.1 Haptic-Kinaesthetic Devices

Haptic-kinaesthetic devices of this category excel primarily due to their extraordinary kinematics and not to very special actuation principles. Nevertheless, every engineer may be encouraged to be aware of the examples of this device class and let this knowledge influence his/her own work.

9.6.1.1 Rope-Based Systems

With rope-based systems, actuators and the point of interaction are connected with ropes, i.e., mechanical elements that can only convey pulling forces. They are especially suited for lightweight systems with large working spaces, as for example simulation of assembly tasks, rehabilitation, and training. VON ZITZEWITZ describes the use of rope-based systems for sport simulation and training (tennis and rowing) as well as an experimental environment to investigate vestibular stimulation in sleeping subjects [131].

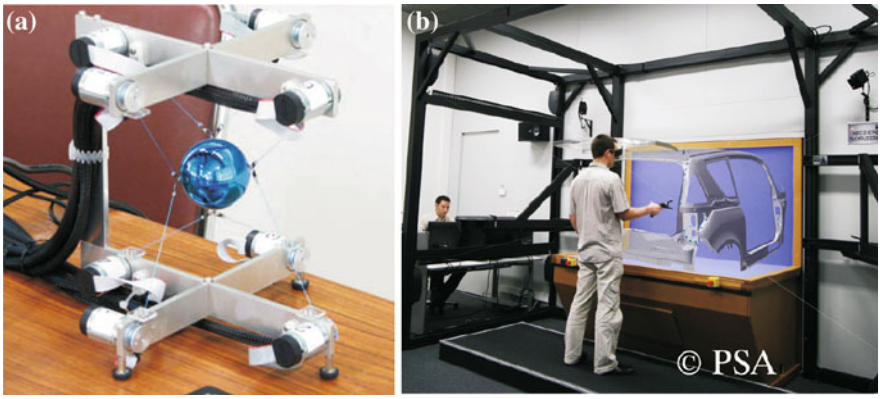

Fig. 9.78 **a** Desktop version of the Spidar with ball-like interaction handle, **b** room-size version INCA 6D with 3D visualization environment by *Haption*

Another system, the Spidar (Fig. 9.78) is based on the work of SATO and has frequently been used in research projects [92, 117] as well as in commercial systems. It is composed of an interaction handle—usually a ball—held by eight strings. Each string is operated by an actuator, which is frequently (but not obligatorily) mounted in the corners of a rectangular volume. The drives are able to generate pulling forces on the strings, enabling the generation of forces and torques in six DoFs on the handle. Typically, the actuators used are based on electrodynamic electronic-commutated units. The Spidar system can be scaled to almost any size, ranging from table-top devices to room-wide installations. It convinces by the small number of mechanical components and the very small friction. As strings are able to provide pull forces only, it is worth noting that just two additional actuators are sufficient to compensate this disadvantage.

9.6.1.2 Screw-and-Cable System

In several projects relating to medical rehabilitation and master slave teleoperation, the CEA-LIST Interactive Robotics Unit use their screw-and-cable system (SCS) shown in a first prototype in 2001 [32, 34–36]. In this prototype six, screw-cable actuators are used to motorize a master arm in a teleoperation system enabling high-fidelity force feedback. In the meantime, the master arm is commercialized by *Haption S.A.* under the name VIRTUOSE 6D 4040 [44]. The patented SCS basic principle can be seen in Fig. 9.79.

A rotative joint is driven by a standard push–pull cable. On one side, the cable is driven by a ball screw that translates directly in its nut (the screw is locked in rotation thanks to rollers moving into slots). The nut is rotating in a fixed bearing and is driven by the motor thanks to a belt transmission [36].

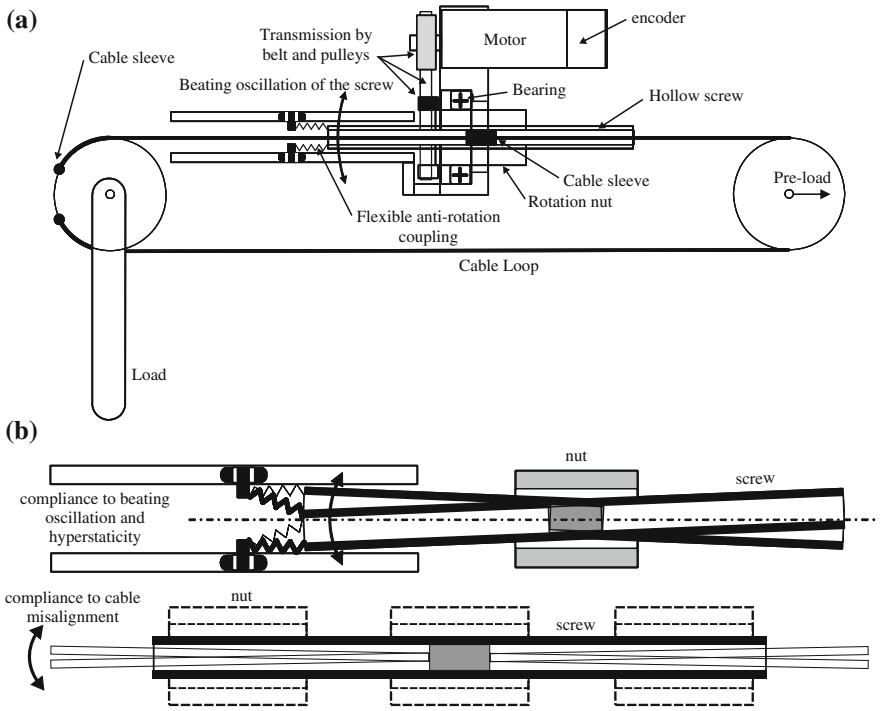

Fig. 9.79 SCS basic principles: **a** driving unit **b** and particular patented mounting [32]. Figure courtesy of *CEA-LIST*

Using SCS allows significantly mass and volume-reduced driving units for joint torque control. The low friction threshold and high backdrivability enable true linear torque control without a sensor, avoiding drift and calibration procedure. Low inertia of the structure leads to high transparency. In the upper-limb exoskeleton ABLE 4D, the SCS is embedded in the moving parts of the arm, resulting in reduced cable length and simplified routing (see Fig. 9.80). The two SCS integrated in the arm module perform alike artificial electrical muscles. Further information about the design of such systems can be found in [33].

9.6.1.3 Magnetorheological Fluids as Three-Dimensional Haptic Display

The wish to generate an artificial haptic impression in a volume for free interaction is one of the major motivations for many developments. The rheological systems shown in Sect. 9.5 provide one option to generate such an effect. For several years, the team of BICCHI has been working on the generation of spatially resolved areas of differing viscosity in a volume (Fig. 9.81) to generate force feedback on an exploring hand. Lately, the results were summarized in [11]. The optimization of such actuators

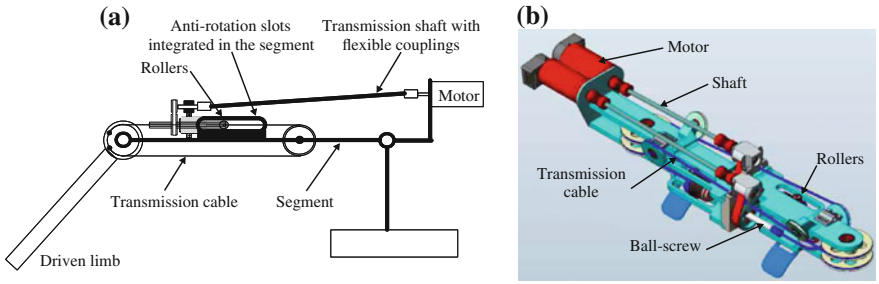

Fig. 9.80 ABLE arm module: **a** optimized architecture to be integrated, **b** structure with its 2 integrated actuators [32]. Figure courtesy of *CEA-LIST*

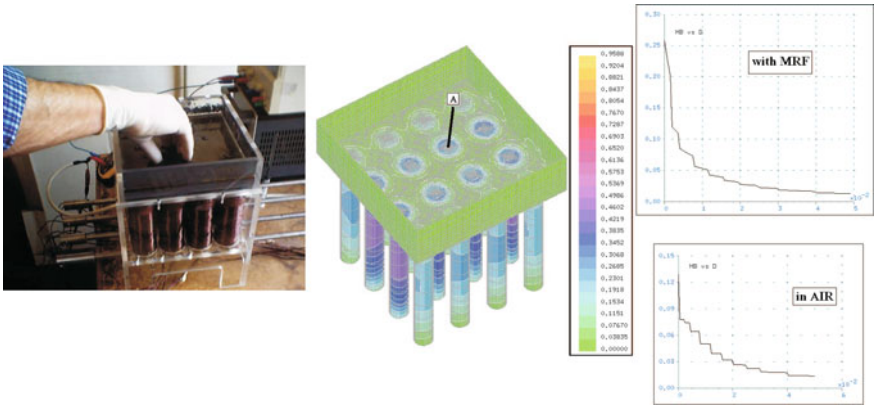

Fig. 9.81 Magnetorheological actuation principle for full-hand interaction based on a 4 × 4 pattern [11]

is largely dependent on the control of the rheological fluid [10]. The psycho-physical experiments performed until today show that the identification of simple geometrical structures can be achieved on the basis of a 4×4 pattern inside the rheological volume.

9.6.1.4 Self-induction and Eddy Currents as Damping

An active haptic device is designed to generate forces, resp., torques in any direction. By the concept of "active" actuation, the whole spectrum of mechanical interaction objects (e.g., masses, springs, dampers, other force sources like muscles, and moving objects) is covered. Nevertheless, only a slight portion of haptic interaction actually is "active." This has the side effect (of control-engineering approaches) that active systems have continuously to be monitored for passivity. An alternative approach to the design of haptic actuators is given by choosing technical solutions able to dissipate mechanical energy. A frictional brake would be such a device, but its properties are

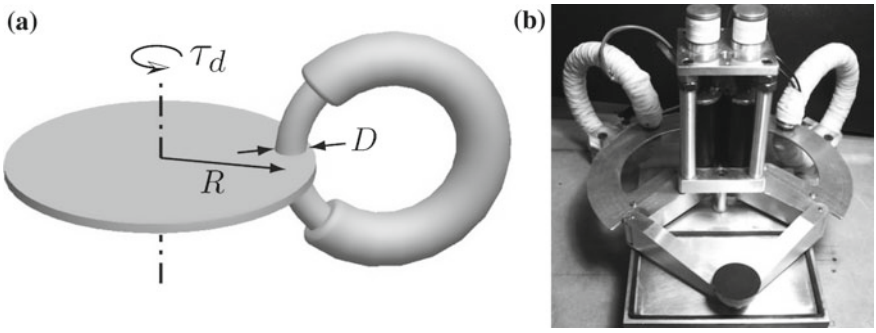

Fig. 9.82 Principle of eddy currents damping a rotating disk (**a**) and realization as a haptic device (**b**) by [41]

strongly nonlinear and hard to control. Alternatives are therefore highly interesting. The team of COLGATE showed in [86] how to increase the impedance of an electronic-commutated electrodynamic actuator, whereby two windings were bypassed by a variable resistor. The mutual induction possible by this bypass damped the motor significantly. In [41], the team of HAYWARD went further by implementing an eddy current break into a pantograph-kinematics (Fig. 9.82). This break is a pure damping element with almost linear properties. By this method, a controlled dynamic damping up to 250 Hz was achieved.

9.6.1.5 Serial Coupled Actuators

Serial coupled actuators include an additional mechanical coupling element between actuator and the driven element of the system. In the majority of cases, this is an elastic element that was originally inserted to ease force control of actuators interacting with stiff environments [138]. These so-called serial elastic actuators allow the replacement of direct force control by the position control of both sides of the series elasticity and are used in applications like rehabilitation or man–machine interaction [104]. An example is shown in Fig. 9.83. For haptic applications, this configuration is especially interesting for the display of null-forces and null-torques, i.e., free space movements.

Another application of serial coupled actuators was introduced by MOHAND- OUSAID ET AL. To increase dynamics, lower the impact of inertia and increase transparency, a serial arrangement of two actuators connected with an viscous coupler based on eddy currents was presented in [88] and is shown in Fig. 9.84. By using two motors, the range of displayable forces/torques can be extended, because of the low inertia of the smaller motor higher dynamics can be archived. The viscous clutch couples slip velocity to transmitted torque that is used in the control of the device. With this approach, inertia is decoupled from the delivered torque effectively.

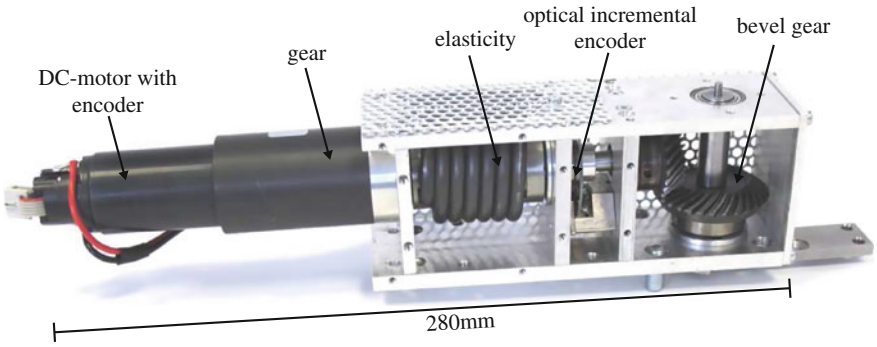

Fig. 9.83 Example for the realization of a serial elastic actuator for use in an active knee orthesis [104]. The bevel gear is needed for better integration of the actuator near the knee of the wearer. Picture courtesy of Roman Müller, Institute of Electromechanical Design, Technische Universität Darmstadt

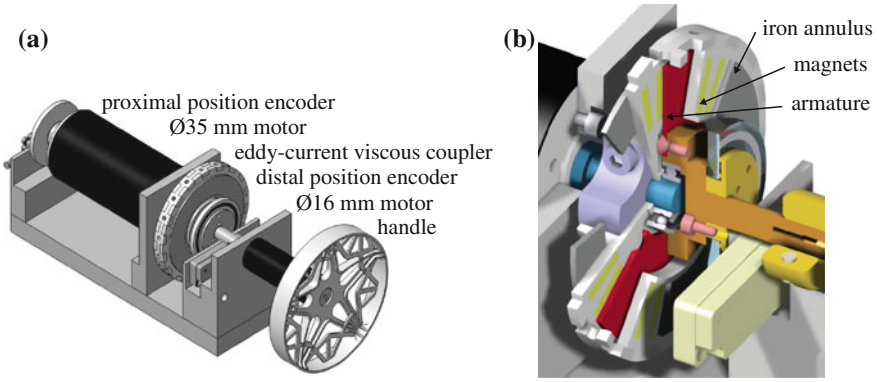

Fig. 9.84 Setup with two serial actuators coupled with an eddy current clutch as presented in [88]

9.6.1.6 MagLev: Butterfly Haptics

In the 1990s, the team of HOLLIS developed a haptic device [9] based on the electrodynamic actuation principle (Fig. 9.85). Since recently, the device has been sold commercially by *Butterfly Haptics*. It is applied to ongoing research projects on psychophysical analysis of texture perception. Six flat coils are mounted in a hemisphere with a magnetic circuit each. The combination of LORENTZ forces of all coils allows an actuation of the hemisphere in three translational and three rotational directions. Via three optical sensors—each of them measuring one translation and one rotation—the total movement of the sphere is acquired. Besides the actuation within its space, the control additionally includes compensation of gravity with the aid of all six actuators. This function realizes a bearing of the hemisphere with Lorentz forces, only. The air-gap of the coils allows a translation of 25 mm and a rotation of $\pm 8°$ in each

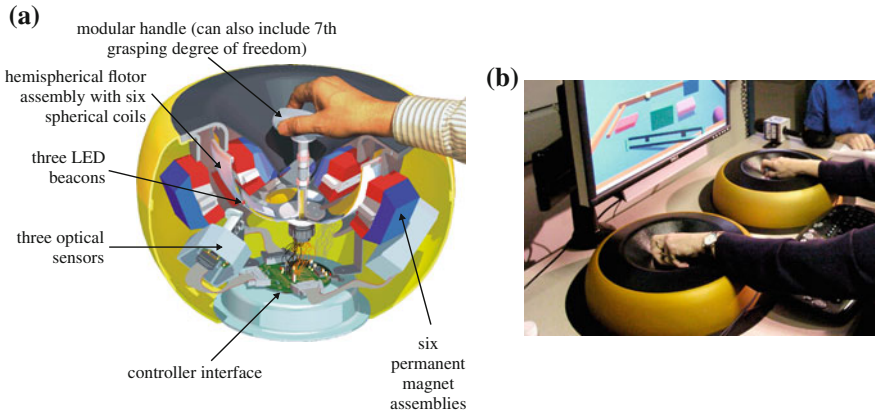

Fig. 9.85 MAGLEV device, **a** inner structure, **b** use of two devices in bimanual interaction. Images courtesy of *Butterfly Haptics, LLC*, Pittsburgh, PA, USA.

direction. Resolutions of 2 µm (1σ) and stiffnesses of up to 50 N mm^{-1} can be reached. As a consequence of the small mass of the hemisphere, the electrodynamic actuator principle as a drive and the abandonment of mechanical bearings, forces of a bandwidth of 1 kHz can be generated.

9.6.2 Haptic-Tactile Devices

Haptic-tactile devices of this category are intelligent combinations of well-known actuator principles of haptic systems with either high position resolutions or extraordinary, dynamic properties.

9.6.2.1 Pneumatic

Due to their working principle, pneumatic systems are a smart way to realize flexible high-resolution tactile displays. But these systems suffer acoustic compliance, low dynamics, and the requirement of pressurized air. A one-piece pneumatically actuated tactile 5×5 matrix molded from silicone rubber is described in [90, 91]. The spacing is 2.5 mm with 1-mm-diameter tactile elements. Instead of actuated pins, an array of pressurized chambers without chamber leakage and seal friction is used (see Fig. 9.86). 25 solenoid 3-way valves are used to control the pressure in each chamber resulting in a working frequency of 5 Hz. Instead of closed pressurized chambers, the direct contact between the fingertip and the compressed air is used for tactile stimulation in [2]. The interface to the skin consists of channels each 2 mm in diameter. A similar display is shown in [82]. Using negative air pressure, the tactile stimulus is generated by suction through 19 channels 2.5 mm in diameter with 5 mm intervals.

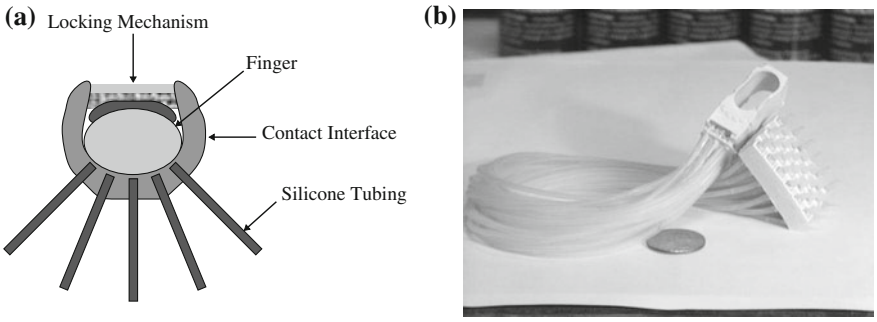

Fig. 9.86 Pneumatic actuated tactile display: sketch (**a**) bidigital teletaction and realization (**b**) [91]

9.6.2.2 Thermopneumatic

A classic problem of tactile pin arrays is given by the high density of stimulator points to be achieved. The space below each pin for control and reconfiguration of the pin's position is notoriously finite. Consequently, a large number of different designs have been tested till date. In [128], a thermopneumatic system is introduced (Fig. 9.87) based on tubes filled with a fluid (methyl chloride) with a low boiling point. The system allows a reconfiguration of the pins within 2 s. However, it has high power requirements, although the individual elements are cheap.

9.6.2.3 Shape-Memory Materials

Materials with shape-memory property are able to remember their initial shape after deformation. When the material is heated up, its internal structure starts to change

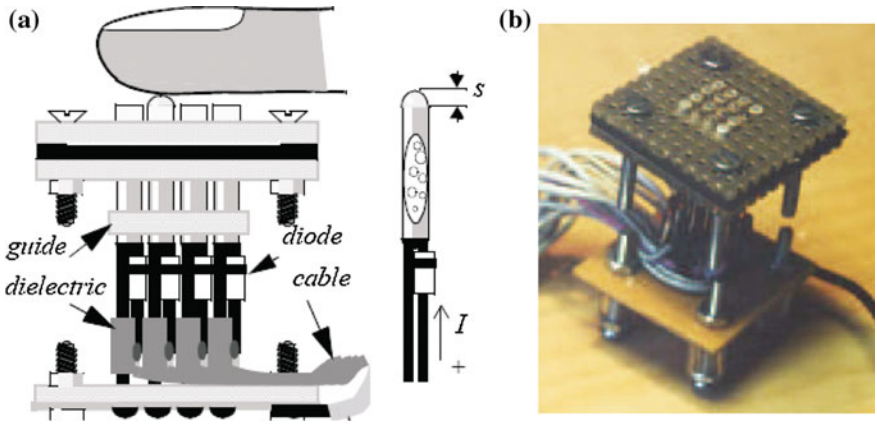

Fig. 9.87 Thermopneumatic actuation principle in a schematic sketch (**a**) and as actual realization (**b**) [128]

and the materials forms back in its pre-deformed state. Due to the material intrinsic actuating effect, high-resolution tactile displays are achievable. The low driving frequencies caused by thermal inertia and needed heating and/or cooling systems are the drawback of this technology.

Shape-Memory Alloys

In [120], a pin array with 64 elements is realized covering an area of $20 \times 40\,\text{mm}^2$. The display consists of 8 modules, each containing eight dots (see Fig. 9.88). Each element comprises a 120 mm length NiTi SMA wire pre-tensioned by a spring. When an electrical current flows through the wire, it heats up and starts to shorten. The result is a contraction of up to 5 mm. Driving frequencies up to a few Hz using a fan to cool the SMA wires down can be reached.

Bistable Electroactive Polymers

Bistable electroactive polymers (BSEP) combine the large-strain actuation of dielectric elastomers with shape-memory properties. The BSEP provide bistable deformation in a rigid structure. These polymers have a glass transition temperature T_g slightly above ambient temperature. Heated above T_g, it is possible to actuate the materials like a conventional dielectric elastomer.

Using a chemically cross-linked poly(tert-butyl acrylate) (PTBA) as BSEP, a tactile display is presented in [94]. The display contains a layer of PTBA diaphragm-actuators and an incorporated heater element array. Figure 9.89 shows the fabricated refreshable Braille display device the size of a smartphone screen.

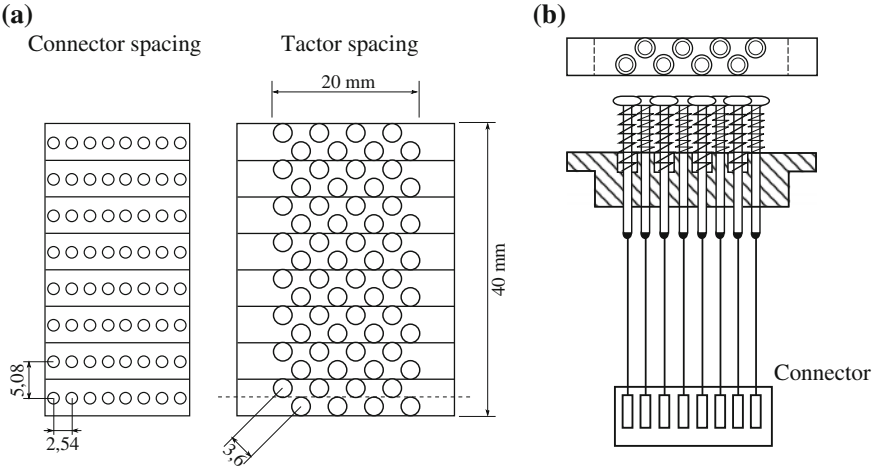

Fig. 9.88 Sketch of tactile display using SMA: Top view (**a**) and side view of one module (**b**) [120]

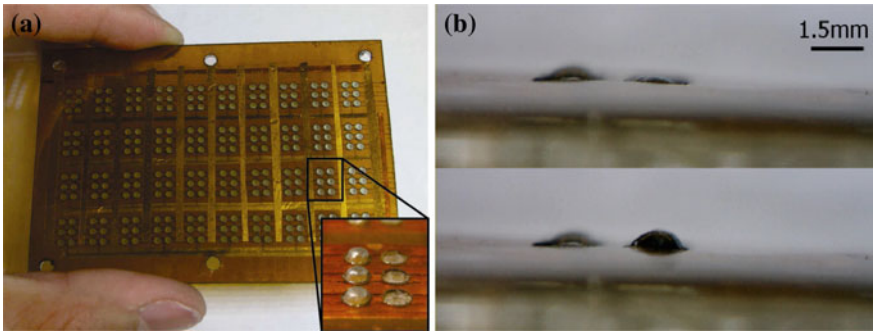

Fig. 9.89 Bistable BSEP Braille display: actuator array (**a**) [94], and zoom of Braille dots in "OFF"? and "ON"? state (**b**) [93]

9.6.2.4 Texture Actuators

Besides an application in Braille-related tasks, the design of tactile displays is also relevant for texture perception. Instead of vibrotactile stimulation on a user's finger, the modification of the friction between a sliding finger and a touchscreen surface is a promising new direction in touchscreen haptics. These kinds of displays are based on two basic technologies. In displays based on the electrovibration effect, a periodic electrical signal is injected into a conductive electrode coated with a thin dielectric layer. The result is an alternating electrostatic force that periodically attracts and releases the finger, producing friction-like rubbery sensations as mentioned in Sect. 9.5.2.4.

In friction displays based on the squeeze film effect, a thin cushion of air under the touching finger is created by a layer placed on top of the screen and is vibrated at an ultrasonic frequency. The modulation of the frequency and intensity of vibrations allows to put the finger touching the surface in different degrees of levitation, thus actually affecting the frictional coefficient between the surface and the sliding finger [68] (Fig. 9.90).

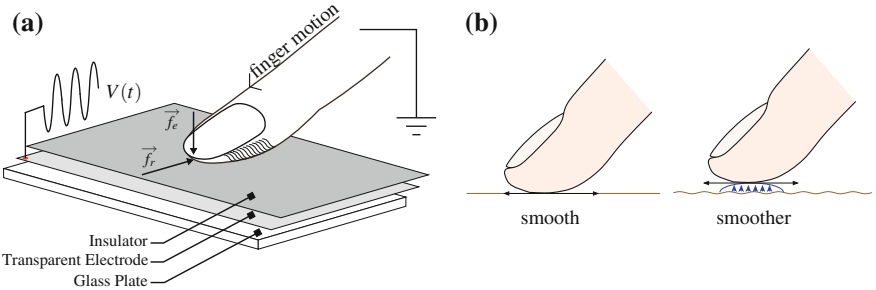

Fig. 9.90 Basic principles of friction tactile displays: **a** Electrovibration effect [7] and **b** squeeze film effect as shown in [20]

In 2007, WINFIELD impressively demonstrated a simple tactile texture display called TPAD based on the squeeze film effect. The actuating element is a piezoelectric bending disk driven in resonance mode [139]. By aid of an optical tracking right above the disk, and with a corresponding modulation of the control signal, perceivable textures with spatial resolutions were generated. The 25-mm-diameter piezoelectric disk is bonded to a 25-mm-diameter glass disk and supported by an annular mount (Fig. 9.91).

A similar display with an increased surface area of $57 \times 76\,\text{mm}^2$ is shown in [83]. The vibrations are created by piezoelectric actuators bonded along one side of a glass plate placed on top of an LCD screen.

9.6.2.5 Flexural Waves

A transparent display providing localized tactile stimuli is presented in [53]. The working principle is based on the concept of computational time reversal and is able to stimulate one or several regions, and hence several fingers, independently. According to the wave propagation equation, the direct solution of a given propagation problem is a diverging wave front and a converging wave front for the time reversed one if the initial condition is an impulse force. Consequently, it is possible to generate peaks of deflection localized in space and in time using constructive interference caused by a multiple of stimulating actuators. Of course, the quality of the focusing process is increasing with the number of transducers and has to be optimized. Depending on the requirements, the noise occurring at the passive areas might be reduced below the tactile perception threshold.

The display shown in Fig. 9.92 consists of a glass sheet with the dimensions of $63 \times 102\,\text{mm}^2$ and 0.2 mm in thickness bonded to a rigid supporting frame at its edges. The used transducers are piezoelectric diaphragms (Murata 7BB-12-9) with a diameter of 12 mm and a thickness of 0.12 mm.

Relating to their patented bending wave technology, the company *Redux Laboratories offers* electromagnetic transducers for medium and large applications as well as piezo-exciters for small form factor applications such as mobile devices (see Fig. 9.93).

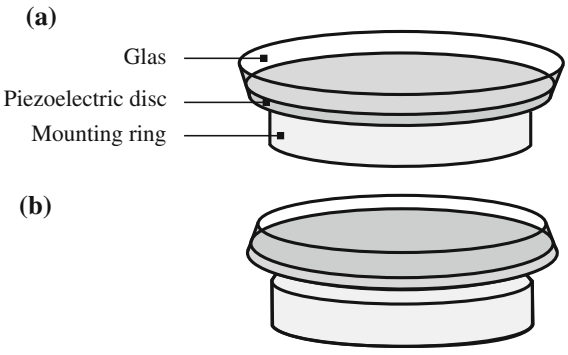

Fig. 9.91 Schematic view of the T-PaD with convex (**a**) and concave (**b**) oscillation states: Piezoelectric disk underneath a glass substrate modulates the friction between finger and display based on the position of the finger and the model of the simulated texture. Figure based on [22]

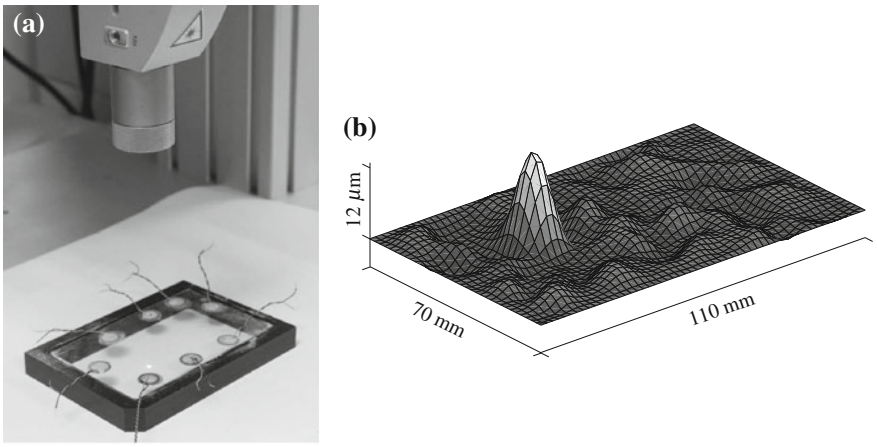

Fig. 9.92 Tactile display using flexural waves: display during characterization with laser vibrometer (**a**) and reconstructed experimental out of plane displacement at focus time without finger load (**b**) [53]

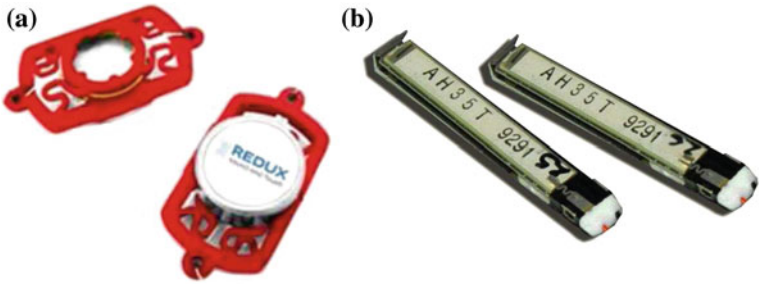

Fig. 9.93 *Redux* transducers for bending wave technology: Moving-coil exciters (**a**), and multi-layered piezos (**b**) [106]

9.6.2.6 Volume-Ultrasonic Actuator

IWAMOTO built tactile displays (Fig. 9.94) that are made of piezoelectric actuators and are actuated in the ultrasonic frequency range. They use sound pressure as a force transmitter. The underlying principle is given by generating a displacement of the skin and a corresponding haptic perception by focused sound pressure. Whereas in the first realization an ultrasonic array had been used to generate tactile dots in a fluid [60], later developments used the air for energy transmission [59]. The pressures generated by the designs (Fig. 9.94) provide a weak tactile impression, only. But

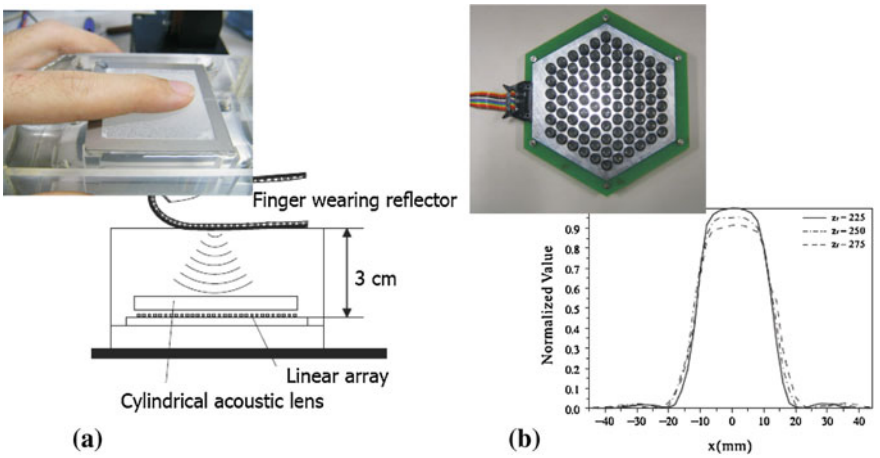

Fig. 9.94 Tactile display based on ultrasonic sound pressure transmitted by a fluid [60] (**a**) or as array of senders for a transmission in the air [59] (**b**)

especially the air-based principle works without any mechanical contact and could therefore become relevant for completely new operation concepts combined with gesture recognition.

9.6.2.7 Ungrounded Haptic Displays

In case of the interaction with large virtual worlds, it is frequently necessary to design devices that are worn on the body, i.e., that do not exhibit a fixed ground connection. An interesting solution has been shown in [123], generating a tactile sensation with belts at the palm and at each finger. The underlying principle is based on two actuators for each belt, generating a shear force to the skin when operated in the same direction, and a normal force when operated in the opposite direction. This enables to provide tactile effects when grasping or touching objects in a virtual world, but without the corresponding kinaesthetic effects.

Other realizations of ungrounded devices include the use of gyro effects and the variation of angular momentum and designs incorporating nonlinear perception properties of the human user as presented in [113]. The device shown in Fig. 9.95 is based on the display of periodical steep inertial forces generated by a spring-mass system and an electrodynamic voice-coil actuator.

9.6.2.8 Electrotactile

As haptic receptors can be stimulated electrically, it is not far-fetched to design haptic devices able to provide low currents to the tactile sense organs. The design

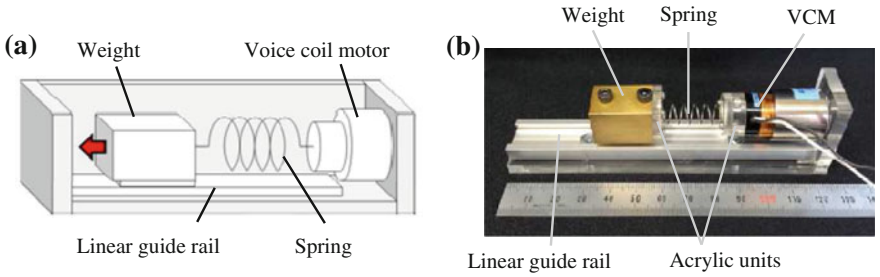

Fig. 9.95 Ungrounded haptic display to convey pulling impressions as shown in [113] **a** scheme , **b** realization

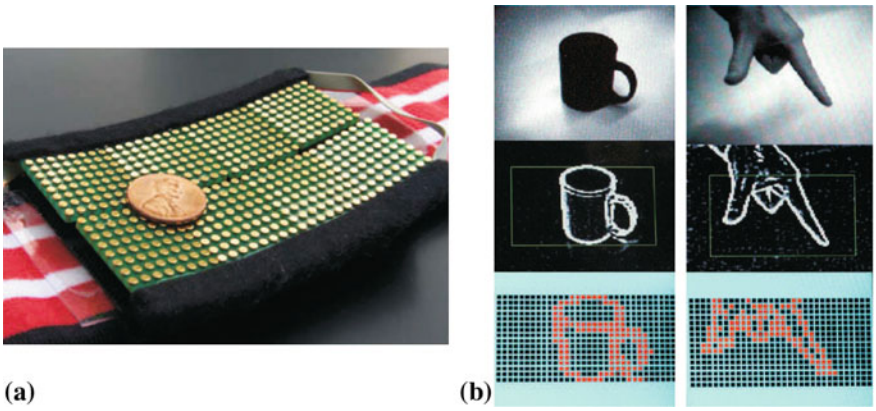

Fig. 9.96 Electrotactile display worn on the forehead: Electrodes (**a**) and edge recognition and signal conditioning principle (**b**) [64]

of such devices can be traced back to the 1970s. One realization is presented in [64] (Fig. 9.96). Electrotactile displays do work—no doubt—however, they have the disadvantage also to stimulate noci-receptors for pain sensation besides the mechano-receptors. Additionally, the electrical conductivity between display and skin is subject to major variations. These variations are inter-person differences due to variations in skin thickness, but they are also a time-dependent result of electrochemical processes between sweat and electrodes. The achievable tactile patterns and the abilities to distinguish tactile patterns are subject to current research.

Recommended Background Reading

[3] Ballas, R.: **Piezoelectric multilayer beam bending actuators: static and dynamic behavior and aspects of sensor integration**. Springer, 2007.
Dynamic modeling of piezoelectric bimorph actuators based on concentrated and distributed network elements.

[52] Huber, J.; Fleck, N. & Ashby, M.: **The Selection of Mechanical Actuators Based on Performance Indices**. In: Proceedings of the Royal Society of London. Series A: Mathematical, Physical and Engineering Sciences, 1997.
Analysis of several performance indices for different actuation principles.

[65] Kallenbach, E.; Stölting, H.-D. & Amrhein, W. (Eds.): **Handbook of Fractional-Horsepower Drives**. Springer, Heidelberg, 2008.
Overview about the most common fractional horsepower actuators and transmissions with focus on the design parameters.

References

1. Ahmadkhanlou F (2008) Design, modeling and control of magnetorheological fluid-based force feedback dampers for telerobotic systems. In: Proceedings of the Edward F. Hayes graduate research forum. http://hdl.handle.net/1811/32023
2. Asamura N, Yokoyama N, Shinoda H (1998) Selectively stimulating skin receptors for tactile display. IEEE Comput Graph Appl 18(6):32–37. ISSN: 02721716. doi:10.1109/38.734977. (Visited on 02/09/2014)
3. Ballas R (2007) Piezoelectric multilayer beam bending actuators: static and dynamic behavior and aspects of sensor integration. Springer, Berlin, pp XIV, 358. ISBN: 978-3-540-32641-0
4. Bar-Cohen Y (2001) Electroactive polymer (EAP) actuators as artificial muscles–reality, potential, and challenges. SPIE Press monograph, vol 98. SPIE Press, Bellingham, pp XIV, 671. ISBN: 0-8194-4054-x
5. Bar-Cohen Y (2006) Biomimetics–biologically inspired technologies. CRC, Taylor und Francis, Boca Raton, pp XVIII, 527. ISBN: 0-8493-3163-3
6. Bar-Cohen Y et al (2001) Virtual reality robotic telesurgery simulations using MEMICA haptic system. In: 8th annual international symposium on smart structures and material—EAPAD. doi:10.1117/12.432667
7. Bau O et al (2010) TeslaTouch: electrovibration for touch surfaces. In: Proceedings of the 23nd annual ACM symposium on user interface software and technology (UIST '10). ACM, New York, pp 283–292. doi:10.1145/1866029.1866074
8. Belford JD The stepped horn–Technical Publication TP-214. Technical report http://www.morganelectroceramics.com/resources/technical-publications/
9. Berkelman PJ, Butler ZJ, Hollis R L (1996) Design of a hemispherical magnetic levitation haptic interface device. In: ASME (ed) ASME international mechanical engineering congress and exposition., pp 483–488. http://www.ri.cmu.edu/pub_files/pub1/berkelman_peter_1996_1/berkelman_peter_1996_1.pdf
10. Bicchi A et al. (2005) Analysis and design of an electromagnetic system for the characterization of magnetorheological fluids for haptic interfaces. IEEE Trans Magn 41(5). Interdepartmental Res. Centre, Pisa University, Italy, pp 1876–1879. doi:10.1109/TMAG.2005.846280
11. Bicchi A (2008) The sense of touch and its rendering—progress in haptics research, vol 45. Springer tracts in advanced robotics. Springer, Berlin, pp XV, 280. ISBN: 9783540790341

12. Biet et al M (2006) A piezoelectric tactile display using travelling lamb wave. In: Proceedings of eurohaptics. Paris, pp 989–992
13. Blume H-J, Boelcke R (1990) Mechanokutane Sprachvermittlung, vol 137. Reihe 10 137. Düsseldorf: VDI-Verl. ISBN: 3-18-143710-7
14. Böse H, Trendler A (2003) Smart fluids–properties and benefit for new electromechanical devices. In: AMAS workshop SMART'03. pp 329–336. http://publica.fraunhofer.de/documents/N-51527.html
15. Böse H et al. (2004) A new haptic sensor-actuator system based on electrorheological fluids. In: Actuator 2004: 9th international conference on new actuators. HVG Hanseatische Veranst. GmbH, Div. Messe Bremen, pp 300–303. doi:10.1016/S0531-5131(03)00443--6
16. Brissaud M (1991) Characterization of piezoceramics. IEEE Trans Ultrason Ferroelectr Freq Control 38(6):603–617. doi:10.1109/58.108859
17. Brochu P, Pei Q (2010) Advances in dielectric elastomers for actuators and artificial muscles. Macromol Rapid Commun 31(1):10–36. doi:10.1002/marc.200900425. (Visited on 04/03/2012)
18. Carlson JD, Stanway R, Johnson AR (2004) Electro-rheological and magneto-rheological fluids: a state of the art report. In: Actuator 2004: 9th international conference on new actuators. HVG Hanseatische Veranst.-GmbH, Div. Messe Bremen, Bremen, pp 283–288
19. Carpi F, Frediani G, De Rossi D (2012) Electroactive elastomeric actuators for biomedical and bioinspired systems. In: IEEE, June 2012, pp 623–627. doi:10.1109/BioRob.6290761. (Visited on 02/26/2014)
20. Casiez G et al. (2011) Surfpad: riding towards targets on a squeeze film effect. In: Proceedings of the SIGCHI conference on human factors in computing systems. ACM Press, New York, p 2491. doi:10.1145/1978942.1979307
21. Chapuis D, Michel X (2007) A haptic knob with a hybrid ultrasonic motor and powder clutch actuator. In: Michel X, Gassert R (eds) Euro haptics conference, 2007 and symposium on haptic interfaces for virtual environment and teleoperator systems. World Haptics 2007. Second Joint. pp 200–205. doi:10.1109/WHC.2007.5
22. Colgate JE, Peshkin M (2009) Haptic device with controlled traction forces. 8525778:B2
23. Conrad H, Fisher M, Sprecher AF (1990) Characterization of the structure of a model electrorheological fluid employing stereology. In: Proceedings of the 2nd international conference on electrorheological fluids
24. Deng K, Enikov E, Zhang H, (2007) Development of a pulsed electromagnetic micro-actuator for 3D tactile displays. In:(2007) IEEE/ASME international conference on advanced intelligent mechatronics. University of Arizona, Tucson, pp 1–5. doi:10.1109/AIM.2007.4412457
25. Doerrer C (2004) Entwurf eines elektromechanischen Systems für flexibel konfigurierbare Eingabefelder mit haptischer Rückmeldung". PhD thesis. Technische Universität Darmstadt, Institut für Elektromechanische Konstruktionen. http://tuprints.ulb.tu-darmstadt.de/435/
26. Dr. Fritz Faulhaber GmbH & Co. KG. Technical Informations. Tech. rep. 2013. www.faulhaber.com
27. Eisner E (1966) Complete solutions of the 'Webster' horn equation. J Acoust Soc Am 41(4B):1126–1146. doi:10.1121/1.1910444
28. El Wahed AK et al (2003) An improved model of ER fluids in squeeze-flow through model updating of the estimated yield stress. J Sound Vibr 268(3):581–599. doi:10.1016/S0022-460X(03)00374-2
29. Fernandez JM, Perriard Y (2003) Comparative analysis and modeling of both standing and travelling wave ultrasonic linear motor. In: IEEE ultrasonic symposium, pp 1770–1773. doi:10.1109/ULTSYM.2003.1293255
30. Fleischer M, Stein D, Meixner H (1989) Ultrasonic piezomotor with longitudinally oscillating amplitude-transforming resonator. IEEE Trans Ultrason Ferroelectr Freq Control 36(6):607–613. doi:10.1109/58.39110
31. Flueckiger M et al. (2005) fMRI compatible haptic interface actuated with traveling wave ultrasonic motor. In: Industry applications conference, 2005. Fortieth IAS annual meeting. Conference record of the 2005, vol 3. pp 2075–2082. ISBN: 0197-2618, doi:10.1109/IAS.2005.1518734

32. Garrec P (2010) Design of an anthropomorphic upper limb exoskeleton actuated by ballscrews and cables. In: University politecnicae of bucharest. Sci Bull D Mech Eng 72(2):23–34. ISSN 1454–2358. http://www.scientificbulletin.upb.ro/rev_docs_arhiva/full9662.pdf
33. Garrec P (2010) Screw and cable actuators SCS and their applications to force feedback teleoperation, exoskeleton and anthropomorphic robotics. In: Abdellatif H (ed) Robotics 2010 current and future challenges. InTech. ISBN: 978-953-7619-78-7. http://www.intechopen.com/download/get/type/pdfs/id/9370 (Visited on 02/09/2014)
34. Garrec P et al. (2006) A new force-feedback, morphologically inspired portable exoskeleton. In: IEEE, pp 674–679. doi:10.1109/ROMAN.2006.314478. (Visited on 02/09/2014)
35. Garrec P et al (2007) Evaluation tests of the telerobotic system MT200-TAO in AREVA NC La Hague hot cells. In: Proceedings of ENC, Brussels. http://www-ist.cea.fr/publicea/exldoc/200800002158.pdf
36. Garrec P et al. (2008) ABLE, an innovative transparent exoskeleton for the upper-limb. In: IEEE, pp 1483–1488. doi:10.1109/IROS.2008.4651012. (Visited on 02/09/2014)
37. Ghoddsi R et al (1996) Development of a tangential tactor using a LIGA/MEMS linear microactuator technology microelectromechanical system (MEMS). In: Microelectromechanical system (MEMS), DSC, vol 59. Atlanta, pp 379–386. ISBN: 978-0791815410
38. Giraud F, Giraud F, Semail B (2004) Analysis and phase control of a piezoelectric travelingwave ultrasonic motor for haptic stick application. In: Semail B, Audren J-T (eds) IEEE Transactions on industry applications, vol 40(6), pp 1541–1549. doi:10.1109/TIA.2004.836317
39. Giraud F, Lemaire-Semail B, Martinot F (2006) A force feedback device actuated by piezoelectric travelling wave ultrasonic motors. In: ACTUATOR 2006, 10th international conference on new actuators. pp 600–603. ISBN: 9783933339089
40. Gong X et al (2008) Influence of liquid phase on nanoparticle-based giant electrorheological fluid. Nanotechnol 19(16):165602. doi:10.1088/0957-4484/19/16/165602
41. Gosline AH, Campion G, Hayward V (2006) On the use of eddy current brakes as tunable, fast turn-on viscous dampers for haptic rendering. In: Eurohaptics conference. Paris, pp 229–234. http://www.cirmmt.org/research/bibliography/GoslineEtAl2006
42. Hagedorn P et al (1998) The importance of rotor flexibility in ultrasonic traveling wave motors. Smart Mater Struct 7:352–368. doi:10.1088/0964-1726/7/3/010
43. Hagood NW, McFarland AJ (1995) Modeling of a piezoelectric rotary ultrasonic motor. IEEE Trans Ultrason Ferroelectr Freq Control 42(2):210–224. doi:10.1109/58.365235
44. Haption SA (2014) http://www.haption.com/ (visited on 02/19/2014)
45. Hayward V, Cruz-Hernandez M (2000) Tactile display device using distributed lateral skin stretch. In: Wikander J (ed) Symposium on haptic interfaces for virtual environment and teleoperator systems, IMECE 2000 conference. http://www.cim.mcgill.ca/jay/index_files/research_files/VH-MC-HAPSYMP-00.pdf
46. He S et al (1998) Standing wave bi-directional linearly moving ultrasonic motor. IEEE Trans Ultrason Ferroelectr Freq Control 45(5):1133–1139. doi:10.1109/58.726435
47. Helin P et al (1997) Linear ultrasonic motors using surface acoustic waves mechanical model for energy transfer. In: Solid state sensors and actuators, TRANSDUCERS '97 Chicago., 1997 international conference on, vol 2. Chicago, IL, pp 1047–1050, 16–19 June 1997. doi:10.1109/SENSOR.1997.635369
48. Heydt R, Chhokar S (2003) Refreshable braille display based on electroactive polymers. In: 23rd international display research conference, pp 111–114
49. Hirata H, Ueha S (1995) Design of a traveling wave type ultrasonic motor. IEEE Trans Ultrason Ferroelectr Freq Control 42(2):225–231. doi:10.1109/58.365236
50. Hu M et al (2005) Performance simulation of traveling wave type ultrasonic motor. In: Proceedings of the eighth international conference on electrical machines and systems, 2005. ICEMS 2005, vol 3. pp 2052–2055, 27–29 Sept 2005. ISBN: 7-5062-7407-8. doi:10.1109/ICEMS.2005.202923
51. Huang X et al (2007) Formation of polarized contact layers and the giant electrorheological effect. Int J Mod Phy B (IJMPB) 21(28/29):4907–4913. doi:10.1142/S0217979207045827

52. Huber J, Fleck N, Ashby M (1997) The selection of mechanical actuators based on performance indices. In: Proceedings of the Royal Society of London. Series A: Mathematical, physical and engineering sciences, vol 453. 1965, pp 2185–2205. doi:10.1098/rspa.1997.0117
53. Hudin C, Lozada J, Hayward V (2013) Localized tactile stimulation by time-reversal of flexural waves: case study with a thin sheet of glass. In: IEEE, pp 67–72. doi:10.1109/WHC.2013.6548386
54. HyperBraille. http://hyperbraille.de/ (visited on 02/09/2014)
55. IEEE (1988) Standard on piezoelectrity. doi:10.1109/IEEESTD.1988.79638
56. Ikeda T (1990) Fundamentals of piezoelectricity. Oxford University Press, Oxford, pp XI, 263. ISBN: 0-19-856339-6
57. Ikei Y, Ikei Y, Shiratori M (2002) TextureExplorer: a tactile and force display for virtual textures. In: Haptic interfaces for virtual environment and teleoperator systems. In: Shiratori M (ed) 10th symposium on HAPTICS 2002. Proceedings, pp 327–334. doi:10.1109/HAPTIC.2002.998976
58. Ikei Y, Yamada M, Fukuda S (1999) Tactile texture presentation by vibratory pin arrays based on surface height maps. In: Olgac N (ed) ASME dynamic systems and control division. 67:97–102. ISBN: 0791816346
59. Iwamoto T, Tatezono M, Shinoda H (2008) Non-contact method for producing tactile sensation using airborne ultrasound. In: Haptics: perception, devices and scenarios. Springer, Berlin, pp 504–513. doi:10.1007/978-3-540-69057-3_64
60. Iwamoto T, Shinoda H (2005) Ultrasound tactile display for stress field reproduction–examination of non-vibratory tactile apparent movement. In: First joint eurohaptics conference and symposium on haptic interfaces for virtual environment and teleoperator systems. WHC 2005, pp 220–228. doi:10.1109/WHC.2005.140
61. Jendritza DJ (1998) Technischer einsatz neuer aktoren: grundlagen, werkstoffe, designregeln und anwendungsbeispiele. 2nd ed. vol 484. Kontakt Studium 484. Renningen-Malmsheim: expert-Verl., p 493. ISBN: 3-8169-1589-2
62. Jolly MR, Carlson JD (1996) Controllable squeeze film damping using magnetorheological fluid. In: Actuator 96, 5th international conference on New Actuators, Bremen
63. Jungmann M (2004) Entwicklung elektrostatischer festkörperaktoren mit elastischen dielektrika für den einsatz in taktilen anzeigefeldern. Technische Universität Darmstadt, Dissertation, p 138. http://tuprints.ulb.tu-darmstadt.de/500/
64. Kajimoto H, Kanno Y, Tachi S (2006) Forehead electro-tactile display for vision substitution. In: Eurohaptics conference. Paris. http://lsc.univ-evry.fr/eurohaptics/upload/cd/papers/f62.pdf
65. Kallenbach E, Stölting H-D, Amrhein W (eds) (2008) Handbook of fractional-horsepower drives. Springer, Berlin. ISBN: 978-3-540-73128-3
66. Kallenbach E et al (2008) Elektromagnete-Grundlagen, Berechnung, Entwurf und Anwendung. Wiesbaden: Vieweg+Teubner, pp XII, 402. ISBN: 978-3-8351-0138-8
67. Kenaley GL, Cutkosky MR (1989) Electrorheological fluid-based robotic fingers with tactile sensing. In: IEEE international conference on robotics and automation. Proceedings, vol 1. pp 132–136. doi:10.1109/ROBOT.1989.99979
68. Kim S-C, Israr A, Poupyrev I (2013) Tactile rendering of 3D features on touch surfaces. In: ACM Press, pp 531–538. doi:10.1145/2501988.2502020. (Visited on 02/17/2014)
69. Kim KJ, Tadokoro S (2007) Electroactive polymers for robotic applications—artificial muscles and sensors. Springer, London
70. Kornbluh R et al. (1999) High-Field electrostriction of elastomeric polymer dielectrics for actuation. In: 6th annual international symposium on smart structures and material—EAPAD, pp 149–161. doi:10.1117/12.349672
71. Kornbluh R, Pelrine R (1998) Electrostrictive polymer artificial muscle actuators. IEEE Int Conf Robotics Autom 3:2147–2154. doi:10.1109/ROBOT.1998.680638
72. Koyama T, Takemura K (2003) Development of an ultrasonic clutch for multi-fingered exoskeleton haptic device using passive force feedback for dexterous teleoperation. In:

Takemura K, Maeno T (eds) Intelligent robots and systems. (IROS 2003). Proceedings. 2003 IEEE/RSJ international conference on, vol 3, pp 2229–2234. doi:10.1109/IROS.2003.1249202
73. Kyung K-U, Lee JY (2007) Haptic stylus and empirical studies on braille, button, and texture display. J Biomed Biotechnol 2008(369651):11. doi:10.1155/2008/369651
74. Kyung K-U, Park J-S (2007) Ubi-pen: development of a compact tactile display module and its application to a haptic stylus. In: Park J-S (ed) EuroHaptics conference, 2007 and symposium on haptic interfaces for virtual environment and teleoperator systems. World Haptics 2007. Second Joint. pp 109–114. doi:10.1109/WHC.2007.121
75. Kyung K-U, Ahn M (2005) A compact broadband tactile display and its effectiveness in the display of tactile form. In: Ahn M, Kwon D-S (eds) Eurohaptics conference, 2005 and symposium on haptic interfaces for virtual environment and teleoperator systems. World Haptics 2005. First Joint, pp 600–601. doi:10.1109/WHC.2005.4
76. Lawrence D, Pao L, Aphanuphong S (2005) Bow spring/tendon actuation for low cost haptic interfaces. In: Haptic interfaces for virtual environment and teleoperator systems. WHC 2005. First joint eurohaptics conference and symposium on (2005). Aerospace Engineering. Colorado University, Boulder, pp 157–166. doi:10.1109/WHC.2005.26
77. Lenk A et al (eds) (2011) Electromechanical systems in microtechnology and mechatronics: electrical, mechanical and acoustic networks, their interactions and applications. Springer, Heidelberg. ISBN: 978-3-642-10806-8
78. Leondes CT (2006) MEMS/NEMS–handbook techniques and applications. Springer, New York. ISBN 0-387-24520-0
79. Levesque V, Levesque V, Pasquero J (2007) Braille display by lateral skin deformation with the STReSS2 tactile transducer. In: Pasquero J, Hayward V (eds) EuroHaptics conference, 2007 and symposium on haptic interfaces for virtual environment and teleoperator systems. World Haptics 2007. Second Joint, pp 115–120. doi:10.1109/WHC.2007.25
80. Li WH et al (2004) Magnetorheological fluids based haptic device. Sensor Rev 24(1):68–73. doi:10.1108/02602280410515842
81. Lotz P, Matysek M, Schlaak HF (2011) Fabrication and application of miniaturized dielectric elastomer stack actuators. IEEE/ASME Trans Mech 16(1):58–66. doi:10.1109/TMECH.2010.2090164. (Visited on 04/11/2012)
82. Makino Y, Asamura N, Shinoda H (2003) A cutaneous feeling display using suction pressure. In: SICE 2003 annual conference (IEEE Cat. No.03TH8734). SICE 2003 annual conference, vol 3. Society of Instrument and Control Engineers, Fukui, Japan. Tokyo, Japan, pp 2931–2934. 4–6 Aug 2003. ISBN: 0-7803-8352-4
83. Marchuk N, Colgate J, Peshkin M (2010) Friction measurements on a large area TPaD. In: Haptics symposium, 2010 IEEE, pp 317–320. doi:10.1109/HAPTIC.2010.5444636
84. Matysek M, Lotz P, Schlaak H (2011) Lifetime investigation of dielectric elastomer stack actuators. IEEE Trans Dielectrics Electr Insul 18(1):89–96. doi:10.1109/TDEI.2011.5704497 (Visited on 04/10/2012)
85. Matysek M et al (2011) Combined driving and sensing circuitry for dielectric elastomer actuators in mobile applications. In: Proceedings of SPIE. vol 7976. San Diego. doi:10.1117/12.879438. (Visited on 03/29/2012)
86. Mehling J, Colgate J, Peshkin M (2005) Increasing the impedance range of a haptic display by adding electrical damping. In: Eurohaptics conference, 2005 and symposium on haptic interfaces for virtual environment and teleoperator systems. World haptics 2005. First Joint. NASA Johnson Space Center, Houston, pp 257–262. doi:10.1109/WHC.2005.79
87. Metec AG. http://web.metec-ag.de/ (Visited on 02/09/2014)
88. Mohand-Ousaid A et al (2012) Haptic interface transparency achieved through viscous coupling. Int J Rob Res 1(3):319–329
89. Mößinger H et al (2014) Tactile feedback to the palm using arbitrarily shaped DEA. In: Proceedings of SPIE, vol 9056. SPIE, San Diego. doi:10.1117/12.2045302
90. Moy G, Wagner C, Fearing R (2014) A compliant tactile display for teletaction. IEEE 4:3409–3415. doi:10.1109/ROBOT.2000.845247. (Visited on 02/09/2014)

91. Moy G (2002) Bidigital teletaction system design and performance. PhD thesis. University of California at Berkeley. http://robotics.eecs.berkeley.edu/ronf/PAPERS/Theses/gmoy-thesis02.pdf
92. Murayama J et al (2004) SPIDAR G&G: two-handed haptic interface for bimanual VR interaction. In: Eurohaptics, vol 1. 1. Universität München, München, pp 138–146
93. Niu X et al (2011) Refreshable tactile displays based on bistable electroactive polymer. In: Proceedings of SPIE, vol 7976. doi:10.1117/12.880185
94. Niu X et al (2012) Bistable electroactive polymer for refreshable Braille display with improved actuation stability. In: Proceedings of SPIE, vol 8340. doi:10.1117/12.915069
95. Nührmann D (1998) Das große Werkbuch Elektronik. 7. Poing: Franzis' Verlag. ISBN: 3772365477
96. Olsson P et al (2012) Rendering stiffness with a prototype haptic glove actuated by an integrated piezoelectric motor. In: Haptics: perception, devices, mobility, and communication. Springer, Berlin, pp 361–372. doi:10.1007/978-3-642-31401-8_33
97. Parthasarathy M, Klingenberg DJ (1996) Electrorheology: mechanisms and models. Mater Sci Eng R Rep 17(2):57–103. doi:10.1016/0927-796X(96)00191-X
98. Pei Q et al (2003) Multifunctional electroelastomer roll actuators and their application for biomimetic walking robots. In: Proceedings of SPIE, vol 5051. [31]. pp 281–290. doi:10.1117/12.484392
99. Pelrine R, Kornbluh R (2008) Electromechanical transduction effects in dielectric elastomers: actuation, sensing, stiffness modulation and electric energy generation. In: Carpi F et al (eds) Dielectric elastomers as electromechanical transducers. 1st edn. Elsevier, Amsterdam, p 344. doi:10.1016/B978-0-08-047488-5.00001-0
100. Phillips RW (1969) Engineering applications of fluids with a variable yield stress. PhD thesis. University of California, Berkeley
101. Physik Instrumete PI GmbH & Co KG (2003) Piezo linear driving mechanism for converting electrical energy into motion, has a group of stacking actuators for driving a rotor in a guiding mechanism
102. Polzin J (2013) Entwurf einer Deltakinematik als angepasste Struktur für die haptische Bedieneinheit eines Chirurgieroboters. Bachelor Thesis. Technische Universität Darmstadt, Institut für Elektromechanische Konstruktionen
103. Popov D, Gaponov I, Ryu J-H (2013) A preliminary study on a twisted strings-based elbow exoskeleton. In: World haptics conference (WHC), 2013. IEEE, pp 479–484. doi:10.1109/WHC.2013.6548455
104. Pott PP et al (2013) Seriell-Elastische Aktoren als Antrieb für aktive Orthesen. In: at-Automatisierungstechnik, vol 61, pp 638–644. doi:10.1524/auto.2013.0053
105. Rajagopal KR, Ruzicka M (2001) Mathematical modeling of electrorheological materials. Continuum Mech Thermodyn 13(1):59–78. doi:10.1007/s001610100034
106. Redux Laboratories. http://www.reduxst.com/ (visited on 02/19/2014)
107. Ren K et al (2008) A compact electroactive polymer actuator suitable for refreshable Braille display. Sens Actuators A Phys 143(2):335–342. doi:10.1016/j.sna.2007.10.083
108. Sattel T (2003) Dynamics of ultrasonic motors. Dissertation. Technische Universität Darmstadt, pp IV, 167. http://tuprints.ulb.tu-darmstadt.de/305/1/d.pdf
109. Schimkat J et al. (1994) Moving wedge actuator: an electrostatic actuator for use in a microrelay. In: MICRO SYSTEM technologies '94, 4th international conference and exhibition on micro, electro, opto, mechanical systems and components. VDE-Verlag, pp 989–996.
110. Senkal D, Gurocak H (2011) Haptic joystick with hybrid actuator using air muscles and spherical MR-brake. Mechatronics 21(6):951–960. doi:10.1016/j.mechatronics.2011.03.001
111. Sheng P (2005) Mechanism of the giant electrorheological effect. Int J Modern Phys B (IJMPB) 19(7/9):1157–1162. doi:10.1016/j.ssc.2006.04.042
112. Sherrit S et al (1999) Modeling of horns for sonic/ultrasonic applications. In: Ultrasonics symposium. Proceedings. IEEE 1:647–651. doi:10.1109/ULTSYM.1999.849482
113. Shima T, Takemura K (2012) An ungrounded pulling force feedback device using periodical vibrationimpact. In: Haptics: perception, devices, mobility, and communication. Springer, Berlin, pp 481–492. doi:10.1007/978-3-642-31401-8_43

114. Sindlinger S (2011) Haptische Darstellung von Interaktionskräften in einem Assistenzsystem für Herzkatheterisierungen. Dissertation. Technische Universität Darmstadt. http://tuprints.ulb.tu-darmstadt.de/2909/
115. Streque J et al (2012) Magnetostatic micro-actuator based on ultrasoft elastomeric membrane and copper—permalloy electrodeposited Structures. In: IEEE international conference on micro electro mechanical systems (MEMS). Paris, pp 1157–1160. doi:10.1109/MEMSYS.2012.6170368
116. Summers IR, Chanter CM (2002) A broadband tactile array on the fingertip. J Acoust Soc Am 112(5):2118–2126. doi:10.1121/1.1510140
117. Takamatsu R, Taniguchi T, Sato M (1998) Space browsing interface based on head posture information. In: Computer human interaction, 1998. Proceedings. 3rd Asia Pacific, pp 298–303. ISBN: 0-8186-8347-3
118. Takasaki M, Kuribayashi Kurosawa M, Higuchi T (2000) Optimum contact conditions for miniaturized surface acoustic wave linear motor. In: Ultrasonics 38:1–8, pp 51–53. doi:10.1016/S0041-624X(99)00093-1
119. Tang H, Beebe DJ (1998) A microfabricated electrostatic haptic display for persons with visual impairments. Rehabilitation Engineering. IEEE Trans Neural Syst Rehabil 6(3):241–248. doi:10.1109/86.712216
120. Taylor P (1997) The design and control of a tactile display based on shape memory alloys. In: Developments in tactile displays (Digest No. 1997/012), IEEE Colloquium on, vol 1997. doi:10.1049/ic:19970080
121. Taylor PM et al (1998) Advances in an electrorheological fluid based tactile array. Displays 18(3):135–141. doi:10.1016/S0141-9382(98)00014-6
122. Tietze U, Schenk C (2002) Halbleiter-Schaltungstechnik. 12th edn. Springer, Berlin, pp. XXV, 1606. ISBN: 3-540-42849-6
123. Tsagarakis N, Horne T, Caldwell D (2005) SLIP AESTHEASIS: a portable 2D slip/skin stretch display for the fingertip. In: First joint eurohaptics conference and symposium on haptic interfaces for virtual environment and teleoperator systems. WHC 2005. pp 214–219. doi:10.1109/WHC.2005.117
124. Uchino K (1997) Piezoelectric actuators and ultrasonic motors. Kluwer, Boston, pp VIII, 349. ISBN: 9780792398110
125. Uchino K, Giniewicz JR (2003) Micromechatronics. Materials engineering, vol 22. Dekker, New York, pp XIV, 489. ISBN: 0-8247-4109-9
126. Uhea S et al (1996) Ultrasonic motors—theory and application. Oxford University Press, Oxford
127. Uhea S (2003) Recent development of ultrasonic actuators, vol 1. Ultrasonics symposium, 2001 IEEE. Atlanta, 7–10 Oct 2001, vol 1, pp 513–520. doi:10.1109/ULTSYM.2001.991675
128. Vidal-Verdú F, Navas-González R (2004) Thermopneumatic approach for tactile displays. In: Mechatronics & robotics. Aachen, Germany, pp 394–399. ISBN: 3-938153-30-X. doi:10.1117/12.607603
129. Vitrani MA et al (2006) Torque control of electrorheological fluidic resistive actuators for haptic vehicular instrument controls. J Dyn Syst Measur Control 128(2):216–226. doi:10.1115/1.2192822. http://link.aip.org/link/?JDS/128/216/1
130. Völkel T, Weber G, Baumann U (2008) Tactile graphics revised: the novel brailledis 9000 pin-matrix device with multitouch input. In: Computers Helping People with Special Needs. Springer, Berlin, pp 835–842. doi:10.1007/978-3-540-70540-6_124
131. von Zitzewitz J (2011) R3—A reconfigurable rope robot as a versatile haptic interface for a cave automatic virtual environment. Dissertation. ETH Zürich
132. Wahed AK (2004) The characteristics of a homogeneous electrorheological fluid in dynamic squeeze. In: Actuator 2004: 9th international conference on new actuators. Bremen, pp 605–608
133. Wallaschek J (1998) Contact mechanics of piezoelectric ultrasonic motors. Smart Mater Struct 3:369–381. doi:10.1088/0964-1726/7/3/011

134. Wang Q, Hayward V (2010) Biomechanically optimized distributed tactile transducer based on lateral skin deformation. Int J Robot Res 29(4):323–335. doi:10.1177/0278364909345289
135. Weaver W, Timosenko SP, Young DH (1990) Vibration problems in engineering, 5th edn. Wiley, New York, pp XIII, 610. ISBN: 0-471-63228-7
136. Weinberg B et al (2005) Development of electro-rheological fluidic resistive actuators for haptic vehicular instrument controls. Smart Mater Struct 14(6):1107–1119. doi:10.1088/0964-1726/14/6/003
137. Wen W, Huang X, Sheng P (2004) Particle size scaling of the giant electrorheological effect. Appl Phys Lett 85(2):299–301. doi:10.1063/1.1772859
138. Williamson MM (1995) Series elastic actuators. Master Thesis. Massachusetts Institute of Technology. http://dspace.mit.edu/handle/1721.1/6776
139. Winfield L et al (2007) T-PaD: tactile pattern display through variable friction reduction. In: IEEE, pp 421–426. doi:10.1109/WHC.2007.105. (Visited on 01/17/2014)
140. Würtz T et al (2010) The twisted string actuation system: modeling and control. In: IEEE/ASME international conference on IEEE/ASME international conference on advanced intelligent mechatronics (AIM). IEEE, pp 1215–1220. doi:10.1109/AIM.2010.5695720
141. Yu O, Zharri (1994) An exact mathematical model of a travelling wave ultrasonic motor, vol 1. Ultrasonics symposium. Proceedings, 1994 IEEE. Cannes, 1–4 Nov 1994, pp 545–548. vol 1. doi:10.1109/ULTSYM.1994.401647
142. Zhu M (2004) Contact analysis and mathematical modeling of traveling wave ultrasonic motors. In: IEEE transactions on ultrasonics, ferroelectrics and frequency control, vol 51, pp 668–679. ISBN: 0885-3010. 6 June 2004